1-1-2003

Micropatterned polymer films for optic nerve regeneration

Jennifer Behr Recknor
Iowa State University

Micropatterned polymer films for optic nerve regeneration

by

Jennifer Behr Recknor

A thesis submitted to the graduate faculty

in partial fulfillment of the requirements for the degree of

MASTER OF SCIENCE

Major: Chemical Engineering

Program of Study Committee:
Surya K. Mallapragada, Major Professor
Donald S. Sakaguchi
Richard Seagrave

Iowa State University

Ames, Iowa

2003

Graduate College
Iowa State University

This is to certify that the master's thesis of

Jennifer Behr Recknor

has met the thesis requirements of Iowa State University

Signatures have been redacted for privacy

TABLE OF CONTENTS

ABSTRACT

In an effort to promote optic nerve regeneration *in vivo*, directional growth of astrocytes has been achieved on polymer substrates *in vitro*. The purpose of this project was to investigate the cellular mechanisms of optic nerve repair using astrocyte cultures. Manipulating a combination of physical and chemical cues, astrocyte adhesion and alignment *in vitro* were examined.

To provide physical guidance, micropatterned polymer films of polystyrene (PS) were fabricated. Laminin was selectively adsorbed onto the grooves of the patterned surface. Rat type-1 astrocytes were seeded onto micropatterned PS substrates of 10 μm groove width, 10 or 20 μm groove spacing and 3 or 4 μm groove depth. The effects of substrate topography and the adsorption of laminin to the PS substrates on the behavior and morphology of the astrocytes were explored. The astrocytes were found to align parallel to the micropatterned grooves at initial seeding densities of approximately 7500, 13,000, and 20,000 cells per cm^2 due to the effects of the physical and chemical guidance mechanisms. Adsorbing laminin in the microgrooves of the micropatterned PS substrates improved cell adhesion and spreading of cytoskeletal filaments significantly. At these initial seeding densities, over 85% alignment in the direction of the grooves was achieved on the micropatterned PS substrates with laminin adsorbed in the grooves. The effects of physical and chemical guidance mechanisms on the behavior and morphology of the astrocytes on the PS substrate were explored to determine their influence on the outgrowth and differentiation of adult neural stem cell cultures *in vitro*. This combination of guidance cues has the potential to provide a permissive substrate for *in vivo* regeneration of the diseased or injured optic nerve and other regions of the central nervous system.

1. INTRODUCTION

Vision is the result of the intricate workings of a complex sensory system. Injury to or malfunction of this delicate system can result in blindness or a sudden loss of sight that has been thought to be completely irreparable until very recently. Accounting for 12 % of all new blindnesses each year, glaucoma is one of the leading causes of blindness in the United States. Glaucoma is a heterogeneous group of nerve disorders that involve a distinct type of optic nerve damage in the central nervous system that can lead to blindness. The death of, or severe damage to, retinal ganglion cells causes this blindness, which disrupts the transmission of electrical impulses from the optic nerve to the visual cortex of the brain. There are other disorders of the optic nerve, including anterior ischemic optic neuropathy and traumatic or compressive optic neuropathy that are extremely difficult to treat if not untreatable. The leading cause of visual loss in the elderly, age-related macular degeneration (AMD) is one of many retinal disorders that involves damage to the retinal ganglion cells. The ability of the central nervous system to transmit signals to the brain is severely hampered when retinal ganglion cells or the optic nerve are affected due to disease or injury. Injury to the adult central nervous system (CNS) is devastating due to the inability of central neurons to regenerate correct axonal and dendritic connections.

The goal of this research project is to create a permissive substrate to facilitate guided growth of neural stem cells with potential for aiding in regeneration of the optic nerve and repair of loss of sight in cases where the optic nerve has been damaged. In an effort to provide an interface between microelectrode components such as retinal prosthesis and the brain, steps were taken for initial characterization of a guidance substrate onto which neural stem cells and microelectrodes could be integrated. Recent evidence has shown that astrocytes of the central nervous system take an active role in the induction of neurogenesis from adult neural stem cells. Combining the biological influence of astrocytes and physical and chemical guidance cues potentially creates a permissive environment for the selective differentiation and outgrowth of neural stem cells. To determine the influence astrocytes can have on adult neural stem cell cultures *in vitro*, the purpose of the research presented here was to investigate physical and chemical mechanisms that direct and guide astrocyte adhesion and alignment *in vitro*. This was achieved by fabricating micropatterned polystyrene substrates to provide physical guidance and chemically modifying these substrates with proteins influential to cell growth. The behavior and morphology of astrocytes on these substrates was extensively explored in order to optimize conditions for controlling their growth and subsequently use the astrocytes to

influence differentiation and outgrowth of adult neural stem cells. If the signals provided by astrocytes have the potential to induce neural stem cells to differentiate into neurons and can provide a permissive environment for neurorepair following injury, these findings may prove to be extremely valuable in developing a strategy for optic nerve regeneration. Furthermore, the understanding gained from the integration of physical, chemical and biological guidance cues to direct neural stem cell differentiation at the cellular level not only has possible applications in controlled regeneration of the optic nerve but in other regions of the CNS.

2. LITERATURE REVIEW

2.1 The Central Nervous System and the Optic Nerve

2.1.1 The mammalian central nervous system

The mammalian central nervous system (CNS) is composed of the spinal cord and brain, including the medulla oblongata, the pons, the cerebellum, the midbrain, the diencephalon and the cerebral hemispheres. The CNS consists of tracts involving nerve fibers that are either myelinated or nonmyelinated. Bundles of nerve fibers, or axons, deliver sensory information to CNS and carry motor commands to the periphery.

There are two distinct classes of cells in the CNS. They are nerve cells and neuroglial cells. Nerve cells, or neurons, collect information from the environment directly or from other neurons and transmit this information to target cells, specifically other neurons in the CNS. Neuroglial cells surround nerve cell bodies and axons. They provide structural support, function in repair processes, provide isolation and insulation of groups of neurons from each other, are involved in metabolic functions and guide the migration of growing axons during development [1]. Neuroglial cells also may regulate neuronal shape and synaptic connectivity [2].

2.1.1.1 Neurons

Neurons of the CNS can appear morphologically different, yet they all have the same functional organization allowing collection and transmission of information. Most have several main features, including a cell body and two types of processes, or nerve fibers, called the dendrites and the axon (Figure 2-1). The diameter of the cell body is 50 μm or larger. It is the center of metabolic activity in the cell and contains the nucleus and the rough and smooth endoplasmic reticulum. Dendrites receive information and axons transmit information to other cells. Dendrites increase the surface area of cellular communication as they branch out receiving signals from hundreds, sometimes thousands, of other neurons. The axon is capable of conveying electrical signals over distances from 0.1 mm to 2 meters. Compared to the cell body, most axons in the CNS are very thin ranging between 0.2 and 20 μm in diameter. Lipoprotein sheaths of myelin provided by a class of

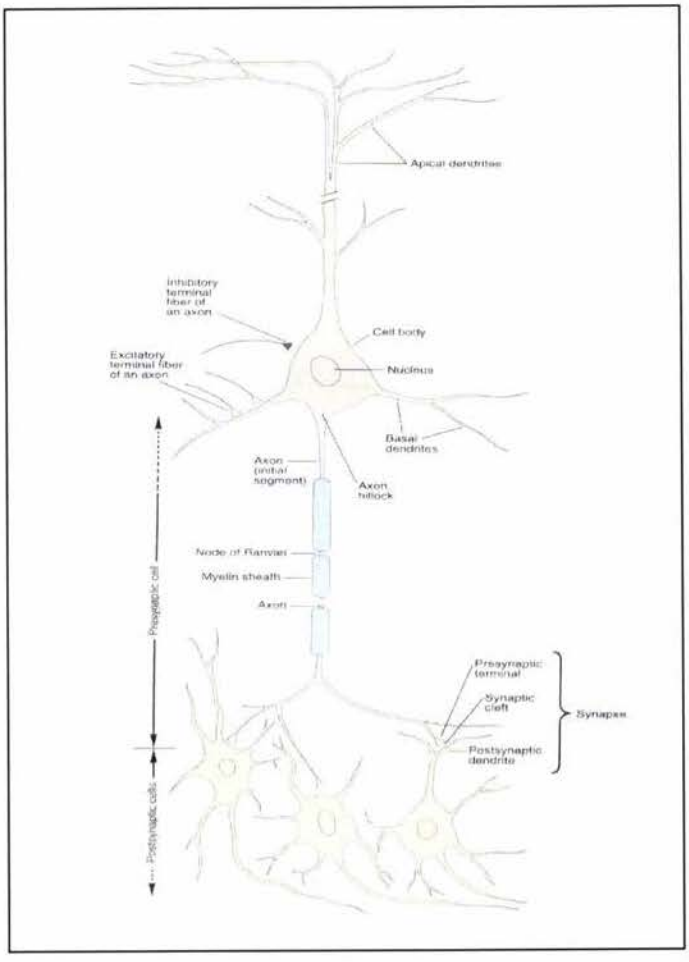

Figure 2-1. The features of neurons in the vertebrate nervous system [1, 3].

glial cells known as oligodendrocytes insulate many axons (myelinated axons). Synapses are specialized terminals where the axon terminals of one neuron (presynaptic neuron) transmit signals to the dendrites of another neuron (postsynaptic neuron). Neurotransmitters released from vesicles at the presynaptic terminal send signals across a synapse to the postsynaptic terminal [1]. Specialized points of synaptic contact are made between neurons determining the function of particular neural networks organized within the CNS.

Neuronal structure provides valuable information about the function of the neuron. The anatomical location of the neuron, its size, origin, and the destination of the axons and dendrites are important features. Connections made with the neuron are also vital in determining neuronal function [2]. The number of processes that a neuron has distinguishes one neuron from another. Bipolar and multipolar are two general classifications for most neurons in the CNS. Bipolar cells, such as those

found in the retina, have two processes, the dendrite and the axon, that have specialized functions. Multipolar cells have an axon and many dendrites. They are the most common neurons in the CNS and are found in the spinal cord, hippocampus, throughout the cerebral cortex and cerebellum. Neurons are also classified by their function. In the mammalian nervous system, afferent neurons carry information toward the CNS from the periphery and motor (or efferent) neurons are motor fibers leading away from the brain and spinal cord [4]. A third class of neurons, known as interneurons, are responsible for relaying or projecting information over long distances as well as within local circuits [1].

2.1.1.2 Glial Cells

Two principal classes of glial cells existing in the CNS are astroglial cells (astrocytes) and oligodendrocytes (Figure 2-2). There is a great deal of information on these macroglial cells and their role in structural and functional support of axons in the central nervous system. However, this discussion will focus mainly on astroglial cells (specfically type 1 astroglial cells) as they are the primary concern in this research.

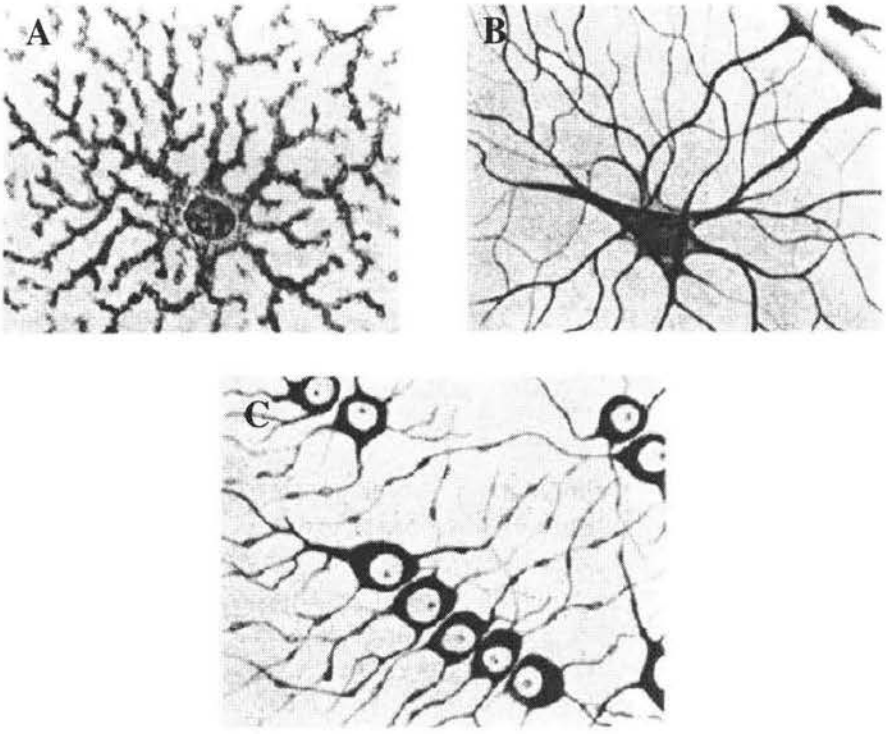

Figure 2-2. Neuroglial cells in the central nervous system. A) Protoplasmic astrocytes. B) Fibrous astrocytes. C) Oligodendrocytes [3].

The oligodendrocytes are small cells with few processes that are responsible for insulating axons by wrapping their processes around them concentrically forming a myelin sheath. These cells are similar to Schwann cells, the ensheathing and myelinating cells of the peripheral nervous system (PNS). However, a single oligodendrocyte enwraps several axons with its plasma membrane whereas in the PNS, one Schwann cell envelops one axon. The sheath is interrupted at regular intervals by gaps, called the nodes of Ranvier. Electrical excitation is confined at the nodes of Ranvier. Nerve impulses, or action potentials, are propagated quickly and efficiently as they travel along the axon jumping from node to node [5]. Oligodendrocytes also surround neuronal cell bodies providing support.

Astrocytes are the most numerous of the glial cells and have multiple functions in the CNS. These cells take on a variety of morpholgies. Typically, astroglial cells have cell bodies that are polygonal or circular in shape usually with many long processes. In culture, astroglial cells are flat, adherent cells. They have a cobblestone-like appearance and lack polarity at confluence. A minority of these cells can also appear irregular in morphology and exhibit one or more long processes. *In vivo*, their appearance closely resembles neurons having polarity and one or more thick processes. Astrocytes are in close contact with neurons and endothelial cells from capillaries and can also envelop synaptic terminals [6] (Figure 2-3). These glial cells are connected to each other through tight junctions, or gap junctions. These specializations allow the passage of small molecules between the cytoplasm of neighboring cells. Due to their position within the CNS, astrocytes have the capability of establishing communication through signaling pathways between neurons, between astrocytes, and between neurons and capillaries [7].

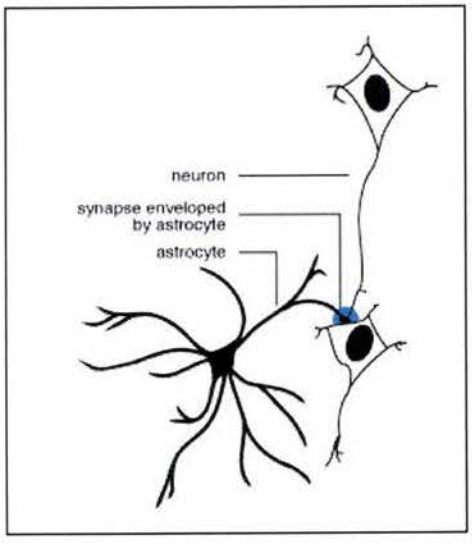

Figure 2-3. Schematic of one synapse enveloped by filopodial extension of one astrocyte [8].

There are various types of astrocytes present in the mammalian brain. Based on the length of the processes of these cells, astrocytes have been placed into two categories: fibrous astrocytes, which have extensive intermediate filaments and protoplasmic astrocytes containing fewer filaments (Figure 2-2 above). A third subclass of astrocytes, reactive astrocytes, appears following injury to the brain. These classifications are typically used to describe astrocytes *in vivo*. Brain cell cultures have revealed two glial cell lineages. These two types of astrocytes are called type-1 and type-2 astroglia [9]. In cell suspensions of the rat optic nerve, it was discovered that type 1 astrocytes appear prenatally and type 2 astrocytes appear at the beginning of the second postnatal week [10]. Morphology, antigenic phenotype, and response to growth factors are used to distinguish these cells from each other [9]. The intermediate filaments of astroglia are composed of glial fibrillary acidic protein (GFAP). The presence of this protein is used as a marker for observing and quantifying astroglial cells. A2B5, a monoclonal antibody directed against gangliosides, is used to differentiate between type-1 and type-2 astrocytes. This antibody labels type-2 astrocytes but not type-1. In addition to the optic nerve, there have been cells of type-1 astroglia and type-2 astroglia observed in cultures of cerebellum [11] and cerebral cortex [12] in addition to optic nerve.

Astrocytes are known primarily to function in supporting roles providing structural support and nutrition to neurons and other cells in the CNS. They form continuous sheets called limiting membranes as they extend processes to the nerve surface and are important in the formation of the blood-brain barrier between the CNS and other tissues. Astrocytes also express a high density of potassium ion (K^+) channels. Due to this characteristic, they are able to buffer extracellular potassium that accumulates when neurons fire action potentials repeatedly and take in excess neurotransmitters released by neurons [13]. *In vivo* and *in vitro* studies have been undertaken revealing that astroglial cells express receptors and function in neurotransmitter uptake. They have also been proposed as a source of trophic factors necessary for neuronal survival [14]. It has been shown that astroglial cells function in neuronal guidance [15]. More recently, Song and colleagues reinforced an emerging view that astrocytes have an active regulatory role in the CNS. Their findings presented strong evidence that astroglia promote neurogenesis from adult neural stem cells [16]. Invaluable experimentation performed in the last two decades has revealed that astrocytes are much more complex than previously thought and are capable of significant influence on neuronal activity.

Type-1 astroglial cells express a variety of functional neurotransmitter receptor and uptake

systems. Type 1 astroglia have been shown to activate second messenger systems including cyclic AMP [17], cyclic GMP [18], and intracellular calcium [19]. These receptor systems also regulate ion channel opening [20]. Voltage dependent ion channels have been demonstrated in astroglia as well [21]. There has been much evidence showing that astrocyte receptors participate in neurotransmitter uptake. Mammalian astrocytes from neonatal rat brain were identified as taking up serotonin by a sodium- dependent mechanism with high-affinity [22]. Astrocytes have been able to respond to amino acids, amines, peptides, purines, and prostaglandins [23]. It has been demonstrated that astrocytes respond to a variety of synaptically released neurotransmitters including glutamate [24], noradrenaline [25], histamine [26], acetylcholine [26], ATP [27, 28], and γ-aminobutyric acid (GABA) [29]. These transmitters induce elevations of astrocytic Ca^{2+}. Astroglial receptor systems are not only involved in response to transmitters, but the integration of inputs and signaling leading to transmitter release.

Type-1 astroglial cells exhibit growth factor secretion. Astrocytes release a variety of soluble factors many of which are involved in neuronal signaling, including glutamate [30-32], ATP [27, 33], and β-chemokines [34]. Cultured glial cells from various regions of the brain synthesize and secrete nerve growth factor (NGF) [35]. In the optic nerve, type-1 astroglia secrete growth factors that induce the proliferation of O-2A progenitor cells [36]. *In vitro* experimental evidence has suggested that platelet-derived growth factor (PDGF) is responsible for this stimulation of O-2A proliferation [37, 38]. Growth factors released from astroglia are also involved in the differentiation of O-2A progenitors to type-2 astroglia. It has been deduced that ciliary neurotrophic factor (CTNF) or a closely related protein plays a role in inducing type-2 astroglia differentiation [39]. Furthermore, various glycoproteins and proteoglycans secreted by astrocytes into the extracellular matrix (ECM) have been shown to influence axonal outgrowth. Laminin, a substrate adhesive molecule, is produced by astroglia and secreted into ECM. This molecule has been shown to promote extensive neurite outgrowth [40]. Chondroitin sulfate proteoglycan (CSPG), an ECM molecule associated with astroglia, was reported by Snow et al. to direct the growth of retinal ganglion cell processes in the rat retina [41]. It has been demonstrated *in vitro* that astroglia release factors in the culture medium that are capable of enhancing growth and prolonging the survival of hippocampal neurons [42] and inducing morphological differentiation in neuroblastoma cells [43]. Astroglia provide supporting elements not only through the release of soluble factors into culture medium but through cell-to-cell contact as well [14].

2.1.1.3 Astroglial-Neuronal interactions

Neurons and astroglial cells interact extensively within the mammalian CNS. Among the functions attributed to astrocytes are the support of the proliferation, survival, and maturation of developing neurons. Astrocytes are thought to guide migrating neuronal precursors and advancing growth cones to their destination [44]. They provide structural, metabolic, trophic as well as tropic support for neurons [1]. Astrocytes regulate neuronal activity through the release of soluble trophic factors, such as glutamate [31, 45]. Haydon reported recently that astrocytes are capable of integrating neuronal inputs and modulating synaptic activity [13, 32]. In the past, it was believed that the role of astrocytes was to provide a passive, supportive mechanism for neurons. They are now believed to take on an active, regulatory role [16, 46].

Astroglia function in the induction and stabilization of CNS synapses. There is *in vitro* evidence that astrocytes might play an important role in determining how well-connected neurons end up by direct influence on their synapses. Pfrieger and Barres reported that culture media from astrocytes caused a tenfold increase in the synaptic activity of RGCs [47]. Work by Ullian and colleagues demonstrated that RGCs that are cultured in the presence of astroglia increased in synaptic number significantly and the synapses were also more mature. They revealed that *in vivo* generation of synapses occurs alongside the development of glia. These results are in agreement with what was previously observed about synapse number *in vivo* in the superior colliculus [48]. Nagler et al. [49] has recently reported that synapse formation in purified CNS neuron cultures is induced by a soluble glia-derived factor. Mauch et al. [50] demonstrated just months later that this factor was cholesterol in a complex with lipoproteins containing apolipoprotein-E. Blondel et al. [51] has also recently presented that a soluble astrocyte-derived factor promotes synapse formation and enhances glutamate sensitivity in cultured hippocampal neurons. Furthermore, there is significant evidence that synapses and the astroglia associated with them form tripartite synaptic structures in the CNS. Synaptic transmission is modulated by such structures in a "feedback" manner [52].

Despite the anatomical simplicity of the optic nerve due to the lack of neuronal cell bodies, a variety of interactions occur between axons and astroglial cells in this pathway both *in vivo* and *in vitro* (Figure 2-4). Changes in chemical composition of the extracellular fluid produced by glial or neuronal stimulation mediate these interactions. Certain interactions have been characterized as lasting for brief periods involving changes in K^+ or H^+ concentrations, or alterations involving small

molecules, including glutamate or ATP, while others involve much longer periods and involve larger signaling molecules such as peptides or proteins [53].

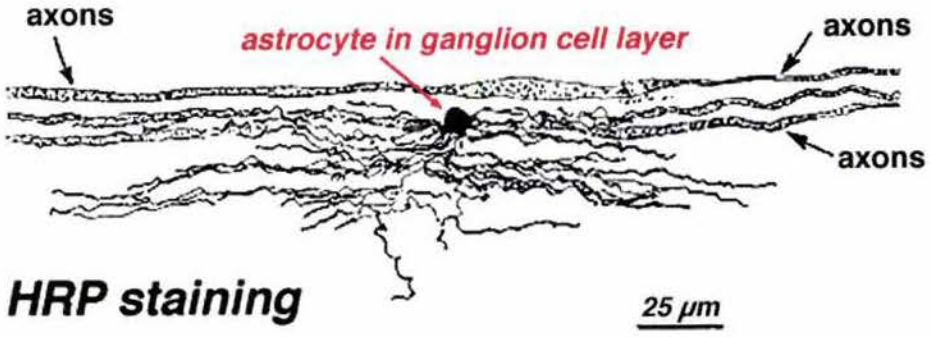

Figure 2-4. Horseradish peroxidase (HRP) staining of astrocytes in the ganglion cell layer [54].

Astroglia also take an active part in neuronal guidance. It has been presented that astroglia play a major role in neuronal migration [15]. Astroglia influence the direction of axonal outgrowth by providing a pathway for axonal outgrowth or by becoming barriers to prevent inappropriate axon pathway growth in certain locations. Astrocytes function actively in neurite extension and patterning [55, 56]. *In vitro* and *in vivo*, evidence has been reported suggesting that neurite pathfinding can be controlled solely by astrocytes in the developing CNS [56, 57]. CSPG has been described as forming barriers to direct growth of retinal ganglion cell axons in the developing retina [41]. Retinal ganglion cell differentiation has also been demonstrated using similar ECM molecules produced by astroglia [58]. Astrocytes take on these active roles through the release of cytokines, proteases, and protease inhibitors [59, 60]. They also have a variety adhesion molecules on their surface that are influential in axon growth and produce various extracellular matrix molecules [56, 61, 62]. The proper combination of astroglia- associated permissive and non-permissive guidance cues produced by astrocytes in the precise locations direct neurites to their destinations. It is thought that astrocytes regulate the expression of these particular guidance cues within the CNS [63].

Furthermore, there has been *in vitro* and *in vivo* evidence reported demonstrating that in response to CNS injury astroglial cells exhibit considerable plasticity and that neuron-glia relationships regulate what occurs in the CNS after injury [64]. Astrocytes produce both soluble and

membrane-associated factors that influence CNS function and provide a surface that may change the "sprouting" of axons following injury [46, 65]. Recently, Song and colleagues revealed that hippocampal astrocytes instruct the neuronal fate commitment of adult neural stem cells [16].

2.1.2 The optic nerve

The optic nerve (ON) consists of the long nerve processes or axons of retinal ganglion neurons projecting from the eye to the brain. These axons reside in narrow extracellular spaces alongside the cell bodies and processes of glial cells [53] (Figure 2-5). Undifferentiated cells, including glial progenitors, are also retained by the optic nerve [66-68]. A wide range of interactions exists between the retinal ganglion cells (RGC) axons and glial cells found within and along the ON.

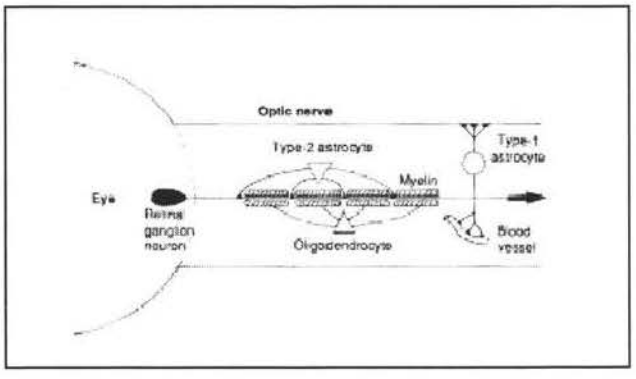

Figure 2-5. A model of how the three types of glial cells are arranged in the adult rat optic nerve [5].

Both *in vitro* and *in vivo* it has been demonstrated that in response to CNS injury astroglial cells exhibit considerable plasticity and that neuron-glia relationships regulate what occurs in the CNS after injury [64]. Neuron-astroglial interactions provide a permissive environment for the prevention of RGC death and restoration of ON function following injury.

2.1.2.1 Organization of the visual system

Vision is an integral part of neural function. The eye consists of a pupil that adjusts lens aperture, a lens that focuses light on the retina, and the retina, or the neural layer of the eye, where photoreceptors are present. The lens is made of many layers of cells that provide translucency. These layers also have viscoelastic properties that are important in focusing, or adjusting lens thickness. The retina receives visual images. It converts the image in to nerve impulses and facilitates feature

analysis of the image. Feature analysis and visual interpretation proceed progressively as signals from the retina are passed to other visual centers in the brain.

The retina is the inner most layer of the eye. It is responsible for receiving light and consists of many retinal cells. There are several layers of cells that make up the retina. The cells in these layers include photoreceptor cells (rods and cones), bipolar cells, ganglion cells, and pigment epithelial cells (Figure 2-6). The pigment epithelium is the most outer layer of the retina and is a single cell-layer of melanin-containing cells. The neural cells are found just outside of this layer. Each cell type forms a cellular layer and they are linked by synapses. The outer segments of the rods and cones form the photoreceptive layer. The cell bodies of the rods and cones make up the outer nuclear layer. The axon terminals of the rods and cones synapse with the dendrites of the bipolar cells (sensory neurons) making up the outer plexiform layer. The nuclei and perikaya of the bipolar cells form the inner nuclear layer. Axon terminals of the bipolar cells synapse with the dendrites of the of ganglion cells forming the inner plexiform layer. The inner most layer of the retina consists of the cell bodies of the ganglion cell, the ganglion cell layer. The axons of the ganglion cells form the optic nerve fiber layer. Light focused by the lens first passes through the nerve cells of the retina to reach the rods and cones at the periphery of the retina. Visual information then moves through the retinal layers, from the photoreceptive layer toward the ganglion cell layer. Finally, the optic nerve transmits visual information from the retinal ganglion cells through the optic disk to three nuclei of the visual system. The axons of RGCs terminate in (1) the lateral geniculate nucleus (thalamic nucleus) of the brain for projection of fibers to the visual cortex, (2) the rostral colliculus for the visual and pupillary light reflexes (pupillary dilation), and (3) the pretectal nucleus for the pupillary light reflex (pupillary constriction).

The optic nerve becomes the central tract along which visual messages are carried out of the eye along the retinal ganglion cell axons. The optic nerves from each eye join its opposite at the optic chiasm. At the chiasm, optic nerve fibers from the nasal halves of each retina cross. The fibers in the temporal halves remain uncrossed. The optic tracts, which extend from the chiasm to the thalamus, contain fibers that convey visual information from both eyes. If there is injury to one optic nerve, the result is total blindness in that particular eye. If the optic tract is damaged on one side, the result is partial blindness in both eyes.

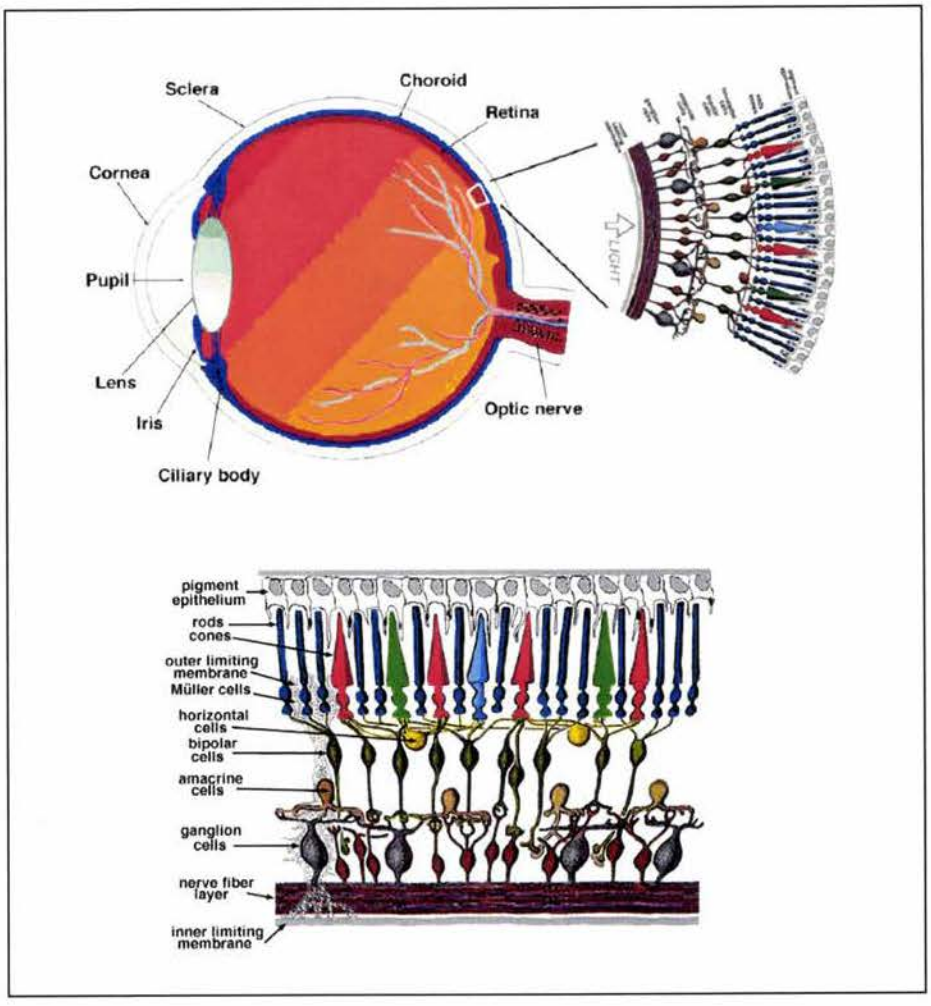

Figure 2-6. The anatomy of the human eye and a cross-section of the human retina [54].

2.1.2.2 Optic nerve injury and regeneration

It is believed that the adult mammalian central nervous system (CNS) is not capable of self-repair or regeneration of the correct axonal and dendritic connections [69, 70]. Adult CNS injury is typically followed by neuronal degeneration, cell death, and the breakdown of synaptic connections. It is established that fish, amphibians, mammalian peripheral nerves as well as developing central nerves respond differently to an injury than the adult mammalian CNS. In these systems, functional axons can regrow after they have been damaged [69]. The adult mammalian optic nerve is thought to be incapable of significant self-repair or regeneration under normal physiological conditions. Presumably injury to the optic nerve, including transection, elevated intraocular pressure, ischemia, and compression is permanent and devastatingly irreversible. Without any capacity for repair, it is

believed that those with damage to the ON will not be able to restore their sight. This belief stems from three major assumptions: (1) the mammalian RGC will die once its cell body or axon has been injured; (2) an injured mammalian RGC whose axon has degenerated cannot be induced to extend a new axon; and (3) even if induced to regenerate, the regenerating axon cannot be guided back to its original target in the CNS. Successful regeneration depends on reinduction of necessary intracellular mechanisms as well as the synthesis of proteins for support of axonal growth. Furthermore, the reactivation of long-range pathfinding functions present during development must occur, and proper conditions must be met for reestablishment of appropriate connections in the target areas of the brain [71]. Studies have provided evidence that under certain conditions a lesioned neuron can survive axotomy, re-extend a regenerated axon and reform patterned connections within the CNS [72].

Following axotomy of the optic nerve, it has been shown that there is a transient state of regeneration followed by a period of retrograde degeneration of ganglion cells. Optic nerve transection results in a cascade of inflammatory events that lead to ganglion cell terminal degeneration followed by phagocytosis of somata in the retina [73-75]. After the axons of the optic nerve are severed, nearly all RGCs survive for about 5 days and then begin to die off. Approximately 90% of the RGCs undergo apoptosis, or programmed cell death, within two weeks [76, 77]. Microglia in the retina that are signaled by the axotomised ganglion cells help this self-destruction [78]. Molecular methods have been shown to increase the survival of lesioned ganglion cells. Among these methods are injections of neurotrophic factors into the eye, including nerve growth factor (NGF), brain derived neurotrophic factor (BDNF), basic fibroblast growth factor (bFGF), and growth factors isolated from the peripheral nervous system, the *in vitro* application of peptides, the intraocular injection of molecules inhibitory to the microglial activity, and the expression of the *bcl*-2 protein [79, 80]. Affecting the external as well as the internal environment of the optic nerve has allowed the ganglion cell to survive axotomy. There seems to be a critical dependency on the availability of exogenous and endogenous neuronal trophic support.

Once the normal programmed degeneration of RGCs following injury is interrupted, the surviving neurons must then re-extend axons within the CNS environment. Experiments have confirmed observations made by Cajal that the myelinated region of the ON (later verified as the myelin of oligodendrocytes) inhibits axon growth in the CNS [73, 81-83]. Therefore, in order for a surviving neuron to re-extend an axon along the CNS, the inhibitory molecules of the myelin must be neutralized. Surgical implantation of hybridoma cells continually secreting monoclonal antibodies

(IN-1) has blocked such inhibitory molecules in the area surrounding lesioned spinal cord [84]. These antibodies used in combination with other growth factors, such as BDNF [85], as well as the inactivation of myelin-associated glycoprotein (MAG) [86] have allowed lesioned RGC axons to regenerate significantly within the optic nerve. Gliosis also exhibits an inhibitory effect to axon growth in the CNS. Gliosis is the scar reaction that results in a massive proliferation of gliotic tissue surrounding the area where the CNS has been injured. This glial reaction is mediated primarily by astrocytes as they are attempting to keep pathogens out of the CNS in an effort to re-establish the blood-brain barrier [87]. Inhibitory molecules are also synthesized during glial scar formation, including chondroitin sulfate proteoglycan (CSPG) [41]. However, it has been revealed that the formation of the glial barrier presents trophic factors and has a role on reconstructing the blood-brain barrier as it isolates intact CNS tissue from secondary lesions [65]. As gliosis presents itself only at the site of injury, regrowing axons are able to grow in parts of the CNS tissue that have not been disrupted [88]. In the retina, there is minimal gliotic reaction with very little CSPG expression following injury [89]. Regenerating adult rat retinal segments have demonstrated axon extension after explantation onto a substrate consisting of Schwann cells [90] or immature astrocytes [91]. These results suggest that the retina may be a more favorable site for regeneration than other regions of the CNS.

Directing a new axon to its correct target in the CNS has proven to be a major challenge in experimental strategies for ON regeneration. The process of synaptic connection and refinement must occur to ensure that the correct retinal ganglion cells are connected to the appropriate targets restoring retinotopic maps and, ultimately, sight [72]. In the opossum, it has been shown that at early stages of development that ganglion cells can regenerate across an incision made in the retina. Regenerating axons were also shown to respond to guidance cues within the optic chiasm [92]. The mechanisms behind the expression of the guidance cues in the adult visual pathway during regeneration are currently under much investigation. This research relies on the close association that exists between development and regeneration.

2.1.3 Neural stem cells in the adult central nervous system

Neural stem cells that have the potential to produce new neurons and glia are present in the adult mammalian CNS. These cells can remain in certain regions of the adult CNS after development even though neurogenesis no longer occurs in most areas after birth. Neural stem cells are described

as generating neural tissue or being derived from the neural system, having capacity for self-renewal, and they are multipotent or possess the ability to adopt a variety of cellular fates. Neural progenitors with more limited capacities in terms of growth and differentiation have been known to proliferate throughout life in a variety of mammalian species, including humans [93, 94]. Progenitor cells isolated from the subventricular zone as well as the dentate gyrus of the hippocampus have demonstrated proliferative neurogenesis into adult life. Cultures that have been initiated from these tissues have revealed both neuronal and glial-restricted progenitor cells as well as multipotent precursors [95, 96]. Palmer and colleagues revealed that the neural progenitors were able to differentiate into neurons after activation by fibroblast growth factor-2 (FGF-2). Furthermore, in the adult optic nerve, exposure to FGF-2 activated a latent neurogenic potential that is retained by precursors in this pathway. The results from this study supported the belief that neurogenesis may be restricted by the local environment cues in the developing and adult brain [16, 97]. This work confirmed that there are stem-like cells existing naturally that are capable of producing neurons within diverse tissues of the adult brain, such as the optic nerve, a structure that is separate from the neurogenic zones within the brain [98].

Neural stem cell transplantation has been proposed as a method of repairing the diseased or damaged CNS through neuronal replacement. Gage and colleagues revealed that transplanted cells capable of proliferation and neurogenesis that were isolated and cultured from the adult rat hippocampus retain the capacity to generate mature neurons when grafted into the adult brain [99]. These cells have also been found to be capable of functionally integrating into the host hippocampal circuitry [100]. Neural stem cell transplantation has been attempted with neonatal and adult eyes [101, 102]. However, the differentiation of transplanted cell into lineages specific to the retina has not been achieved. In the past, the capacity of the retina to support transplanted neural stem cells has only been observed in diseased or damaged mature neural retinas [101, 103]. However, the work of Van Hoffelen et al. has recently shown that transplanting brain progenitor cells from the opossum into the developing and mature opossum eye led to survival and differentiation *in vivo* with extensive morphologic integration in the host retina. It was revealed that these cells displayed characteristic morphologies of retinal neurons and that age of the host appeared to play a role in determining cell fate[104]. Neuronal replacement strategies, such as neural stem cell transplantation, that incorporate the insight gained from exploring cues the influence proliferation and differentiation of neuronal

progenitor cells are valuable to the study of CNS, and more specifically, optic nerve regeneration and repair.

2.1.4 Adult neural stem cell- astroglial interactions

Local environments have a profound influence on the fate of adult neural stem cells. In the postnatal period in which the proliferation of progenitor cells progressively decreases, there is correspondence to a period of maturation of astrocytes. In the subventricular zone and the dentate gyrus of the hippocampus (the germinative zones of the brain), where proliferation of neuronal progenitors continues throughout adulthood, astrocytes are present that exhibit the morphology and phenotype of immature astrocytes. Alvarez-Buylla and Lim showed that *in vitro* direct cell to cell contact between the progenitors of the adult subventricular zone and astrocytes stimulated proliferation of progenitors [105]. In recent *in vivo* work by Alonso, it was revealed that astrocytes present in the germinative zones of the CNS provide a microenvironment that supports the proliferation of neuronal progenitors [106].

It has been further demonstrated that astroglial cells provide a permissive environment for neurogenesis. Song and colleagues recently established that factors from astrocytes increase the rates of neuronal fate commitment nearly six-fold and proliferation of progenitor cells twofold [16]. They have shown that neonatal as well as mature hippocampal astrocytes in the adult brain promote neurogenesis. Astroglial cells were observed as taking an active, regulatory role in neuronal production in the adult CNS. It was deduced that regionally specified astroglial cells have the potential to function as cues for neural stem cell differentiation of FGF-2 dependent, adult-derived stem cells [16].

2.2 Techniques for Optic Nerve Regeneration

For nearly twenty years, optic nerve regeneration has been attempted in the laboratory at certain critical stages of CNS development, with the involvement of existing pathways using antibodies to neutralize inhibitory factors, the manipulation of peripheral nerve grafts, and the use of embryonic CNS transplants [79, 107-109]. Adult mammalian RGCs possess the capacity for self-repair. It has been well established that peripheral nerve segments exert trophic influences on survival and regeneration of axotomized ganglion cells [109-111]. Work by Videl-Sanz and colleagues [110]

demonstrated regeneration of ON axons into and through a sciatic nerve graft and to the superior colliculus. Regeneration of ON axons through transection was also induced by Lazarov-Spiegler et al. by bathing a transected and subsequently reconnected mouse ON in a solution containing macrophages incubated with sciatic nerve [112]. Porous conduits have been used in the past to guide axons on a macroscopic scale toward the distal stump and prevent severe axonal branching [113]. Semipermeable acrylic copolymer tubes have been reported to bridge transections of the rabbit optic nerve using entubulization techniques [114]. The use of an electric field for regeneration of the optic nerve has also been investigated [115]. It has been revealed through much experimentation that the environment surrounding the retinal ganglion cell and its axon has been proven to be extremely important for the successful regeneration of the injured ON.

Neural stem cells have extraordinary potential to restore sight after injury to the ON. These cells are capable of long-term survival, migrate in response to injury cues, and are capable of differentiating along multiple CNS neural cell lineages. Stem cells integrate with host cells, will not initiate immune response or grow abnormally leading to tumor formation [72]. Stem cells have been found in the retina and ciliary body of embryonic and adult mice and rats, and human embryos [116]. They can be induced to differentiate into RGCs using the appropriate conditions [116-118]. Transplanted characterized stem cells, such as adult hippocampal-derived neural stem cells, can be grafted back into the retina. Young and colleagues were the first to experiment with transplanting neural stem cells- derived from the adult rat hippocampus- into a diseased retina. In these studies, the researchers found that the neural stem cells morphologically integrated into the eye. They not only migrated to the right place and appear to take on the right characteristics, but they also show signs of trying to connect from the retina to the brain [101]. Kurimoto and colleagues had similar success with the injection of transplanted neural stem cells into retinas injured by transient ischemia [103]. The results of these studies suggest that transplanted neural stem cells can potentially be used as donor cells in cell replacement therapies to repair the damaged optic nerve.

Neural stem cells have the potential to replace dead or damaged RGCS, provide the "enzymatic machinery" to correct metabolic defects, be sources of growth factor delivery to cells, or cellularly "bridge" disconnected cells [72]. The interactive relationship that exists between astrocytes and neural stem cells can provide an extremely permissive environment for regeneration. There is strong evidence that astrocytes, particularly hippocampal astrocytes, provide signals locally that support both neuronal fate commitment of adult neural stem cells and proliferation of neural

progenitors [16]. With the potential of neural stem cells to give rise to progeny that can form multiple cell types, it is possible that differentiation of such cells into RGCs can occur using appropriate growth cues.

2.2.1 Cell guidance: *In vitro* experimentation

Providing a permissive environment for retinal ganglion cells that have suffered trauma is essential for the regeneration of these neurons in the central nervous system. Clearly, retinal ganglion cell axons have the capacity to repair themselves [109, 110, 112, 114]. Regeneration requires stimulating damaged RGCs to extend new axons to appropriate targets in the central nervous system and restoration of a normal retinotopic distribution. These axons must be guided through the optic chiasm and eventually synapse in the correct locations within the brain. In order to generate an environment that supports optic nerve regeneration, biological, physical and chemical manipulations must be made. Guidance cues must be provided that aid in control of nerve outgrowth and navigate neuronal growth cones to distant targets *in vivo*. "Intelligent" substrates combining such cues will provide insight into the mechanisms behind axon growth and regeneration in the optic nerve. These substrates can enhance regeneration and help repair severed or injured neural tissue.

Astrocytes have the potential to provide the external growth factors that a permissive regenerative environment needs. During development, astrocytes play key roles in axon guidance. They are not only influential in the development of axonal pathways but also in the processes of degeneration and regeneration following injury in the CNS. Astrocyte and neuronal interactions can potentially aid in guiding regenerating retinal ganglion axons to central targets within the CNS following injury to the optic nerve. Providing a substrate upon which astrocytes act as biological guidance cues promoting the differentiation of neural stem cells into retinal ganglion cells provides a promising therapeutic strategy for repair of the optic nerve following injury. *In vitro*, it is evident that cells and growth cones have an absolute response to adhesive proteins while they respond to topography in a probabilistic manner [119]. By combining physical and chemical guidance mechanisms, permissive environmental cues can be precisely oriented and regeneration can be achieved.

2.2.1.1 Physical substratum patterning

Substrate topography can have a tremendous effect on cell morphology and behavior.

Topographic guidance is the tendency of cells to be guided in their direction of movement by the shape of the substrate onto which they are attached [120]. The susceptibility of a cell to topography is determined by the organization of the cytoskeleton, cell adhesion, and cell-to-cell interactions [121]. Cellular response to topographical features is thought to be "predictable" on a probabalistic basis. Cells recognize three-dimensional geometric configurations of substrate surfaces. Their growth can be controlled at the cellular level through the fabrication of microgrooves and other patterns on these surfaces [122]. The response of a cell to topography depends on the characteristics of the substrate, including the types, densities and magnitudes of the features, as well as cell type and interactions with surrounding cells [121, 122].

The development of microfabrication and nanofabrication techniques has allowed precise control over patterned features using a variety of materials. Isolating large numbers of individual cells and having control over their shape and distribution is extremely valuable in the analyzing functional changes in individual cells in culture. Substrates with various feature shapes and dimensions result from these techniques involving photolithography and reactive ion etching and can be used to study cell behavior and morphology. In the recent past, our group developed micropatterned biodegradable substrates using microfabrication and transfer patterning techniques [123-125]. Microcontact printing techniques involving elastomeric polydimethylsiloxane (PDMS) stamps have been used to create adhesive islands for the control of cell shape, growth and function [126, 127]. Cell behavior has been studied using such techniques on different substrate materials, including Perspex [119, 121, 122], silicon wafers [128-130], polymers such as polystyrene [131] and biodegradable polymers, including poly(lactide-*co*-glycolide) and poly(DL-lactide)[124, 125], and quartz [132, 133]. The techniques for microfabrication and nanofabrication of non-biodegradable substrates have been well established.

Guidance has been demonstrated using various shapes and feature sizes with several cell types. V-shaped grooves have been used to align fibroblasts and epithelial cells. Rectangular shapes [121, 134] [135], hexagonal [129] as well as circular features [136] have been successful in controlling cellular behavior. The shape and expression of a differentiated phenotype of retinal pigment epithelium (RPE) can be controlled using octadecyltrichlorosilane (OTS)- modified glass micropatterned substrates [136]. Webb et al. [133] demonstrated that rat optic nerve astrocytes aligned on surface features as small as 100 nm depth with 260 nm pattern spacing on quartz discs. The oligodendrocyte lineage displayed a high degree of sensitivity to topography as well [133]. Our group has exhibited Schwann cell and neurite alignment on micropatterned biodegradable

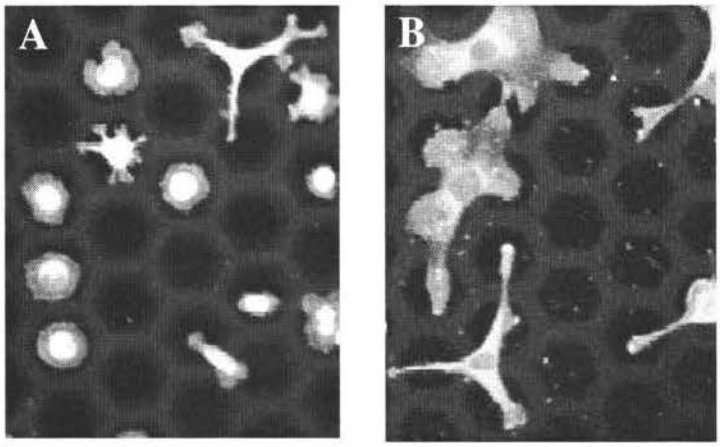

Figure 2-7. Astroglial cells on hexagonal micro-patterned surfaces at (A) 6 hours and (B) 1 day [129].

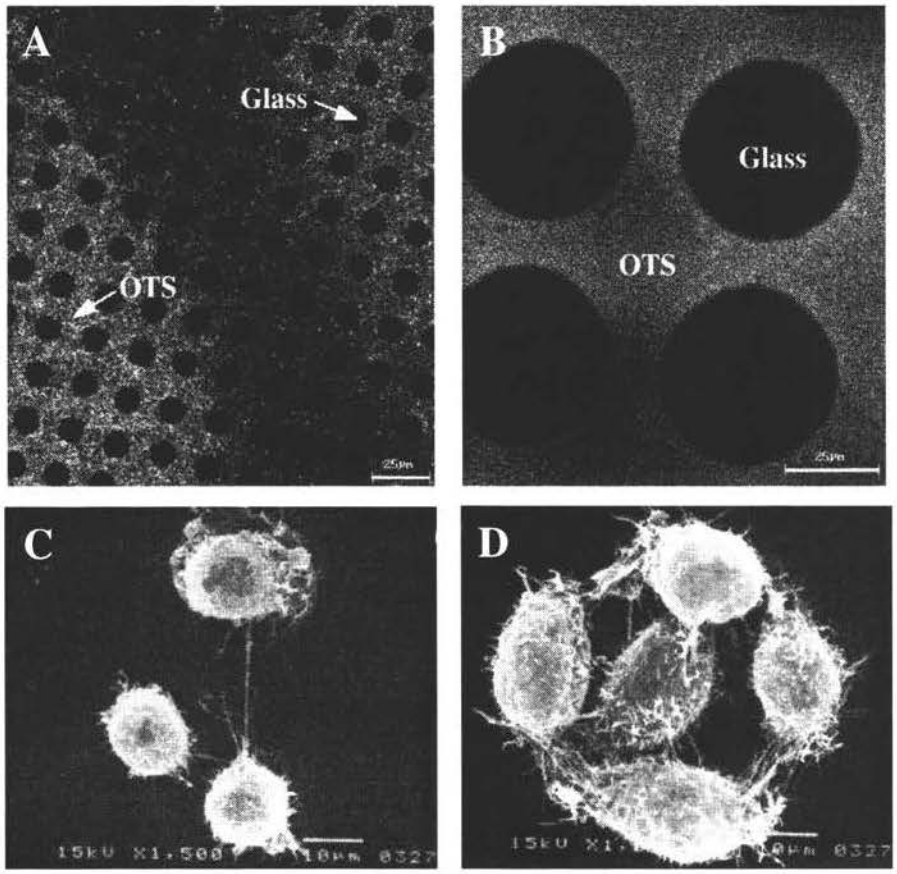

Figure 2-8. (A, B) Fluorescent micrographs of OTS-modified glass surfaces with circular (A) 10 μm and (B) 50 μm diameter features of unmodified glass. Scale bars, 25 μm. (C, D) Scanning electron micrographs of RPE cells adhering to (C) 10 μm and (D) 50 μm diameter circular patterns. Scale bars, 10 μm [136].

substrates. In these studies, groove width had the most influence on cell alignment with groove spacings of 10 to 20 μm being optimal for Schwann cell alignment. There is also evidence that groove depth affects the proportion of neurites aligned. Deeper grooves have a stronger effect on cellular behavior [121-123, 125, 130]. Clark et al. [137] has also studied the interaction between groove depth and spacing. It was reported that the higher the density of topographic cues, the increase in response to the features of a given depth.

Cell processes interact with substrate surfaces in different ways. Studies of fibroblasts [130, 135] and epithelial cells [134] have demonstrated cellular processes exhibiting extensive contact and extending into the grooves of microfabricated surfaces. Meyle et al. [135] observed interaction between cell bodies and surface contours where the shear stress required for detachment of the cell was increased. This led to an explanation for increased cell numbers adhering to rougher surfaces as was seen in prior *in vitro* studies. Interactions between cells in close proximity to each other also affect cell behavior on patterned substrates [121, 138].

Mechanisms of contact guidance have also been studied using microfabrication techniques for the design of patterned substrates. The intracellular distribution of cytoskeletal elements such as microtubules, microfilaments, intermediate filaments, and adhesive structures on cells as they respond to various geometric configurations has been analyzed. Various filaments have exhibited preferential attachment to particular locations on the substrate with time [120]. Astrocytes aligned on micropatterned quartz discs have shown incredible arrangements of actin stress fibers whereas oligodendrocyte-type 2 astrocyte progenitors nor oligodendrocytes showed high order F-actin cytoskeletal networks on the same substrates [133]. It has been suggested that the cytoskeleton is an essential part of the mechanism for topographical guidance for many cells [121, 122, 130, 131, 137].

2.2.1.2 Chemical substratum patterning

Providing an adhesive substrate for cells and neurites to grow on is an important mechanism for guidance. Several studies have been performed using various methods for generating patterns of adhesive domains on various materials. These studies have largely consisted of two-dimensional substrates where adhesive areas are patterned adjacent to nonadhesive areas. However, chemical patterning of three-dimensional substrates has also been demonstrated. Patterning techniques have been used that manipulate surface chemistry and photolithographic techniques. They have involved microstamping hexadecanethiol on gold in a self-assembled monolayer (SAM) creating islands of various shapes that support the adsorption of many proteins [127]. Similar methods have also been

used in the photolithographic patterning of organosilanes to silicon wafers [128, 129], quartz and standard glass [136, 139]. Microfabrication techniques using photolithographic photomasks have aided in the reproducible creation of desired patterns of molecules on substrates of various materials, such as glass coverslips [140]. Several chemicals and proteins have been employed to create regions of two-dimensional patterns of adhesive domains: laminin [140]; nerve growth factor [141]; fibronectin; collagen; albumin; and laminin paired with other chemicals including laminin-denatured laminin, laminin-albumin and laminin-collagen [142]. In the experiments involving multiple, parallel patterns, neurite outgrowth was guided in a similar fashion. Neurons exhibited outgrowth on the adhesive, highly permissive regions in instances where the period of the parallel pattern was wider. On patterns with narrower periods, neurites were observed as bridging nonadhesive regions. In studies involving adhesive islands or microdomains, cell spreading was limited with few cells extending membranes onto nonadhesive areas. These results also suggested that chemical patterning might play a stronger role in inducing cellular response (i.e. attachment, spreading, and alignment) than topography. Furthermore, since the response of cells to physical patterning is probabilistic, efforts have been made to combine the chemical and physical cues by chemical patterning of three-dimensional substrates[124, 125].

Relative adhesivity of different chemically modified substrates has also been studied using patterned substrates [143, 144]. Cells have been examined on the following patterns: protein (or polylysine) and glass; protein (or polylysine) and amine; and amine or alkane [145]. In these experiments it was observed that different cells preferred different adhesive substrates [146]. Relative adhesiveness was not a good predictor of the rate of axon growth or degree of axon fasciculation [144]. The results also suggested that certain adhesion molecules acting as permissive substrates can define pathways for growth, but information on pathway navigation is not provided [144].

The concentration of the adhesive protein applied to a substrate has been observed as affecting the guidance effect of the substrate. Neurite guidance on the laminin regions, as measured by percentage of neurite length on the protein pathway and number of growth cones, was improved by increasing the concentration of laminin [147]. However, large increases in laminin concentration, however, demonstrated little effect on neurite outgrowth [148]. The migration of growth cones was slowed by increased interactions between substrate boundaries and the growth cone [140]. These results suggest that laminin serves as a permissive substrate rather than instructive substrate [144, 148].

Evidence has been presented that laminin provides pathways of adhesiveness in both peripheral and central nervous system tissues [149]. It has been reported that *in vitro* laminin is a potent neurite-promoting factor for PNS and CNS neurons [150]. This ECM protein is capable of initiating and supporting neurite extension [139]. The projection from the retina to the optic tectum has been shown to be a preformed pathway consisting of both neural cell adhesion molecule (NCAM) [151] and laminin [152]. However, it has been observed that laminin is not as abundant in the CNS as it is in the PNS [150]. It is possible, therefore, that the availability of laminin in the CNS may have a role in axonal regeneration. Combining chemical patterning techniques using laminin and other ECM molecules with other guidance mechanisms such as physical patterning leads to the creation of permissive substrates for *in vitro* experimentation into the regenerative potential of the optic nerve, and ultimately, the central nervous system as a whole. Using this approach, we are transferring patterns of micron scale dimensions onto synthetic polymers and chemically modifying them with laminin to demonstrate the successful, guided alignment of cortical astrocytes on micropatterned polystyrene substrates.

References Cited

1. Kandel, E.R., J.H. Schwartz, and T.M. Jessell, *Essentials of Neural Science and Behavior.* 1995, Norwalk, CT: Appleton and Lange.
2. Greenstein, B. and A. Greenstein, *Color Atlas of Neuroscience.* 2000, New York, NY: Thieme.
3. Pannese, E., *Neurocytology: fine structure of neurons, nerve proceses and neuroglial cells.* 1994, New York: Stuttgart; New York: G. Thieme Verlag; New York: Thieme Medical Publishers.
4. Gould, J. and W. Keeton, *Biological Science.* 1996, New York, NY: W.W. Norton & Company, Inc.
5. Raff, M.C., *Glial Cell Diversification in the Rat Optic Nerve.* Science, 1989. **243**: p. 1450-1455.
6. Ventura, R. and K.M. Harris, *Three-dimensional relationships between hippocampal synapses and astrocytes.* Journal of Neuroscience, 1999. **19**: p. 6897-6906.
7. Haydon, P., *GLIA: listening and talking to the synapse.* Nature Reviews Neuroscience, 2001. **2**: p. 185-93.
8. Antanitus, D.S., *A Theory of Cortical Neuron-Astrocyte Interaction.* 1998.
9. Raff, M.C., et al., *Two types of astrocytes in cultures of developing rat white matter: differences in morphology, surface gangliosides, and growth characteristics.* Journal of Neuroscience, 1983a. **3**: p. 1289-1300.
10. Miller, R.H., et al., *A quantitative immunohistochemical study of macroglial cell development in the rat optic nerve: in vivo evidence for two distinct astrocyte lineages.* Developmental Biology, 1985. **111**(1): p. 35-41.
11. Levi, G., V. Gallo, and M.T. Ciotti, *Bipotential precursors of putative fibrous astrocytes and oligodendrocytes in rat cerebellar cultures express distinct surface features and "neuron-like" gamma-aminobutyric acid transport.* Proceedings of the Natl Academy of Sciences, USA, 1986. **83**: p. 1504-1508.
12. Goldman, J.E., S.S. Geier, and M. Hirano, *Differentiation of astrocytes and oligodendrocytes from germinal matrix cells in primary culture.* Journal of Neuroscience, 1986. **6**: p. 52-60.
13. LoTurco, J., *Neural circuits in the 21st century: Synaptic networks of neurons and glia.* Proceedings of the Natl Academy of Sciences, USA, 2000. **97**(15): p. 8196-8197.
14. Manthorpe, M.B., B. Pettman, and S. Varon, *Modulation of astroglial cell output of neuronotrophic and neurite promoting factors*, in *The Biochemical Pathology of Astrocytes*, L.H. M.D. Norenberg, and A. Schousboe, Editor. 1988, Alan R. Liss: New York. p. 41-58.
15. Rakic, P., *Principles of neural migration.* Experimentia, 1990. **46**: p. 882-891.
16. Song, H., C. Stevens, and F. Gage, *Astroglia induce neurogenesis from adult neural stem cells.* Nature, 2002. **417**: p. 39-44.
17. McCarthy, K.D. and J. DeVellis, *Alpha-adrenergic receptor modulation of beta-adrenergic, adenosine, and prostaglandin E_1 increased adenosine 3':5'-cyclic monophosphate levels in primary culture of glia.* J. Cyclic Nucleotide Research, 1978. **4**: p. 15-26.
18. Friedl, A.C., et al., *Rat atrial natriuretic peptide elevates the level of cyclic GMP in astroglia-rich brain cell cultures.* Eur. J. Pharmacolgy, 1985. **111**: p. 141-142.
19. Salm, A.K., et al., *Distinct subsets of astroglia can be defined by their expression of neuroligand receptors that regulate intracellular calcium levels*, in *Differentiation and Functions of Glial Cells*, G. Levi, Editor. 1990, Alan R. Liss: New York, NY. p. 275-288.
20. Barres, B., *Ion channels in vertebrate glia.* Annual Review of Neuroscience, 1990. **13**: p. 441-474.

21. Bevan, S. and M.C. Raff, *Voltage-dependent potassium currents in cultured astrocytes.* Nature, 1985. **315**: p. 229-232.
22. Kimelberg, H.K. and D.M. Katz, *High-affinity uptake of serotonin into immunocytochemically identified astrocytes.* Science, 1985. **228**: p. 889-891.
23. Wilkin , G.P., D. Marriott, and B. Pearce, *Peptide receptors on astrocytes*, in *Neuroglia*, B.R. Ransom, Editor. 1995, Oxford University Press: New York, NY.
24. Cornell Bell, A.H., et al., *Glutamate induces calcium waves in cultured astrocytes: long-range glial signaling.* Science, 1990. **247**: p. 470-473.
25. Duffy, S. and B.A. MacVicar, *Adrenergic calcium signaling in astrocyte networks within the hippocampal slice.* Journal of Neuroscience, 1995. **15**: p. 5535-5550.
26. Shelton, M.K. and K.D. McCarthy, *Hippocampal astrocytes exhibit Ca^{2+}-elevating muscarinic, cholinergic, and histaminergic receptors in situ.* Journal of Neurochemistry, 2000. **74**: p. 555-563.
27. Wang, Z., P.G. Haydon, and E.S. Yeung, *Direct observation of calcium-independent intracellular ATP signaling in astrocytes.* Analytical Chemistry, 2000. **72**: p. 2000-2007.
28. Guthrie, P.B. and *e. al., ATP released from astrocytes mediates glial calcium waves.* Journal of Neuroscience, 1999. **19**: p. 520-528.
29. Kang, J., et al., *Astrocyte-mediated potentiation of inhibitory synaptic transmission.* Nature Neuroscience, 1998. **1**: p. 683-692.
30. Nedergaard, M., *Direct signaling from astrocytes to neurons in cultures of mammalian cells.* Science, 1994. **263**: p. 1768-1771.
31. Parpura, V., et al., *Glutamate-mediated astrocyte-neuron signaling.* Nature, 1994. **369**: p. 744-747.
32. Parpura, V. and P.G. Haydon, *Physiological astrocytic calcium levels stimulate glutamate release to modulate adjacent neurons.* Proceedings of the Natl Academy of Sciences, USA, 2000. **97**: p. 8629-8634.
33. Cotrina, M.L.e.a., *Connexins regulate calcium signaling by controlling ATP release.* Proceedings of the Natl Academy of Sciences, USA, 1998. **95**: p. 15735-15740.
34. Brenneman, D.E., et al., *VIP and D-alanine peptide T-amide release chemokines which prevent HIV-1 GP120-induced neuronal death.* Brain Research, 1999a. **838**: p. 27-36.
35. Zafra, F., et al., *Regulation of brain-derived neurotrophic factor and nerve growth factor mRNA in primary cultures of hippocampal neurons and astrocytes.* Journal of Neuroscience, 1992. **12**: p. 4793-4799.
36. Noble, M. and K. Murray, *Purified astrocytes promote the in vitro division of a bipotential glial progenitor cell.* EMBO J., 1984. **3**: p. 2243-2247.
37. Noble, M., et al., *Platelet-derived growth factor promotes division and motility and inhibits premature differentiation of the oligodendrocyte/type-2 astrocyte progenitor cell.* Nature, 1988. **333**: p. 560-562.
38. Richardson, W.D., et al., *A role for platelet-derived growth factor in gliogenesis in the central nervous system.* Cell, 1988. **53**: p. 309-319.
39. Lillien, L.E., et al., *Type-2 astrocyte development in rat brain cultures initiated by a CNTF-like protein produced by type-1 astrocytes.* Neuron, 1988. **1**: p. 485-494.
40. Liesi, P., D. Dahl, and A. Vaheri, *Neurons cultured from developing rat brain attach and spread preferentially on laminin.* Journal of Neuroscience Research, 1983. **11**: p. 241-251.
41. Snow, D.M., et al., *A chondroitin sulfate proteoglycan may influence the direction of retinal ganglion cell outgrowth.* Development, 1991. **113**: p. 1473-1485.
42. Banker, G., *Trophic Interactions between Astroglial Cells and Hippocampal Neurons in Culture.* Science, 1980. **209**: p. 809-810.

43. Monard, D., et al., *Glia-Induced Morphological Differentiation in Neuroblastoma Cells.* Proceedings of the Natl Academy of Sciences, USA, 1973. **70**(6): p. 1894-1897.
44. Faissner, A., *Tenascin glycoproteins in neural pattern formation: facets of a complex picture.* Perspectives in Developmental Biology, 1993. **1**(3): p. 155-64.
45. Araque, A., et al., *Glutamate-dependent astrocyte modulation of synaptic transmission between cultured hippocampal neurons.* Eur. J. Neuroscience, 1998. **10**: p. 2129-2142.
46. Powell, E., et al., *Mechanisms of astrocyte-directed neurite guidance.* Cell and Tissue Research, 1997. **290**: p. 385-393.
47. Pfrieger, F.W. and B.A. Barres, *Synaptic efficiency enhanced by glial cells in vitro.* Science, 1997. **277**: p. 1684-1687.
48. Ullian, E.M., et al., *Control of Synapse Number by Glia.* Science, 2001. **291**: p. 657-660.
49. Nagler, K., D.H. Mauch, and F.W. Pfrieger, *Glia-derived signals induce synapse formation in neurones of the rat central nervous system.* Journal of Physiology, 2001. **533**(Pt 3): p. 665-79.
50. Mauch, D.H., et al., *CNS synaptogenesis promoted by glia-derived cholesterol.* Science, 2001. **294**(5545): p. 1354-7.
51. Blondel, O., et al., *A glia-derived signal regulating neuronal differentiation.* Journal of Neuroscience, 2000. **20**(21): p. 8012-20.
52. Araque, A., et al., *Tripartite synapses: glia, the unacknowledged partner.* Trends in Neurosciences, 1999. **22**: p. 208-215.
53. Ransom, B.R. and R. Orkand, *Glial-neuronal interactions in non-synaptic areas of the brain: studies in the optic nerve.* Trends in Neurosciences, 1996. **19**(8): p. 352-58.
54. Kolb, H., E. Fernandez, and R. Nelson, *Webvision: http://webvision.med.utah.edu*. 2002, University of Utah.
55. Steindler, D., A. Faissner, and M. Schachner, *"Brain cordones": glial and adhesion molecule transient boundaries define developing functional units.* Comments Developmental Neurobiology, 1989b. **1**: p. 29-60.
56. McKeon, R.J. and J. Silver, *Functional significance of glial-derived matrix during development and regeneration*, in *Neuroglia*, H. Kettenmann and B.R. Ransom, Editors. 1995, Oxford University Press: New York, NY.
57. Smith, G., et al., *Maturation of astrocytes in vitro alters the extent and molecular basis of neurite outgrowth.* Developmental Biology, 1990. **138**: p. 377-390.
58. Brittis, P.A., D.R. Canning, and J. Silver, *Chondroitin sulfate as a regulator of neuronal patterning in the retina.* Science, 1992. **255**: p. 733-736.
59. Labourdette, G. and M. Sensenbrenner, *Growth factors and their receptors in the central nervous system*, in *Neuroglia*, H. Kettenmann and B.R. Ransom, Editors. 1995, Oxford University Press: New York, NY.
60. Mizuno, T., M. Sawada, and A. Suzumura, *Expression of cytokines during glial differentiation.* Brain Research, 1994. **656**: p. 141-146.
61. Sanes, J., *Extracellular matrix molecules that influence neural development.* Annual Review of Neuroscience, 1989. **12**: p. 491-516.
62. Letourneau, P., M. Condic, and D. Snow, *Interactions of developing neurons with the extracellular matrix.* Journal of Neuroscience, 1994. **14**: p. 915-928.
63. Steindler, D., et al., *Boundaries during normal and abnormal brain development: in vivo and in vitro studies of glia and glycoconjugates.* Experimental Neurology, 1990. **109**: p. 35-56.
64. Hatten, M., *Astroglia in CNS injury.* Glia, 1991. **4**(2): p. 233-43.
65. Ridet, J.L., et al., *Reactive astrocytes:cellular and molecular cues to biological function.* Trends in Neurosciences, 1997. **20**(12): p. 570-577.

66. Omlin, F.X. and J. Waldmeyer, *Differentiation of neuron-like cells in cultured rat optic nerves: a neuron or common neuron-glia progenitor?* Developmental Biology, 1989. **133**(1): p. 247-53.
67. Wolswijk, G. and M. Noble, *Identification of adult-specific glial progenitor cell.* Development, 1989. **105**: p. 387-400.
68. Raff, M., S. Temple, and C. Ffrench-Constant, *Glial cell development and function in the rat optic nerve.* Progress in Brain Research, 1987. **71**: p. 435-438.
69. Horner, P.J. and F.H. Gage, *Regenerating the damaged central nervous system.* Nature, 2000. **407**: p. 963-970.
70. Bjorklund, A. and O. Lindvall, *Cell replacement therapies for central nervous system disorders.* Nature Neuroscience, 2000. **3**: p. 537-544.
71. Stuermer, C.A.O., *Glial cells and axonal regeneration in the central nervous system*, in *Neuroglia*, H. Kettenmann and B.R. Ransom, Editors. 1996, Oxford University Press: New York, NY. p. 905-915.
72. Miller, N., *Optic Nerve Protection, Regeneration, and Repair in the 21st Century: LVIII Edward Jackson Memorial Lecture.* American Journal of Ophthalmology, 2001. **132**(6): p. 811-819.
73. Cajal, S.R., *Traumatic degeneration and regeneration of the optic nerve and retina.*, in *Degeneration and regeneration of the central nervous system.*, R. May, Editor. 1928, Hafner: New, York, NY. p. 583-596.
74. Richardson, P.M., I. V.M.K., and S. S., *Regeneration and retrograde degeneration of axons in the rat optic nerve.* Journal of Neurocytology, 1982. **11**: p. 949-966.
75. Thanos, S. and H. Thiel, *Mechanisms governing neuronal degeneration and axonal regeneration in the mature retinofugal system.* Journal of Cell Science, 1991. **15**: p. 125-134.
76. Berkelaar, M., et al., *Axotomy results in delayed death and apoptosis of retinal ganglion cells in adult rats.* Journal of Neuroscience, 1994. **14**: p. 4368-4374.
77. Garcia-Valenzuela, E., et al., *Apoptosis in adult retinal ganglion cells after axotomy.* Journal of Neurobiology, 1994. **25**: p. 431-438.
78. Thanos, S., *The relationship of microglial cells to dying neurons during natural neuronal cell death and axotomy-induced degeneration of the rat retina.* European Journal of Neuroscience, 1991. **3**: p. 1189-1207.
79. MacLaren, R.E., *Regeneration and Transplantation of the Optic Nerve: Developing a Clinical Strategy.* British Journal of Ophthalmology, 1998. **82**: p. 577-583.
80. Chierzi, S. and J. Fawcett, *Regeneration in the mammalian optic nerve.* Restorative Neurology and Neuroscience, 2001. **19**: p. 109-118.
81. Fawcett, J., J. Rokos, and I. Bakst, *Oligodendrocytes repel axons and cause growth cone collapse.* J Cell Science, 1989. **92**: p. 93-100.
82. Caroni, P. and M. Schwab, *Two membrane protein fractions from rat central myelin with inhibitory properties for neurite growth and fibroblast spreading.* J Cell Biology, 1988. **106**: p. 1281-1288.
83. McConnell, P. and M. Berry, *Regeneration of retinal ganglion cells in the adult mouse retina.* Brain Research, 1982. **241**: p. 362-365.
84. Schnell, L., R. Schneider, and R. Kolbeck, *et al., Neurotrophin-3 enhances sprouting of corticospinal tract during development and after adult spinal cord lesion.* Nature, 1994. **367**: p. 170-173.
85. Wiebel, D., G. Kreutzberg, and M. Schwab, *Brain-derived neurotrophic factor (BDNF) prevents lesion-induced axonal die-back in young rat optic nerve.* Brain Research, 1995. **679**: p. 249-254.

86. Wong, E.V., et al., *Inactivation of myelin-associated glycoprotein enhances optic nerve regeneration.* Journal of Neuroscience, 2003. **23**(8): p. 3112-3117.
87. Canning, D., et al., *A potent inhibitor of neurite outgrowth that predominates in the extracellular matrix of reactive astrocytes.* Int J Developmental Neuroscience, 1996. **14**: p. 153-175.
88. MacLaren, R.E. and J.S.H. Taylor, *Regeneration in the Developing Optic Nerve: Correlating Observations in the Opossum to Other Mammalian Systems.* Progress in Neurobiology, 1997. **53**: p. 381-98.
89. MacLaren, R.E., *Development and role of retinal glia in regeneration of ganglion cells following retinal injury.* Br J Opthalmology, 1996. **80**: p. 458-464.
90. Baehr, M. and R.P. Bunge, *Functional status influences the ability of Schwann cells to support adult rat retinal ganglion cell survival and axonal regrowth.* Experimental Neurology, 1989. **106**(1): p. 27-40.
91. Baehr, M. and R.P. Bunge, *Growth of adult rat retinal ganglion cell neurites on astrocytes.* Glia, 1990. **3**(4): p. 293-300.
92. MacLaren, R.E. and J.S.H. Taylor, *Chiasmatic specificity on the regenerating mammalian optic nerve.* Exp. Neurology, 1997. **147**: p. 279-286.
93. Temple, S., *The development of neural stem cells.* Nature, 2001. **414**: p. 112-117.
94. Lowenstein, D.H. and J.M. Parent, *Brain, Heal Thyself.* Science, 1999. **283**: p. 1126-7.
95. Gage, F.H., J. Ray, and L.J. Fisher, *Isolation, characterization, and use of stem cells from the CNS.* Annual Review of Neuroscience, 1995. **18**: p. 159-192.
96. McKay, R., *Stem cells in the central nervous system.* Science, 1997. **276**: p. 66-71.
97. Palmer, T.D., J. Ray, and F.H. Gage, *FGF-2 responsive neuronal progenitors reside in proliferative and quiescent regions of the adult rodent brain.* Molecular and Cellular Neurosciences, 1995. **6**(5): p. 474-486.
98. Palmer, T.D., et al., *Fibroblast Growth Factor-2 Activates a Latent Neurogenic Program in Neural Stem Cells from Diverse Regions of the Adult CNS.* The Journal of Neuroscience, 1999. **19**(19): p. 8487-8497.
99. Gage, F.H., et al., *Survival and differentiation of adult neural progenitor cells transplanted to the adult brain.* Proceedings of the Natl Academy of Sciences, USA, 1995.
100. Song, H., C. F. Stevens, and F.H. Gage, *Neural stem cells from adult hippocampus develop essential properties of functional CNS neurons.* Nature Neuroscience, 2002. **5**(5): p. 438-45.
101. Young, M.J., et al., *Neuronal differentiation and morphological integration of hippocampal progenitor cells transplanted to the retina of immature and mature dystrophic rats.* Molecular and Cellular Neuroscience, 2000. **16**(3): p. 197-205.
102. Takahashi, M., et al., *Widespread integration and survival of adult neural progenitor cells in the developing retina.* Molecular and Cellular Neuroscience, 1998. **12**: p. 340-48.
103. Kurimoto, Y., et al., *Transplantation of Adult Rat Hippocampus-Derived Neural Stem Cells into Retina Injured by Transient Ischemia.* Neuroscience Letters, 2001. **306**: p. 57-60.
104. Van Hoffelen, S.J., et al., *Incorporation of murine brain progenitor cells into the developing mammalian retina.* Investigative Ophthalmology and Visual Science, 2003. **44**(1): p. 426-34.
105. Lim, D.A. and A. Alvarez-Buylla, *Interaction between astrocytes and adult subventricular zone precursors stimulate neurogenesis.* Proceedings of the Natl Academy Sciences, USA, 1999. **96**: p. 7526-7531.
106. Alonso, G., *Proliferation of Progenitor Cells in the Adult Rat Brian Correlates With the Presence of Vimentin-Expressing Astrocytes.* Glia, 2001. **34**: p. 253-266.
107. MacLaren, R.E. and J.S.H. Taylor, *A critical period for axon regrowth through a lesion in the developing mammalian retina.* European Journal of Neuroscience, 1995. **10**: p. 2111-2118.

108. Negishi, H., et al., *Optic nerve regeneration within artificial Schwann cell graft in the adult rat.* Brain Research Bulletin, 2001. **55**(3): p. 409-419.
109. So, K.F. and A.J. Agauyo, *Lengthy regrowth of cut axons from ganglion cells after peripheral nerve transplantation into the retina of adult rats.* Brain Research, 1985. **328**: p. 349-354.
110. Vidal-Sanz, M., et al., *Axonal regeneration and synapse formation in the superior colliculus by retinal ganglion cells in the adult rat.* The Journal of Neuroscience, 1987. **7**: p. 2894-2909.
111. Villegas-Perez, M.P., et al., *Influences of peripheral nerve grafts on the survival and regrowth of axotomized retinal ganglion cells in adult rats.* Journal of Neuroscience, 1988. **8**(1): p. 265-80.
112. Lazarov-Spiegler, O., et al., *Transplantation of activated macrophages overcomes central nervous system regrowth failure.* FASEB Journal, 1996. **10**: p. 1296-1302.
113. Dubey, N., P.C. Letourneau, and R.T. Tranquillo, *Guided Neurite Elongation and Schwann Cell Invasion into Magnetically Aligned Collagen in Simulated Peripheral Nerve Regeneration.* Experimental Neurology, 1999. **158**(2): p. 338-350.
114. Aebischer, P., et al., *The use of a semi-permeable guidance channel for a transected rabbit optic nerve.* Brain Research, 1988. **78**(599-603).
115. Politis, M., M. Zanakis, and B. Albala, *Mammalian Optic-Nerve Regeneration Following Application of Electric Fields.* Journal of Trauma, 1988. **28**: p. 1548-1552.
116. Ahmad, I., L. Tang, and H. Pham, *Identification of neural progenitors in the adult mammalian eye.* Biochem Biophys Res Commun, 2000. **270**: p. 517-521.
117. Ge, J., et al., *Preliminary study on in vitro induced differentiation of embryonic stem cells into neurons.* Eye Science, 2000. **16**: p. 1-6.
118. Tropepe, V., et al., *Retinal Stem Cells in the Adult Mammalian Eye.* Science, 2000. **287**: p. 2032-2036.
119. Clark, P., *Cell and neuron growth cone behavior on micropatterned surfaces*, in *Nanofabrication and biosystems: Integrating materials, science, engineering, and biology*, H.C. Hoch, L.W. Jelinski, and H.G. Craighead, Editors. 1996, Cambridge University Press: New York, NY. p. 356-366.
120. Brunette, D.M., *Effects of surface topography of implant materials on cell behavior in vitro and in vivo*, in *Nanofabrication and biosystems: Integrating materials, science, engineering, and biology*, H.C. Hoch, L.W. Jelinski, and H.G. Craighead, Editors. 1996, Cambridge University Press: New York, NY. p. 335-355.
121. Clark, P., et al., *Topographical control of cell behaviour:II. Multiple grooved substrata.* Development, 1990. **108**: p. 635-644.
122. Clark, P., et al., *Topographical control of cell behaviour. I. Simple step cues.* Development, 1987. **99**: p. 439-448.
123. Miller, C., S. Jeftinija, and S. Mallapragada, *Synergistic effects of physical and chemical guidance cues on neurite alignment and outgrowth on biodegradable polymer substrates.* Tissue Engineering, 2002. **8**(3): p. 367-378.
124. Miller, C.A., S. Jeftinija, and S.K. Mallapragada, *Micropatterned Schwann Cell-Seeded Polymer Substrates Significantly Enhance Neurite Alignment and Outgrowth.* Tissue Engineering, 2001. **7**: p. 705-715.
125. Miller, C.A., et al., *Oriented Schwann cell growth on micropatterned biodegradable polymer substrates.* Biomaterials, 2001. **22**: p. 1263-1269.
126. Chen, C., et al., *Geometric Control of Life and Death.* Science, 1997. **276**: p. 1425-1428.
127. Singhvi, R., et al., *Engineering Cell Shape and Function.* Science, 1994. **264**: p. 696-698.
128. Kleinfeld, D., K. Kahler, and P. Hockberger, *Controlled Outgrowth of Dissociated Neurons on Patterned Substrates.* Journal of Neuroscience, 1988. **8**(11): p. 4098-4120.

129. Kam, L., et al., *Correlation of astroglial cell function on micropatterned surfaces with specific geometric parameters.* Biomaterials, 1999. **20**(23/24): p. 2343-2350.
130. Brunette, D.M., *Fibroblasts on micromachined substrata orient hierarchically to grooves of different dimensions.* Experimental Cell Research, 1986. **164**(1): p. 11-26.
131. Ohara, P.T. and R.C. Buck, *Contact guidance in vitro. A light, transmission, and scanning electron microscopic study.* Experimental Cell Research, 1979. **121**(2): p. 235-49.
132. Kawana, A., *Formation of a simple model brain on microfabricated electrode arrays*, in *Nanofabrication and biosystems: Integrating materials, science, engineering, and biology*, H.C. Hoch, L.W. Jelinski, and H.G. Craighead, Editors. 1996, Cambridge University Press: New York, NY. p. 258-275.
133. Webb, A., et al., *Guidance of oligodendrocytes and their progenitors by substratum topography.* Journal of Cell Science, 1995. **108**(8): p. 2747-2760.
134. Brunette, D.M., *Spreading and orientation of epithelial cells on grooved substrata.* Experimental Cell Research, 1986. **167**(1): p. 203-17.
135. Meyle, J., et al., *Fibroblast anchorage to microtextured surfaces.* Journal of Biomedical Materials Research, 1993. **27**(12): p. 1553-7.
136. Lu, L., et al., *Retinal pigment epithelial cell function on substrates with chemically micropatterned surfaces.* Biomaterials, 1999. **20**(23/24): p. 2351-2361.
137. Clark, P., et al., *Cell guidance by ultrafine topography in vitro.* Journal of Cell Science, 1991. **99 (Pt 1)**: p. 73-7.
138. Lu, L., et al., *Retinal pigment epithelial cell adhesion on novel micropatterned surfaces fabricated from synthetic biodegradable polymers.* Biomaterials, 2000. **22**(3): p. 291-297.
139. Clark, P., S. Britland, and P. Connolly, *Growth cone guidance and neuron morphology on micropatterned laminin surfaces.* Journal of Cell Science, 1993. **105**(1): p. 203-12.
140. Tai, H.C. and H.M. Buettner, *Neurite outgrowth and growth cone morphology on micropatterned surfaces.* Biotechnology Progress, 1998. **14**(3): p. 364-70.
141. Gundersen, R.W., *Sensory neurite growth cone guidance by substrate adsorbed nerve growth factor.* Journal of Neuroscience Research, 1985. **13**(1-2): p. 199-212.
142. Buettner, H.M., *Microcontrol of neuronal outgrowth*, in *Nanofabrication and biosystems: Integrating materials, science, engineering, and biology*, H.C. Hoch, L.W. Jelinski, and H.G. Craighead, Editors. 1996, Cambridge University Press: New York, NY. p. 300-314.
143. Lom, B., K. Healy, and P. Hockberger, *A versatile technique for patterning biomaterials onto glass substrates.* Journal of Neuroscience Methods, 1993. **50**: p. 385-397.
144. Lemmon, V., et al., *Neurite growth on different substrates: permissive vs. instructive influences on the role of adhesive strengths.* Journal of Neuroscience, 1992. **12**: p. 818-826.
145. Hockberger, P., et al., *Cellular engineering: control of cell-substrate interactions*, in *Nanofabrication and biosystems: Integrating materials, science, engineering, and biology*, H.C. Hoch, L.W. Jelinski, and H.G. Craighead, Editors. 1996, Cambridge University Press: New York, NY. p. 276-299.
146. Lom, B. and P. Hockberger, *Laminin-1 is non-preferred and anti-adhesive for developing cerebellar cells.* Society of Neuroscience Abstracts, 1995. **21**: p. 1037.
147. Hammarback, J.A., et al., *Growth cone guidance by substrate-bound laminin pathways is correlated with neuron-to-pathway adhesivity.* Developmental Biology, 1988. **126**(1): p. 29-39.
148. Buettner, H.M. and R.N. Pittman, *Quantitative effects of laminin concentration on neurite outgrowth in vitro.* Developmental Biology, 1991. **145**(2): p. 266-76.
149. Letourneau, P.C., et al., *Immunoreactivity for laminin in the developing ventral longitudinal pathway of the brain.* Developmental Biology, 1988. **125**(1): p. 135-44.

150. Manthorpe, M., et al., *Laminin promotes neuritic regeneration from cultured peripheral and central neurons.* Journal of Cell Biology, 1983. **97**(6): p. 1882-90.
151. Silver, J. and U. Rutishauser, *Guidance of optic axons in vivo by a preformed adhesive pathway on neuroepithelial endfeet.* Developmental Biology, 1984. **106**(2): p. 485-99.
152. Cohen, J., et al., *The role of laminin and the laminin/fibronectin receptor complex in the outgrowth of retinal ganglion cell axons.* Developmental Biology, 1987. **122**(2): p. 407-18.

3. MATERIALS AND METHODS

3.1 Materials

3.1.1 Polystyrene substrates

The polymer used to construct the micropatterned substrates was polystyrene (PS). PS is a hard, rigid transparent plastic with good dimensional stability. PS has a specific gravity of 1.04 g/ml and a glass transition temperature (T_g) of 100 °C -105 °C. Atactic polystyrene is highly amorphous. It is soluble in organic solvents including toluene and acetone. Polystyrene atatic beads (Polysciences, Inc., Warrington, PA) with molecular weight range of 125,000 to 250,000 were dissolved in toluene to make 7-10 % solutions (w/v) used in the solvent casting of the PS films.

3.1.2 Materials for cell culturing and processing

All substances used for cell culture and processing are listed in the Appendix. The primary and secondary antibodies used for immunocytochemical procedures are also listed in the Appendix.

3.2 Methods

3.2.1 Silicon wafer fabrication

Conventional photolithographic techniques were used to prepare silicon wafers having desired micropatterns. These micropatterns were then transferred to the polymer substrates. The fabrication of the silicon microdies began by producing a chrome lithographic photomask. This mask served as a template to produce desired geometric patterns on a silicon wafer (Figure 3-1). The pattern the mask generates on the silicon wafer protects sections of the silicon while it is being etched. Following the creation of a photomask, the silicon microdies were created using a process that included surface preparation, metal deposition, photolithography and etching.

The surfaces of four-inch diameter silicon wafers were cleaned using the following procedure. To remove any unwanted substances the silicon wafers were exposed to a 5 minute acetone bath, a 1 minute methanol bath, a 3 minute de-ionized (DI) water bath and finally an RCA clean (standard clean). After the silicon wafers were dried, they were placed in the electron beam

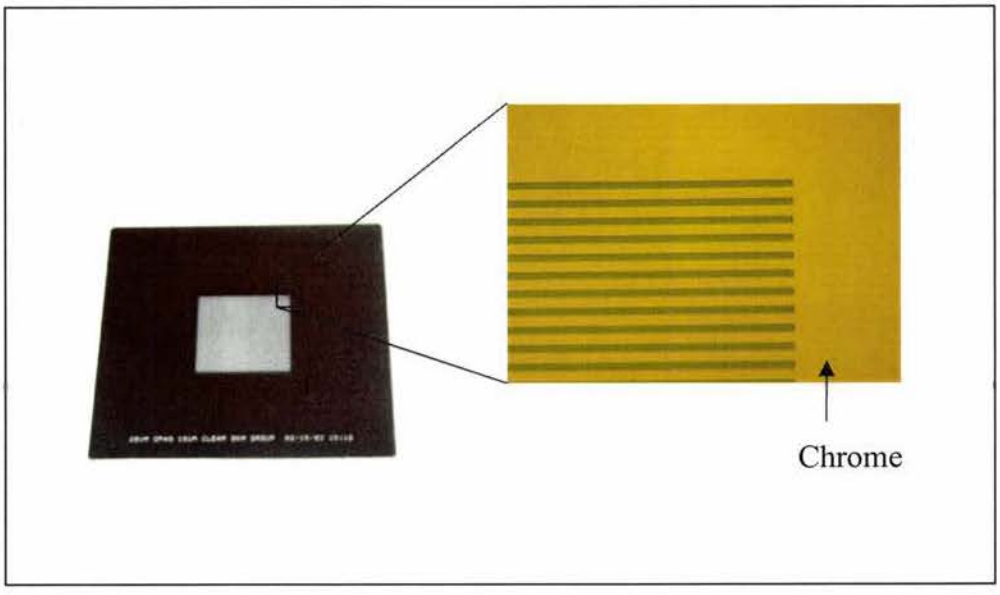

Figure 3-1. Glass mask patterned with chrome used for generating desired patterns on a silicon wafer using photolithographic techniques.

evaporator for chrome deposition. This metal deposition was performed under an ultra-high vacuum in a chamber purged with nitrogen at a pressure of less than 1μTorr. A focused electron beam bombards a cup of metallic chrome with electrons causing the chrome to sublimate and deposit on the surface of the silicon wafer. After 1 kÅ of chrome was deposited, the wafers were removed from the evaporator (Figure 3-2 - Step 1).

The silicon wafers were spin-coated with AZ 5209E positive photoresist (Clariant, Somerville, NJ) (Figure 3-2 - Step 2) and prebaked at 100°C for 1 minute on a hotplate. After the wafers cooled, they were placed onto a mask aligner and the photoresist was exposed to ultra-violet radiation through a patterned photomask (Figure 3-2 - Step 3). The exposed wafers were placed in AZ 312 MIF developer (Clariant, Somerville, NJ), a commercial photoresist etchant, for 60 seconds to etch the exposed photoresist (Figure 3-2 - Step 4). Since the photoresist is positive photoresist, the regions exposed to UV light were rendered soluble in the developer solution (Figure 3-2 - Step 5). The wafers were then rinsed in DI water, sprayed dry with nitrogen and postbaked at 120°C for 25 minutes to harden the resist.

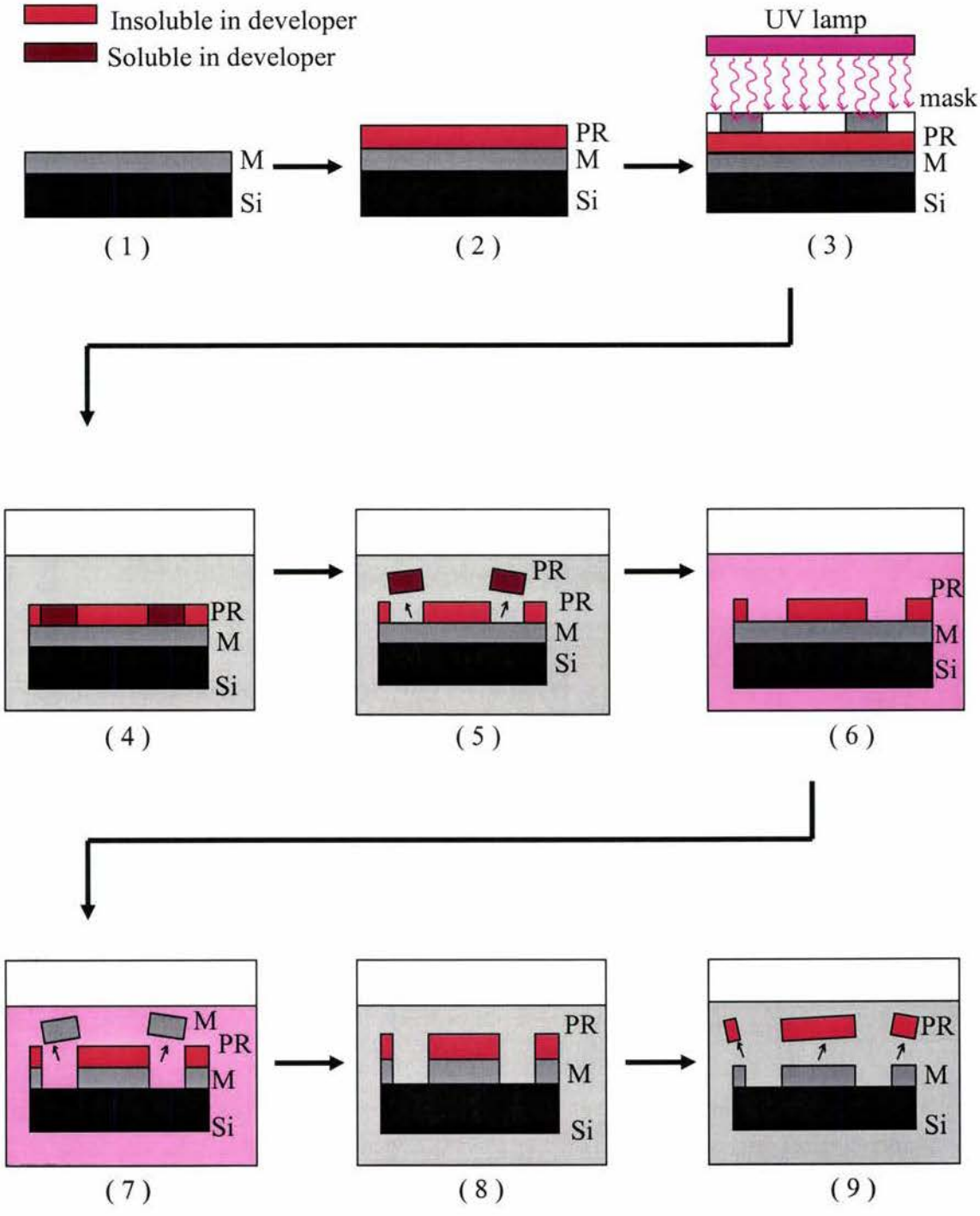

Figure 3-2. The steps in the photolithography process following the creation of a photomask and surface preparation of the silicon wafers. These photolithographic techniques allow the preparation of silicon wafers having desired micropatterns. PR = photoresist, M= metal, Si = Silicon Wafer.

After the photolithography was complete, the silicon wafers covered with patterned photoresist were immersed in CR4 commercial chrome etch (82% water, 9% nitric acid and 9% ceric ammonium nitrate) (Figure 3-2 - Step 6). The chrome that was exposed during photolithography was removed to expose the silicon surface while the photoresist kept the non-exposed chrome from being etched (Figure 3-2 - Steps 7 and 8). The photoresist was removed by flowing acetone over the silicon wafers for 3 minutes followed by a second 3-minute acetone bath (Figure 3-2 - Step 9). The wafers were then rinsed for one minute in a methanol bath. Finally, the wafers were cascade rinsed with DI water and sprayed dry.

After patterning the metal with the desired dimensions, the silicon wafer was placed in the Reactive Ion Etcher (Plasma-Therm 720, dual-chamber, Leybold 360 turbo-pump, St. Petersburg, FL) (Figure 3-3 - Step 2 and 3). The chamber was evacuated and filled with atmospheric oxygen and CF_4 (Freon 14) at flow rates of 7.5 sccm and 50 sccm, respectively. The chamber pressure was maintained at 50 mTorr. The base pressure in the reactive ion etch system was 8 μTorr. A radio frequency (RF) plasma was formed over the wafers creating an ion bombardment voltage of 100 V DC resulting in an etch rate of 16.8 nm per minute for the silicon surface. After the silicon was etched, the wafers were submerged in CR4 chrome etch to remove the chrome covering the mesas (Figure 3-3 - Steps 4 and 5). The grooves etched into the silicon imprint the mesas onto the polymer films (Figure 3-3 - Step 6).

Silicon wafers used as microdies for solvent cast films were also created using the Deep Reactive Ion Etcher (DRIE) (Alcatel 601E Micromachining Etch System, Annecy, France). The processing of the wafers before deep reactive ion etching involved similar steps to those mentioned above for the RIE with exception of metal deposition. Only patterned photoresist was necessary to use as a mask with the DRIE because of the relatively short etch times as compared to the RIE. After the surfaces of the wafers were cleaned using the same procedures as above, the photoresist was patterned to serve as a mask while the silicon wafer was being etched in the DRIE. First, three drops of hexamethyldisilazane (HMDS is an adhesion promoter for the photoresist) were spun onto the wafer at 4000 rpm for 20 seconds. The wafer was then spin-coated with a thick layer of positive photoresist (0.9 μm thick) (AZ 5209E made by Clariant, Somerville, NJ) at 4000 rpm for 40 seconds and prebaked on a hotplate at 100°C for 60 seconds. After the wafers cooled, they were placed onto a mask aligner and the photoresist was exposed to ultra-violet (UV) radiation through a patterned

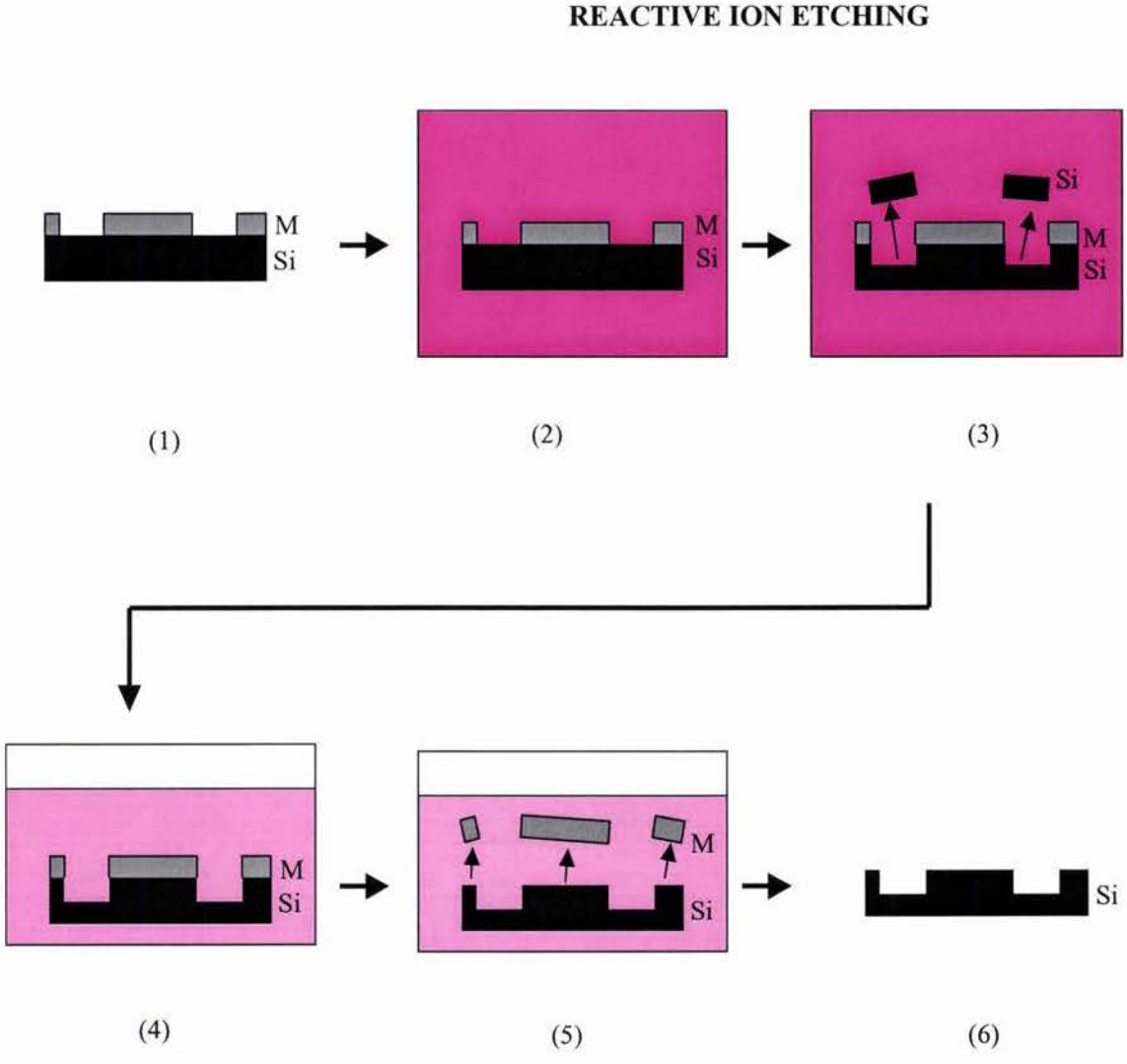

Figure 3-3. The steps of the reactive ion etching process followed by the removal of chrome metal on the mesas of the pattern. Reactive ion etching results in a three dimensional pattern with desired depth etched into the silicon wafer. This wafer was then be used as a microdie for imprinting the pattern onto polystyrene films.

photomask for 32 seconds (Dose = 416 mJ @ 13 mW/cm^2). The exposed wafers were placed in AZ 312 MIF developer (Clariant, Somerville, NJ), a commercial photoresist etchant, for 60 seconds to etch the exposed photoresist. The wafers were rinsed in DI water, sprayed dry with nitrogen and postbaked at 120°C for 25 minutes to harden the resist.

The patterned silicon wafer was then placed in the DRIE chamber and the silicon was etched with the silicon etch program for 30 seconds. The etch was performed by pulsing sulfur hexafluoride (SF6) etch gas and octafluorocyclobutane (C4F8) for passivation to achieve straight sidewalls. A flow rate of 300 sccm for 3 seconds was used for etching and a flow rate of 150 sccm for 1.25 seconds was used for passivation. The pressure changes depending on which gas is flowing by setting the open position of the throttle valve. This is different than what is used for most plasma systems (i.e. RIE) where pressure is controlled with gas flows. The valve was set to 46 degrees open resulting in pressures of ~45 mTorr during etching and ~20 mTorr during passivation. The substrate temperature was held to 25 °C. The source power used for the RF generators was 1800 Watts and the substrate bias power used was 75 Watts. The DRIE etch rate for silicon is 8 μm/minute.

After the silicon was etched, the photoresist was removed by flowing acetone over the silicon wafers for 3 minutes followed by a second 3-minute acetone bath. The wafers were then rinsed for one minute in a methanol bath. Finally, the wafers were cascade rinsed with DI water and sprayed dry. After solvent casting, the grooves etched into the silicon imprint the mesas onto the polymer films.

Conventional photolithography was also used for directly etching micropatterns into the polystyrene. The procedures used to create and etch the micropattern into the silicon wafer were applied to the polymer itself. First, polystyrene was solvent cast onto a bare silicon wafer that been cleaned with standard procedures. Chrome or aluminum (1 kÅ) was then deposited onto the PS by e-beam evaporation. The rest of the procedures used for direct etching were similar to those used for patterning the silicon wafer. However, care was taken with the polystyrene layer as certain solvent washes used in conventional photolithography attack the polymer. To remove the photoresist, a blanket exposure was performed where the entire surface was exposed to UV light without the use of a photomask. The RIE was then used to etch the PS layer to the desired depth by exposure to oxygen plasma. After processing, the wafer was scored with a razor and the patterned PS film was removed by floating the wafer in DI water.

3.2.2 Micropatterned polystyrene substrates

3.2.2.1 Solvent cast polystyrene films

The solvent cast polymer substrates were fabricated by dissolving 7-10 grams of polystyrene atactic beads (MW 125,000-250,000) into 100 ml of toluene making a 7-10% (w/v) solution. The micropatterned polysytrene films were created using both spin casting and gravity casting onto the etched silicon wafer with the desired pattern. Polystyrene solutions were first passed through syringes with attached PDVF (polyvinylidene fluoride) and PTFE (polytetrafluoroethylene) filters (Fisher Scientific, Pittsburgh, PA) of 0.22 μm pore size. For spin casting, various combinations of spin speeds and spin times were used to create a film of uniform thickness. For a micropatterned film of optimal thickness (50 μm), polystyrene solution was spun onto the patterned silicon wafer at 150 - 280 rpm for 30 -60 seconds. For gravity casting, typically 8 ml of 7-8% (w/v) polystyrene solution was deposited onto a 4-inch diameter silicon wafer via syringe after passing the solution through a 0.22 μm filter. Gravity casting resulted in a film thickness of approximately 50-70 μm. After casting, the polystyrene was covered with a glass petri dish and allowed to dry for a minimum of 24 hours. In this time, the majority of the toluene evaporated leaving a solvent cast film with a pattern opposite to that etched into the wafer.

The polystyrene film was removed by soaking the wafer in DI water for 4-12 hours. The film was floated on DI water with the grooves facing down for 24 hours at 37°C and then sterilized with 70% ethanol before storing at room temperature.

3.2.2.2 Imaging polystyrene films – scanning electron microscopy

The micropatterned substrates were imaged using scanning electron microscopy (SEM). The samples were prepared by cutting the substrates followed by mounting the sample and sputter coating the substrate with a conductive metal. The substrates were cut using dissecting scissors or a razor blade. They were cut perpendicular to the axial direction of the grooves in order for a cross sectional view of the substrate to be imaged.

The substrates were mounted with silver paint onto conductive tape-covered aluminum studs. After mounting, the samples were sputter coated to prevent the buildup of high voltage static charges that would degrade the quality of the SEM images and cause heat damage to the polymer. Sputter coating (SEM Coating Unit E5100, Polaron Instruments, Inc., Watford Hertfordshire, UK) was performed with 15 nm of conductive metal (100% gold).

Upon completion of the processing of the substrate, the JEOL JSM- 840A SEM was used to view the samples. The SEM images were taken using an accelerating voltage of 20 kV, a 50 μm diameter aperture and a vacuum level of 1 x 10^{-6} Torr.

3.2.3 Growth chambers for cell seeding

Chambers for the cells to grow within were constructed using PTFE (Teflon®) o-rings (Small Parts, Inc., Miami Lakes, FL) with inner diameters of 9/16 inches, outer diameters of 0.75 inches and widths of 3/32 inches. The process for making the growth chambers began with the sterilzation of glass coverslips (22 mm by 22 mm, Corning, Corning, NY) in 70% ethanol. The o-rings were stored in 70% ethanol until just before use. They were then autoclaved and left to cool to room temperature. After the coverslips dried under sterile conditions, the o-rings were applied to the coverslips using Syl-Gard®, a silicone elastomer (Dow Corning Corp., Midland, MI). The coverslip and o-ring set-up was allowed to cure for 24 hours before using. After 70% ethanol sterilization, the PS films were cut into square films approximately 1 cm^2 in area. The square films consisted of 0.5 cm^2 of patterned substrate adjacent to 0.5 cm^2 of non-patterned substrate (used as a control) (Figure 3-4). The PS films were then secured to the glass coverslips within the inner diameter of the o-ring using Silastic®, a silicone based medical adhesive (Dow Corning Corp., Midland, MI). This procedure resulted in a growth chamber for the cells. Each chamber was then placed inside a sterile, untreated 35 mm petri dish (Falcon, Franklin Lakes, NJ) (Figure 3-4). Laminin was applied to the PS film within this chamber prior to the seeding of the cells (See Section 3.2.3 below). The chambers provided an area where the cells grew strictly within the boundaries of the patterned/non-patterned PS film.

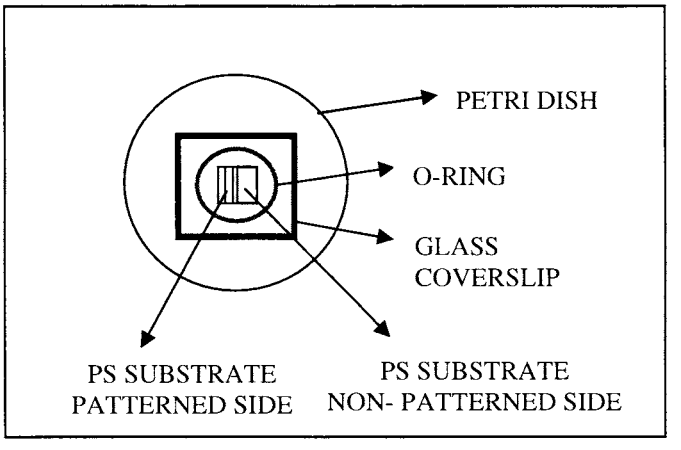

Figure 3-4. A schematic of the growth chamber consisting of the polystyrene substrate having both patterned and non-patterned sides.

3.2.4 Laminin adsorption onto polystyrene substrates

A solution of laminin was prepared by diluting 1 mg/ml of laminin in Earle's Balanced Salt Solution (EBSS) to concentrations ranging from 10-100 μg/ml. Approximately 0.5 ml of laminin solution was placed onto the polystyrene film (within the Teflon o-ring growth chamber) using a micropipettor (Figure 3-5). The laminin was allowed to adsorb for 15-20 minutes at room temperature and was removed with a micropipette tip placed perpendicular to the surface of the polystyrene film and pipetting up the fluid. The excess solution was allowed to dry on the surface for at least 4 hours at room temperature. This was the primary method of laminin application used in experimentation with the astrocytes.

Other techniques were also used for application of laminin as well as observe the distribution of laminin on the surface of the micropatterned film. In the second method, 0.5 ml laminin was applied to PS substrates within the o-ring chamber. This solution was left overnight at 4 °C. The following day the solution was removed with a micropipette tip placed perpendicular to the surface of the polystyrene film and pipetting up the fluid and the films were washed with sterile-filtered phosphate buffered saline (PBS, 137 mM NaCl, 2.68 mM KCl, 8.1 mM Na_2HPO_4, 1.47 mM KH_2PO_4). The third method was adapted from Buettner and colleagues [1]. Laminin was coated onto the PS substrates by placing 0.5 ml of laminin solution within the o-ring chambers. The laminin was allowed to adsorb to the surface of the substrate at room temperature for two hours. The solution was then removed with a micropipette tip placed perpendicular to the surface of the polystyrene film and pipetting up the fluid. The chamber was subsequently washed with PBS. A second wash of PBS was placed in chamber and removed in the same manner as above four hours later.

3.2.4.1 Laminin distribution assay

To observe the distribution of laminin on the surface of the micropatterned film, an immunocytochemical assay for laminin was performed. Laminin solution, diluted to a concentration of 0.01 mg/ml in EBSS, was applied to the PS substrate using the three different methods of application mentioned above with three replicates for each method of laminin application. Indirect immmunocytochemistry was performed immediately following the laminin application procedures (see Section 3.2.7.1.2 *Immunocytochemistry and histological labeling* for protocol). Laminin was identified using polyclonal antibodies raised against laminin (Anti-laminin, rabbit IgG, Sigma, St. Louis, MO). Anti-laminin was diluted at 1:50. Goat anti-rabbit IgG secondary antibody conjugated with TRITC (Sigma, St. Louis, MO) was diluted at 1:100. After immunocytochemistry, the laminin

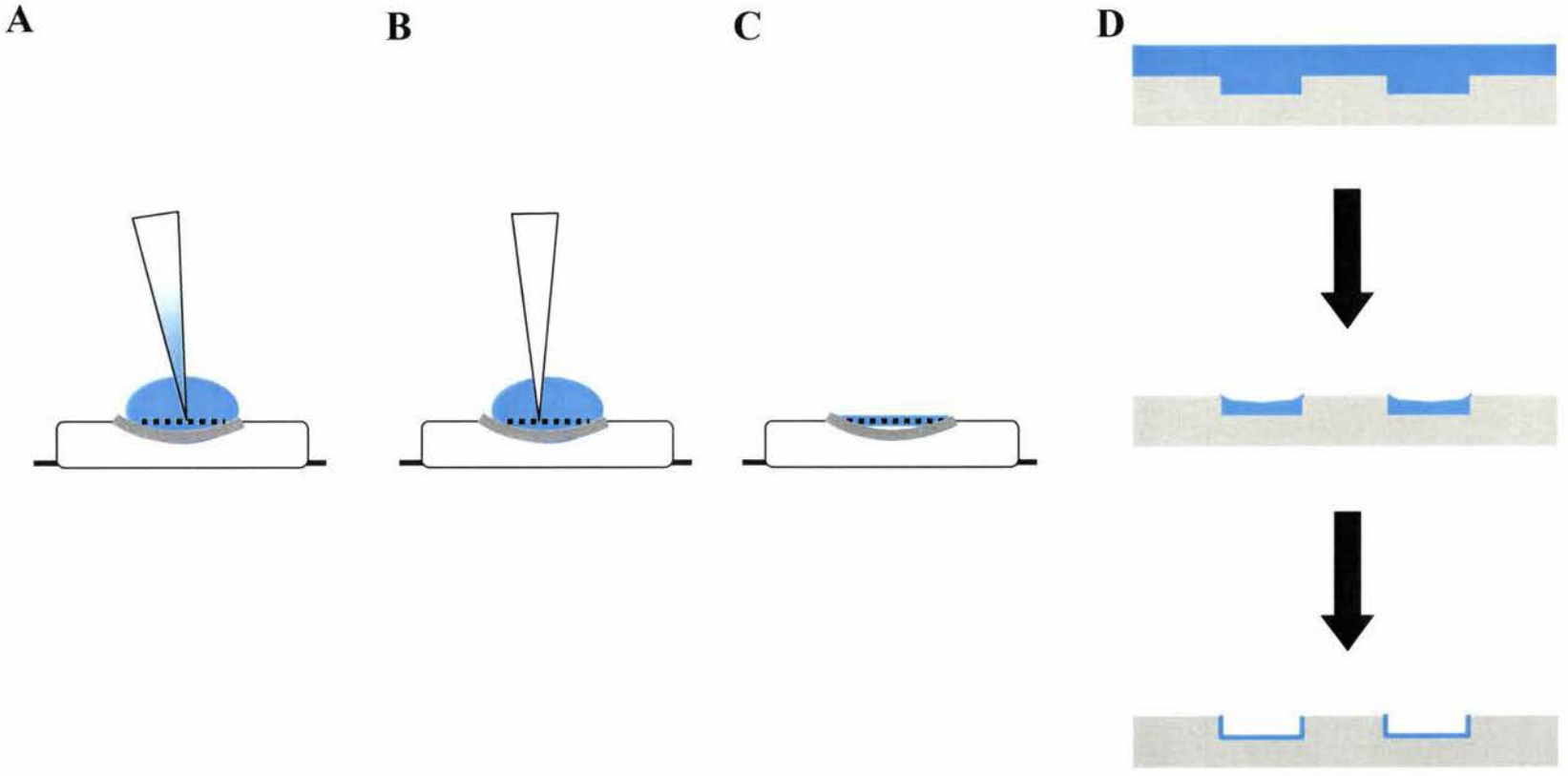

Figure 3-5. (A) Laminin deposition within the Teflon® o-ring growth chamber. (B) Removal of laminin with micropipette tip. (C) Drying of laminin on PS substrate. (D) The laminin puddles evenly over the surface. After removal, more fluid lines the grooves than the mesas. As a result, more laminin remains inside the grooves upon drying.

coated PS substrates were visualized with a tetramethyl-rhodamine isothiocyanate (TRITC) filter having a 555 nm absorption cutoff.

To further observe the distribution of laminin on the surface of the micropatterned film, fluorescein isothiocyanate (FITC) was conjugated to laminin using protein labeling techniques. Prior to labeling, laminin (Sigma) at 1 mg/ml in Tris-HCl with 150mM NaCl, pH=7.5, was exchanged into borate buffer (310 mg H_3BO_3, 475 mg $Na_2B_4O_7 \bullet 10\ H_20$ in 100 ml ddH_20, pH 8.4) by dialysis. A Slide-A-Lyzer Dialysis Unit (Pierce Biotechnology, Rockford, IL) with a molecular weight cut-off (MWCO) of 10,000 was used for dialysis. Following dialysis, the protein labeling reaction was performed. Laminin was reacted with 2 µl of FITC at 10 mg/ml in DMSO. This mixture was incubated for one hour at room temperature. To remove excess fluorescent dye, the sample was then dialyzed in a beaker filled with 500 ml of phosphate buffered saline (PBS, 137 mM NaCl, 2.68 mM KCl, 8.1 mM Na_2HPO_4, 1.47 mM KH_2PO_4) using a 10,000 MWCO Slide-A-Lyzer Dialysis Unit. The beaker was covered with foil to protect the FITC from light. The FITC-conjugated laminin was then applied to the patterned PS substrates using the first and second application methods mentioned above using 0.1 ml of laminin solution for each substrate. The FITC-conjugated laminin coated PS substrates were visualized with fluorescence microscopy using a FITC filter having a 495 nm absorption cutoff and confocal microscopy using an 488 nm Argon laser.

3.2.5 Astroglial cells

3.2.5.1 Rat astrocyte purification and culture

A population of purified astrocytes was obtained from the cerebral cortex of post-natal, one to three day old rat pups. The methods described below were modified from [2, 3]. Strategies used include the selection of nervous tissue where neurogenesis is completed but immature astroglial cells are present as the major proliferative cell population. Vigorous mechanical tissue dissociation procedures are used that destroy the majority of neurons but allow the survival of small undifferentiated glial precursor cells.

Primary cultures of astrocytes were obtained as follows. Sprague-Dawley rat pups, one to three days old, were anesthetized. The brain of the rat pup was isolated by severing the spinal cord and cutting the skull surrounding the brain of the pup. Upon isolation, the cerebrum with the midbrain still attached was removed and placed into a petri dish filled with of cold EBSS. The cerebral hemispheres were removed from the midbrain and separated. The meninges were removed from each

cerebral hemisphere using fine forceps. The hemispheres were then placed in a centrifuge tube containing cold EBSS. The tissue was washed in EBSS and enzymatically treated with papain solution (20 IU/ml; 37 °C, 5% CO_2/ 95% air, 1 hour). After the enzymatic treatment, the papain was decanted and the tissue was washed in EBSS for 5 minutes. The EBSS was replaced with 10 mg/ml of a trypsin inhibitor solution for 5 minutes. The tissue was washed again with EBSS for 5 minutes and the EBSS is replaced with modified minimum essential culture medium (MMEM). The tissue was mechanically dissociated and approximately 1 ml of cell suspension was added to each 25 cm^2 tissue culture flask (T-25; Falcon, Franklin Lakes, NJ) (2 flasks per pup). The flasks were then placed in a humidified 5% CO2/ 95% air atmosphere for 1 hour. After 1 hour, 5 ml of medium was added to each flask. After one day, the medium was removed and the cultures were washed with EBSS. Cultures were fed with new medium. The culture medium, MMEM, consisted of minimum essential medium (MEM) supplemented with 40 mM glucose, 2 mM *L*-glutamine, 1 mM pyruvate and 14 mM $NaHCO_3$, penicillin (100 IU/ml) and streptomycin (100 µg/ml) with 10% v/v fetal bovine serum (FBS), pH 7.35.

After the cultures reached confluency (~8 days), an enriched population of astrocyte type-1 cultures was prepared. This was achieved by taking steps to eliminate both neurons and microglia from the flask. Neurons do not survive after washing with cold MMEM. Microglia are jarred loose from the astrocyte bed by shaking the flasks. After ~8 days, the cells were washed with cold medium two times. The flasks were then shaken twice on a horizontal shaker at 260 RPM at 37 °C, first for 1.5 hours and then after replacement of the medium, again for 18 hours. The remaining adherent cells were enzymatically detached with trypsin (0.1%). Cells were then pelleted (100 X *g*, 10 min.), resuspended in MMEM and passaged into 25 cm^2 tissue culture flasks. The astrocytes attached to the flask within 18 hours. Cultures were fed every three days. Cells were not passaged more than 8 times.

3.2.5.2 Seeding of astrocytes onto micropatterned substrates

Astrocytes were seeded onto micropatterned/non-patterned film surfaces coated with poly-L-lysine (PLL) (100 or 1000 µg/ml EBSS) or laminin (10 or 100 µg/ml EBSS) and those not coated with PLL or laminin at initial densities varying from 7,500 to 100,000 cells/cm^2. The process for seeding purified astrocytes began by washing the cells with 5 ml of EBSS. After rinsing with EBSS, 4.5 ml of EBSS was added to the flask followed by 0.5 ml of a 1% trypsin stock. The trypsin was left in the flask for about 5 minutes and incubated at 37 °C during which time the cells were detached from the flask. The flask was gently tapped at this point to free loosely attached cells. Then 9 ml of

medium was added to flask and the solution was poured into a 15 ml centrifuge tube. The mixture was pelleted (100 x *g*, 10 min) and the supernatant was removed. The cells were resuspended in the appropriate volume of medium or EBSS for live staining of the astrocytes prior to cell counting. The astrocytes were typically stained with $DiIC_{18}$ (DiI) or carboxyfluorescein diacetate succinimidyl ester (CFDA SE).

In order to image the astrocytes *in vitro* throughout experimentation, the cells were fluorescently labeled prior to cell counting using DiI at 2.68 μM or CFDA SE at 5 μM. After addition of the DiI or the CFDA SE at the appropriate dilution, the cells were incubated for 20 minutes and 30 minutes, respectively, at 37 °C. The cells were washed three times using centrifugation following incubation. After the last wash, the appropriate volume of medium was added to the pellet to reconstitute the cells for counting.

Total cell counts and viable cell numbers for the astrocytes were determined by trypan blue cell exclusion using a hemacytometer. Counts were performed in triplicate and averages were calculated. The number of astrocytes per ml of medium was calculated by multiplying the dilution factor by the average cell count multiplied by 10^4. The desired amount of medium for the appropriate seeding density was added to the astrocytes. The cell suspension was triturated with a sterile Pasteur pipette with a flamed tip to ensure cell separation. A cell suspension volume of 150-200 μl was used for seeding the cells on the micropatterned substrates inside the growth chamber. The cells were incubated at 37 °C for 1 hour. After 1 hour, enough medium was added to cover the cells adhered to the substrates (approximately 2 ml).

3.2.6 Adult rat hippocampal progenitor cells

Adult rat hippocampal progenitor cells (AHPCs) were used in preliminary studies with the micropatterned PS substrates. They were originally isolated from the adult brains of Fischer 344 rats as reported by Palmer and colleagues. The expanded cultures of single clones were infected with retrovirus to express enhanced GFP (eGFP) [4, 5]. The AHPCs were maintained in polyornithine/laminin-coated plastic tissue culture flasks (T-75, Fisher Scientific, Pittsburgh, PA) in complete culture media containing Dulbecco's modified Eagle's medium/Ham's F12 (DMEM/F12, 1:1; Gibco BRL, Gaitherburg,MD) supplemented with N2 (Gibco BRL, Gaitherburg,MD), 20 ng/ml fibroblast growth factor (Promega Corporation, Madison, WI), and L-glutamine (2.5 mM L-glu; Gibco BRL, Gaitherburg,MD). For *in vitro* analysis on PS substrates, the AHPCs were detached from

the T-75 flask using ATV solution (Gibco BRL, Gaitherburg,MD) after media removal. The flask was gently tapped at this point to free loosely attached cells. The cells were resuspended in DMEM/F12 and transferred to a centrifuge tube. The cells were collected by centrifugation at 1000 g for 3 minutes and the pellets were resuspended in cell conditioned media and triturated gently. The cells were then plated on the PS substrates coated with 0.01 mg/ml laminin in EBSS using the procedures described above (Section 3.2.3). Cells were maintained for three days in the culture media stated above without FGF (referred to as differentiation media).

3.2.7 Histological procedures and imaging

3.2.7.1 Light and fluorescence microscopy

The astrocytes were imaged using light and fluorescence microscopy. An Olympus IMT-2 bright field/phase contrast microscope was used to view the cells during culture. Digital images were taken throughout experimentation using an epifluorescence microscope equipped with a cooled digital camera (ORCA, Hamamatsu) that was controlled by MetaMorph software (Universal Imaging Corporation, West Chester, PA). Cultured astrocytes were also examined using a Nikon Microphot-FXA photomicroscope (Nikon, Inc. Garden City, NY) equipped with epifluorescence. Images were captured from this microscope with a Kodak Megaplus CCD camera connected to a Perceptics Megagrabber Framemaker in a Macintosh computer (Apple Computer, Cupertino, CA) using NIH Image 1.58 VDM software (Wayne Rasband, National Institutes of Health, Bethesda, MD).

Histological and immunocytochemical staining procedures were used to enhance the visibility of the astrocytes on the polystyrene substrates as well as determine if the cultures used for experimentation were type-1 astrocytes that were free of neurons and other types of glial cells.

3.2.7.1.1 *Labeling live cells* Live cell staining procedures were used to monitor and image the astrocytes as they grew on the substrates. One of two tracers was used to enhance the visibility of the cells during experimentation. The first method involved staining the cells with $DiIC_{18}$ (DiI). In the second method, the cells were stained with the membrane permeant tracer, carboxyfluorescein diacetate succinimdyl ester (CFDA SE).

The lipophilic tracer, DiI, is typically used as an anterograde and retrograde neuronal tracer in living and fixed cells. This dye can label the plasma membrane of cells with high specificity. DiI laterally diffuses into the plasma membranes of living cells at a 6 mm per day and can remain viable

for up to four weeks in culture [6]. This tracer has an absorption wavelength of 549 nm and an emission maximum of 565 nm and was visualized with a TRITC filter.

DiI was used to label astrocytes in cell suspension and to re-label the astrocytes adhered onto the substrates. First, the dye solution was prepared by dissolving DiI crystals in dimethylsulfoxide (DMSO) at 2.5 mg/ml. This stock solution was then diluted in medium to 2.68 μM when used to label the astrocytes. While the cells were in suspension, 1 μl of DiI was added to every 1 ml of medium used to resuspend the astrocytes. This mixture was incubated for 20 minutes at 37 °C. Following incubation, the cells were washed three times using centrifugation (100 x *g*, 5 minutes). After the last wash, the supernatant was removed and the cells were resuspended in the appropriate volume of medium to either count the cells or achieve the desired density for seeding. To stain adherent cells, staining medium was prepared by adding 1 μl of stock solution to 1 ml of normal growth medium. Then, approximately 100 μL of staining medium was pipetted onto the corner of the substrate and gently agitated until all of the cells were covered. The substrates were incubated for 30 minutes at 37 °C. The substrates were washed three times with fresh medium. During each wash, the substrates were placed in the incubator at 37 °C for 8-10 minutes. Then, the medium was drained off following incubation and replaced with fresh medium.

The second staining method involved the membrane permeant tracer, carboxyfluorescein diacetate succinimidyl ester (CFDA SE). CFDA SE is a nonpolar molecule that penetrates cell membranes spontaneously. This tracer irreversibly couples to both intracellular and cell-surface proteins by reaction with lysine side chains and other available amines. CFDA SE is converted to anionic CFSE by intracellular esterases. It is the amine-reactive coupling of CFSE to proteins that results in a stable, long-term intracellular retention of the dye inside the cell membrane. Depending on cell type, the fluorescence of resting cells labeled with CFDA SE is stable over several months. When cells divide, CFDA SE labeling is distributed equally between daughter cells. The daughter cells become half as fluorescent as the parent cell. CFDA SE has an absorption wavelength of 495 nm and an emission maximum of 525 nm and was visualized with a FITC filter.

CFDA SE was used to label astrocytes in cell suspension and to re-label the astrocytes adhered onto the substrates. A 5mM stock solution of was prepared by dissolving 25 mg of concentrated dye in 8-9 ml of DMSO. This stock solution was then diluted in EBSS to a working dilution of 1-10 μM when used to label the astrocytes. While the cells were in suspension, 1 μl of CFDA SE was added every 1 ml of EBSS used to resuspend the astrocytes. This mixture was

incubated for 30 minutes at 37 °C. Following incubation, the cells were washed three times with serum-free MMEM using centrifugation (100 x *g*, 5 minutes). After the last wash, the supernatant was removed and the cells were resuspended in the appropriate volume of medium to either count the astrocytes or achieve the desired density for seeding. To stain adherent cells, staining medium was prepared by adding 1 µl of stock solution to 1 ml of normal growth medium. The cells were initially washed with EBSS. Then, approximately 100 µL of staining medium was pipetted onto the corner of the substrate and gently agitated until all of the cells were covered. The substrates were incubated for 30 minutes at 37 °C. The substrates were washed three times with serum-free MMEM. Then, the medium was drained off following incubation and replaced with fresh MMEM (with serum).

3.2.7.1.2 *Immunocytochemistry and histological labeling* Astrocytes were fixed at various time points throughout experimentation. These time points were typically at 24 hours and 72 hours after seeding the astrocytes onto the substrates. Fixed astrocytes were labeled using histological and/or immunocytochemical labeling procedures. When histological and immunocytochemical techniques were used in combination, the immunocytochemical procedures preceeded the histological staining of the astrocytes. Indirect immunocytochemistry with conjugated fluorochrome secondary antibodies was performed on cells cultured on glass coverslips coated with 1 mg/ml poly-L-lysine (Sigma) prepared in borate buffer (310 mg H_3BO_3, 475 mg $Na_2B_4O_7 \bullet 10\ H_20$ in 100 ml ddH_20, pH 8.4) 72 hours after seeding and on PS substrates coated with 0.01 mg/ml laminin in EBSS and PS films not coated with laminin 24 or 72 hours after seeding. First, the astrocytes were rinsed in 0.1 M PO_4 buffer, fixed with 4% paraformaldehyde in 0.1 M PO_4 for 20 minutes and then gently rinsed with phosphate buffered saline (PBS, 137 mM NaCl, 2.68 mM KCl, 8.1 mM Na_2HPO_4, 1.47 mM KH_2PO_4) 3 times for 7 minutes each. The cultures were blocked in 5% goat serum, containing 0.4% bovine serum albumin (BSA) and 0.2% Triton-X-100 in PBS for 30 minutes at room temperature. Primary antibodies were prepared at the proper dilutions in the blocking solution. The primary antibody was applied to the substrates (coverslips or PS films) with astrocytes seeded on them and incubated overnight at 4 °C. On the following day, the substrates were rinsed with sterile- filtered PBS 4 times for 8 minutes each and incubated with appropriate secondary antibodies conjugated to Alexa 546, TRITC or Alexa 488 in the dark for 90 minutes at room temperature. The secondary antibody was applied to the preparations (coverslips or PS films seeded with astrocytes) after dilution in the blocking solution prior to incubation. The substrates were subsequently rinsed with sterile-filtered PBS 8 times for 6 minutes each. If no histological labeling was used on the cultures, the substrates

were then mounted using Gel Mount mounting media (Biomeda Corp., Foster City, CA). Negative controls were performed in parallel during all immunocytochemical processing by the omission of the primary and secondary antibodies. There was no antibody labeling observed in the negative controls.

Immuncytochemistry involved specific primary and secondary antibodies. The presence of glial fibrillary acidic protein (GFAP) was identified using monoclonal antibodies raised against GFAP (Anti-GFAP, G-A-5, mouse IgG) purchased from ICN Immunobiologicals, Inc. (Costa Mesa, CA) and diluted 1:200 in blocking solution, and polyclonal anti-GFAP antibody (rabbit IgG, Sigma) diluted 1:100 in blocking solution. These antibodies were used as markers for astrocytes, as GFAP is a type of intermediate filament found in astrocytes. Microtubule associated protein 2 was identified using anti-MAP-2ab (1:150), purchased from Sigma (mouse IgG) and used as a neuronal marker. Terminally differentiated oligodendrocytes and their myelin sheaths were identified using Anti-RIP (1:50), obtained from the Developmental Studies Hybridoma Bank, maintained by the Department of Biology, University of Iowa, under contract NO1-HD-2-3144 from the NICHD (mouse IgG). Goat anti-mouse IgG secondary antibodies conjugated with Alexa 546 (diluted 1:100) or Alexa 488 (1:150) were purchased from Southern Biotechnology (Birmingham, AL) or Molecular Probes (Eugene, OR). Goat anti-rabbit IgG secondary antibody conjugated with RITC (1:150) was purchased from Southern Biotechnology (Birmingham, AL). All primary and secondary antibodies were diluted in blocking solution.

Two histological stains were used on the preparations following immunocytochemistry. F-actin cytoskeletal filaments were labeled with Alexa Fluor 568 phalloidin. Alexa phalloidin was diluted at 1:40 in PBS and applied for 45 minutes followed by 3 washes with sterile-filtered PBS of 5 minutes each. Nuclei of the astrocytes were stained with 4', 6-diamidino-2-phenylindole, dilactate (DAPI), a semi-permeant nucleic acid stain. DAPI was diluted at 10:1000 in PBS and applied for 15 minutes followed by 3 washes with sterile-filtered PBS of 5 minutes each. Following labeling with phalloidin and then DAPI, the preparations were mounted using Gel Mount mounting media. Alexa Fluor 568 has an absorption wavelength of 578 nm and an emission maximum of 600 nm and was visualized with the TRITC filter set. DAPI has an absorption wavelength of 358 nm and an emission maximum of 461 nm and was visualized with the DAPI filter set.

3.2.7.2 Confocal microscopy

The PS substrates used in the FITC- conjugated laminin distribution assay were imaged with a Prairie Technologies Confocal Microscope (Prairie Technologies, Madison, WI). All imaging was

controlled by Prairie Technologies software. The 488 nm laser and the 40X objective were used to view the FITC-conjugated laminin applied to the patterned PS substrates using the techniques mentioned in Section 3.2.3.1. Confocal images 0.5 μm apart were taken through each substrate analyzed. These sequential images were used to reconstruct a three-dimensional representation of the sample. Confocal microscopy 'builds' an image with 'in focus' light only. Out of focus light was physically rejected from the detector by a 75 μm pinhole. Images were constructed by scanning the excitation light in an X-Y fashion over the sample while the resulting emission light was detected with a photomultiplier tube and reported to a computer file. Image analysis was done with MetaMorph software (Universal Imaging Corporation, West Chester, PA).

3.2.8 Analysis of astrocytes *in vitro*

3.2.8.1 Assessment of GFAP immunoreactivity

Following immunocytochemical procedures on the coverslips and PS substrates on microscope slides, the preparations were examined on a Microphot- FXA photomicroscope (Nikon Inc., Garden City, NY). A 20X objective was used to examine 10 to 20 microscope fields, each field representing 0.1 mm^2 (360 μm by 280 μm). The following counts were made in each microscope field for the coverslips and the PS substrates: the total number of cells (using a DAPI filter cube) and the number of cells expressing the primary antibody of interest (using a TRITC and FITC filter cube, respectively). This data was used to calculate the percentage of cells labeled with one of the antibody markers (mentioned above) on each coverslip and anti-GFAP alone on the PS substrates. For PS substrates, the data collected after 24 and 72 hours was compared and analyzed.

3.2.8.2 Determination of cell alignment

At twenty-four hours and seventy-two hours after seeding, the cells were fixed, labeled and mounted onto glass microscope slides (Fisher Scientific, Pittsburgh, PA). The astrocytes were examined and photographed under light and fluorescence microscopy using 10X and 20X objectives. The effect of initial seeding density and laminin (100 μg/ml EBSS) adsorbed on the substrate was evaluated for the pattern dimensions 10 x 20 x 3 μm at initial densities varying from 7,500 to 20,000 cells/cm^2. The orientation of the astrocytes on the PS substrates was measured quantitatively using MetaMorph software (Universal Imaging Corp., West Chester, PA). Orientation was measured as the angle of the longest chord through each astrocyte relative to the horizontal axis of the imported image (Figure 3-6). The data were grouped in 10° sectors between -90° to 90°. Orientations of the groove

position in the images were measured in the same way. Control data were taken from measurements made on astrocytes on non-patterned PS film areas adjacent to the patterned areas. The angle of orientation in these controls was measured relative to the horizontal axis (0°). Statistical analysis was performed on the values of the differences between the orientation of the cell and the orientation of the groove on the substrate with a difference of 0° indicating perfect alignment.

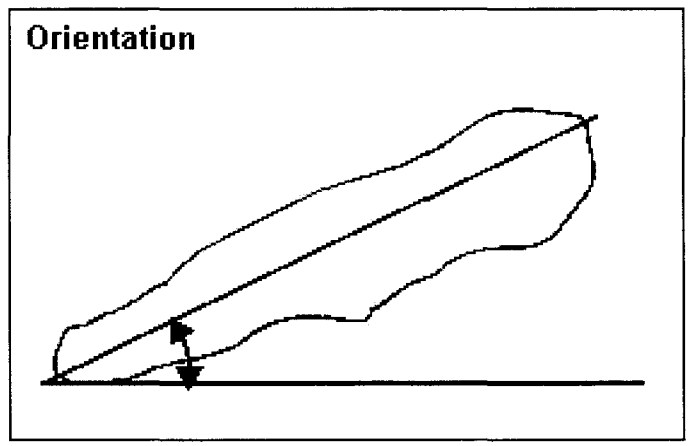

Figure 3-6. A schematic of the method by which MetaMorph defines and measures orientation. Orientation is measured as the angle between the longest chord through the object and the horizontal axis. The orientation ranges from -90° to 90°.

Before statistically evaluating the orientation of the astrocytes, the measurement scale for the orientation values measured by MetaMorph was changed from –90° to +90° to 0° to 180°. This was done in order to obtain a uniform, positive measurement of each cell relative to the groove orientation on the substrate. If the orientation value of the cell was negative, then it was rescaled to where it ranged from 0° to +90° by adding the negative value to 180°. The position of the grooves of the pattern was taken into account for the difference measurement. If the groove orientation was a negative value it was also added to 180°. The difference between the groove orientation and the orientation of each cell was then evaluated. These were the values used for statistical analysis performed on the orientation of the astrocytes.

There were various reasons for the change in measurement scale. Due to the way the substrates were cut away from the patterned film generated by casting the polystyrene solution onto the silicon wafer, there were substrates that had grooves oriented vertically and those that had grooves that were oriented horizontally when placed randomly in the growth chamber. Secondly, MetaMorph

measured orientation from –90° to +90°. Therefore, to make analysis easier, all measurements were corrected back to a positive scale. Furthermore, it was not always possible to take an image where the horizontally positioned grooves ended up at exactly 0° and the vertically positioned grooves ended up at exactly 90° so each groove orientation was calculated to determine what degree, if any, the pattern was off from 0° or 90°. This orientation was then taken into account when evaluating the orientation of each cell relative to the grooves of the pattern.

Cell alignment was measured as the proportion of astrocytes whose longest chord makes an angle of ≤ 20° with the direction of the grooves in these studies. The proportions of cells falling in this group as well as those astrocytes whose longest chord made an angle of ≤ 10° with the direction of the grooves were estimated. There were four types of substrates examined: (1) micropatterned PS substrates with laminin adsorbed on the surface (LAM -PATT); (2) micropatterned PS substrates without laminin (NO LAM - PATT); (3) non-patterned PS substrates with laminin adsorbed on the surface (LAM - NO PATT); and (4) non-patterned PS substrates without laminin (NO LAM - NO PATT). Table 1 displays a summary of the experimental set-up used in analysis of the astrocytes on the micropatterned PS substrates. Three replicates of each treatment or control were analyzed. Statistical analyses were performed on (1) the astrocyte alignment to within 10° and 20° of groove direction and (2) on the number of cells adhering to substrates with laminin as compared to those without. The analysis was performed using the PROC MIXED procedure in SAS statistical software.

Table 1. A summary of the experimental design used in the analysis of astrocyte behavior on 10 x 20 x 3 μm patterned and non-patterned polystyrene (PS) substrates.

STUDY	PHYSICAL GUIDANCE	CHEMICAL GUIDANCE	CHEMICAL and PHYSICAL GUIDANCE
TREATMENT (PS Substrate)	NO LAM - PATT (10 x 20 x 3 μm)	LAM - NO PATT	LAM - PATT (10 x 20 x 3 μm)
CONTROL(S) (PS Substrate)	NO LAM - NO PATT	NO LAM - NO PATT	LAM - NO PATT NO LAM - PATT (10 x 20 x 3 μm) NO LAM - NO PATT
INITIAL SEEDING DENSITY (cells/cm^2)	20,000 13,000 7,500	20,000 13,000 7,500	20,000 13,000 7,500

The data was analyzed using an ANOVA with three error terms to account for (1) the whole plot effect, (2) the split plot effect, and (3) the subsampling due to the experimental design. The whole plot experimental unit was the entire polystyrene substrate (approximately 1 cm^2 in area) while the split plot experimental unit was the half of the substrate that was either patterned or not patterned. Multiple observations were made on each half of a substrate. The numbers of observations were not balanced, and this accounted for the subsampling variation. A natural log transformation was used to account for the exponential rate of growth of the astrocytes.

References Cited

1. Buettner, H.M. and R.N. Pittman, *Quantitative effects of laminin concentration on neurite outgrowth in vitro.* Developmental Biology, 1991. **145**(2): p. 266-76.
2. Innocenti, B., V. Parpura, and P.G. Haydon, *Imaging extracellular waves of glutamate during calcium signaling in cultured astrocytes.* Journal of Neuroscience, 2000. **20**(5): p. 1800-8.
3. Parpura, V., et al., *Expression of synaptobrevin II, cellubrevin and syntaxin but not SNAP-25 in cultured astrocytes.* FEBS LETTERS, 1995. **377**(3): p. 489-92.
4. Takahashi, J., T.D. Palmer, and F.H. Gage, *Retinoic acid and neurotrophins collaborate to regulate neurogenesis in adult-derived neural stem cells cultures.* Journal of Neurobiology, 1999. **38**: p. 65-81.
5. Palmer, T.D., J. Takahashi, and F.H. Gage, *The adult rat hippocampus contains primordial neural stem cells.* Molecular and Cellular Neurosciences, 1997. **8**(6): p. 389-404.
6. *Neuroscience Protocols*, ed. F. Wouterlood. 1993: Elsevier Science Publishers. 1-20.

4. RESULTS AND DISCUSSION

4.1 Micropatterned Substrate Fabrication

An efficient system was developed to produce micropatterns on polymer substrates. Various polymers were experimented with to determine the most desirable substrate for cell culture. Among these polymers were epoxy, poly (methyl methacrylate), and polystyrene. Polystyrene was used because it was the most suitable for astrocyte culture. Using this polymer involved the least disruption to normal *in vitro* cell morphology and growth as observed by seeding astrocytes onto substrates made of the various polymers and evaluating cell behavior. Two fabrication methods using photolithographic techniques were tested to produce micropatterns on the polymer substrates. One method involved a direct etch of the polymer film and the other fabrication method involved creating a microdie that was then used to transfer the desired pattern onto the polymer substrate using solvent casting. The method that was found to be the most reproducible and least time consuming was to create a die with the desired micropattern and cast the pattern onto the polystyrene (PS).

Conventional photolithographic techniques were used to prepare silicon wafers having desired micropatterns. The micropatterns were etched into silicon using either reactive ion etching or deep reactive ion etching to produce patterns of various depths. The reactive ion etch (RIE) etched silicon at 16.8 nm per minute. RIE is designed to etch thin films at depths from less than 1 μm to 10 μm. The resulting etch from RIE was isotropic. The deep reactive ion etch (DRIE) etched silicon at 8 μm per minute. DRIE is designed for micromachining processes. It can be used to etch silicon substrates as deep as 1 mm. The etch resulting from DRIE was more of an anisotropic etch where the wall profile is vertical. Due to the nature of the deep reactive ion etch, the silicon wafer did not have to be deposited with metal prior to photolithography. The photoresist remained on the wafer when the patterned wafer was placed in the DRIE chamber and protected the non-exposed areas on the wafer from being etched. After the silicon was etched, the photoresist was removed.

Using the patterned and etched silicon as a microdie (Figure 4-1), the patterns were transferred to the polymer substrates by applying a solvent casting technique. Solvent casting allows easy creation of a polymer film (Figure 4-1) having desired thickness. The micropatterned polymer substrates created using solvent casting were described using the following nomenclature: groove

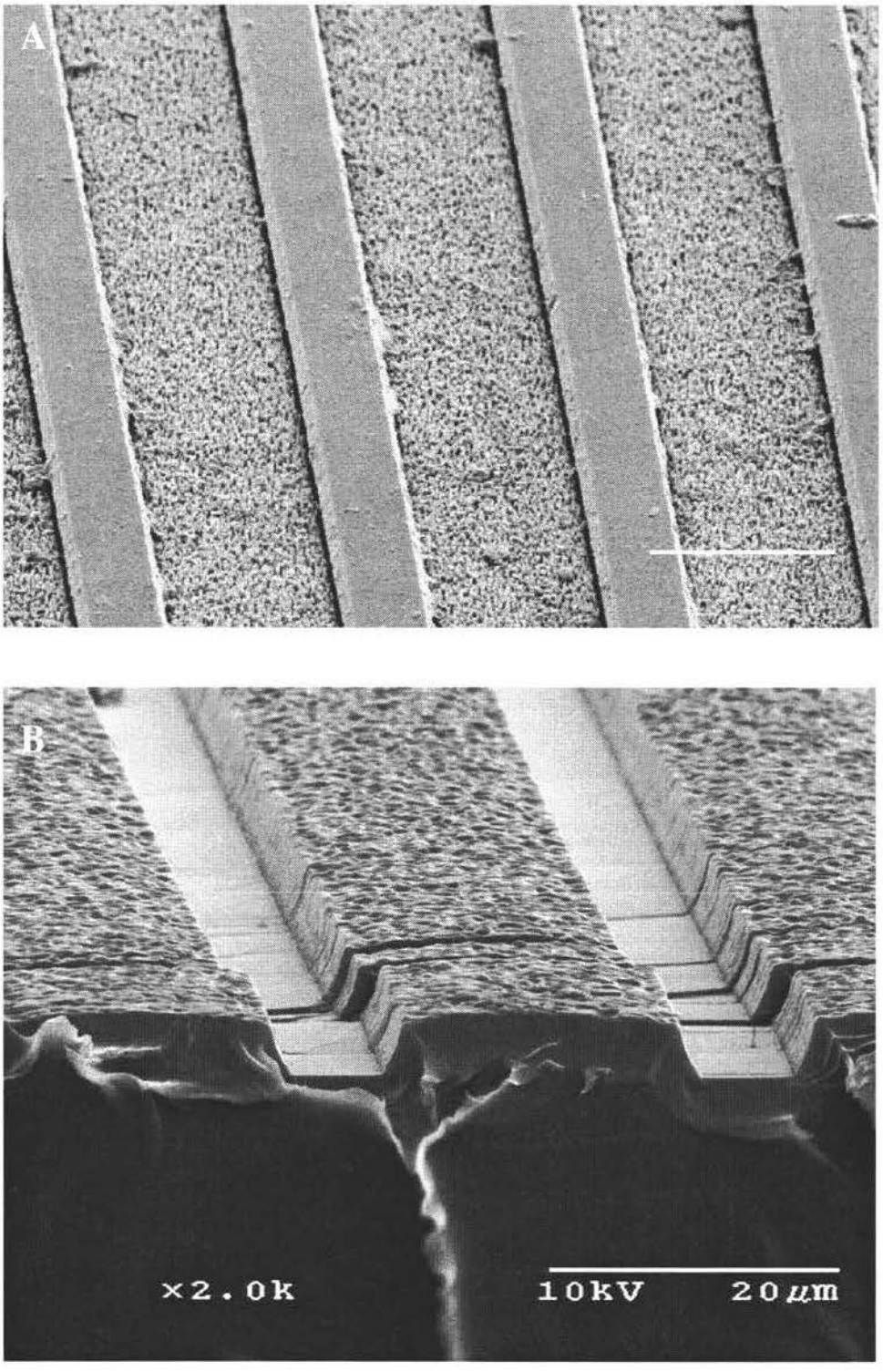

Figure 4-1. (A) A 20 x 10 x 3 µm silicon wafer used as microdie. (B) An SEM image of a polystyrene substrate having groove dimensions of 10 x 20 x 3 µm created by solvent casting onto the microdie. Scale bars, 20 µm.

width (μm) x groove spacing (or mesa width) (μm) x groove depth (μm). The dimension sets used in these studies were 10 x 10 x 3 μm, 10 x 10 x 4 μm or 10 x 20 x 3 μm micropatterns. Solvent casting was accomplished either by gravity casting or spin casting onto the etched silicon wafer with the desired pattern. Varying the amount and concentration of the PS solution used was found to change the thickness of the polymer film. When spin casting, spin speed and spin time were found to be other variables that can change the film thickness. The solutions used for casting varied from 7 to 10 % PS (w/v) dissolved in toluene. PS films were cast using volumes of solution that varied from 4 to 8 ml. Depositing 8 ml of 7-8% (w/v) PS dissolved in toluene onto a 4- inch diameter silicon wafer, the film thickness resulting from gravity casting was approximately 50-70 μm. The thickness of the films was consistent for the concentration and the volume of solution used. These PS films were easier to work with than those made by spinning the polymer solution onto the patterned silicon wafer. The spin speeds used for spin casting varied from 150 to 280 RPM for times ranging between 30-60 seconds. These films were approximately 50 μm in thickness. Different combinations of spin speed and time spinning resulted in films with various thicknesses. Generally, it was found that using PS solution in the 7-10% (w/v) range at lower speeds for less time resulted in thicker films. In order for the polymer solution to distribute evenly over a wafer surface producing a smooth film, approximately 4 ml of 10% PS dissolved in toluene and spin settings typically at a minimum of 150 RPM for 30 seconds were used. These specifications also depended on the shape and surface area of the wafer as well. In general, using the same specifications for spin casting on the same patterned wafer did not result in films with the same appearance. There were many variables that affected film quality making spin casting less efficient than gravity casting. Overall, spin casting resulted in thinner, more brittle films than gravity casting. Gravity casting allowed a more even distribution of PS solution across the wafer surface resulting in smooth films that were uniform in thickness. Furthermore, gravity casting a film was more reproducible than spin casting. Therefore, gravity casting was the method used primarily for casting the PS films.

4.2 Protein Distribution Assays

To chemically modify the PS micropatterned substrates, poly-L-lysine (PLL) and laminin were adsorbed onto the substrates using a surface tension based technique. Poly-L-lysine and laminin were used as they were found to promote cell adhesion in previous studies with astrocytes as well as

neural stem cells. Assays were performed on the PLL and laminin coated substrates to determine where the proteins were distributed on the patterned PS films upon adsorption. The PLL was conjugated to FITC, applied to the PS substrate and analyzed by fluorescence microscopy. As a result of surface tension, more PLL appeared to be deposited in the grooves and was fluorescing with higher intensity than on the mesa surfaces where there was little fluorescence if any (Figure 4-2). Substrates that had been rinsed with de-ionized (DI) water after adsorption were compared to those that were left to dry after the removal of excess PLL with no rinsing. The results revealed that those substrates that had been rinsed had an overall lower intensity of fluorescence. The FITC-conjugated PLL did not appear to be concentrated in the groove corners but was spread evenly over the entire surface of the substrate. Based on these results, PLL was adsorbed onto the PS substrates without a rinse with DI water after adsorption and removal of excess PLL.

Laminin distribution on the PS substrates was assayed using FITC-conjugated laminin as well as immunocytochemistry (ICC) for laminin. After each of three different methods for adsorbing laminin to the PS films, ICC with an antibody against laminin was performed. The results revealed that the laminin was spread evenly over the entire surface of the substrate -on both the grooves and the mesas. The same observations were made regardless of the method used for adsorbing the laminin on the PS film. The intensities of fluorescence were similar for each method tested. In addition to ICC, distribution was studied with FITC-conjugated laminin due to less washing of the substrates with this technique and laminin location could be observed immediately following adsorption. After applying the FITC-conjugated laminin to the PS substrates using two different methods of adsorption, the laminin was observed as spreading over the entire surface of the substrate upon adsorption. For the substrates that were not rinsed after adsorption, more laminin was observed lining the walls and base of the groove region than on the mesa surface due to surface tension (Figure 4-2). The groove regions fluoresced with higher intensities but the mesas were fluorescing as well. There were also spots on the mesas with a higher intensity of fluorescence equal to that lining the grooves. These observations were made initially using fluorescence microscopy and were confirmed using confocal microscopy (Figure 4-3). The substrates that had been rinsed (after sitting overnight coated with laminin and removal of the excess laminin) had an overall lower intensity of fluorescence of FITC-conjugated laminin. The laminin was evenly distributed over the entire surface of the substrate (Figure 4-4). Rinsing with PBS resulted in a washing effect on the laminin that was concentrated in

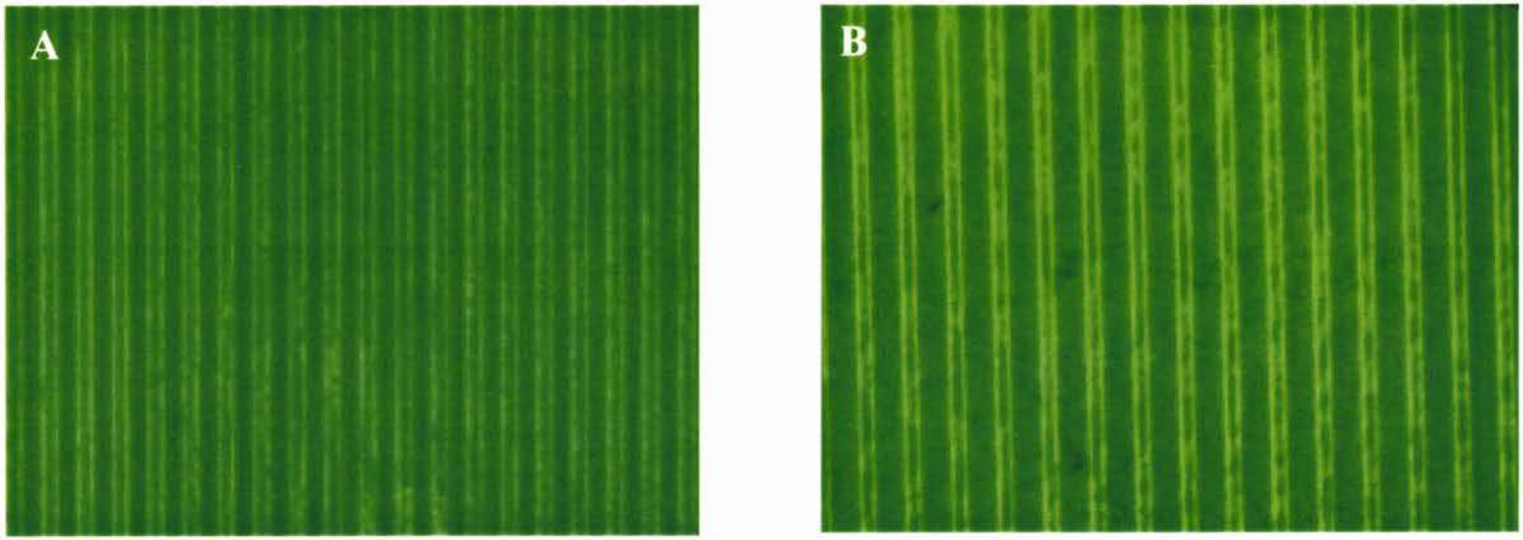

Figure 4-2. Fluorescent images of FITC-conjugated protein distributions on micropatterned PS substrates. (A) FITC-conjugated PLL deposited in the grooves on a 10 x 10 x 4 μm PS substrate. (B) FITC-conjugated laminin lining the walls and base of the groove region on a 10 x 20 x 3 μm PS substrate.

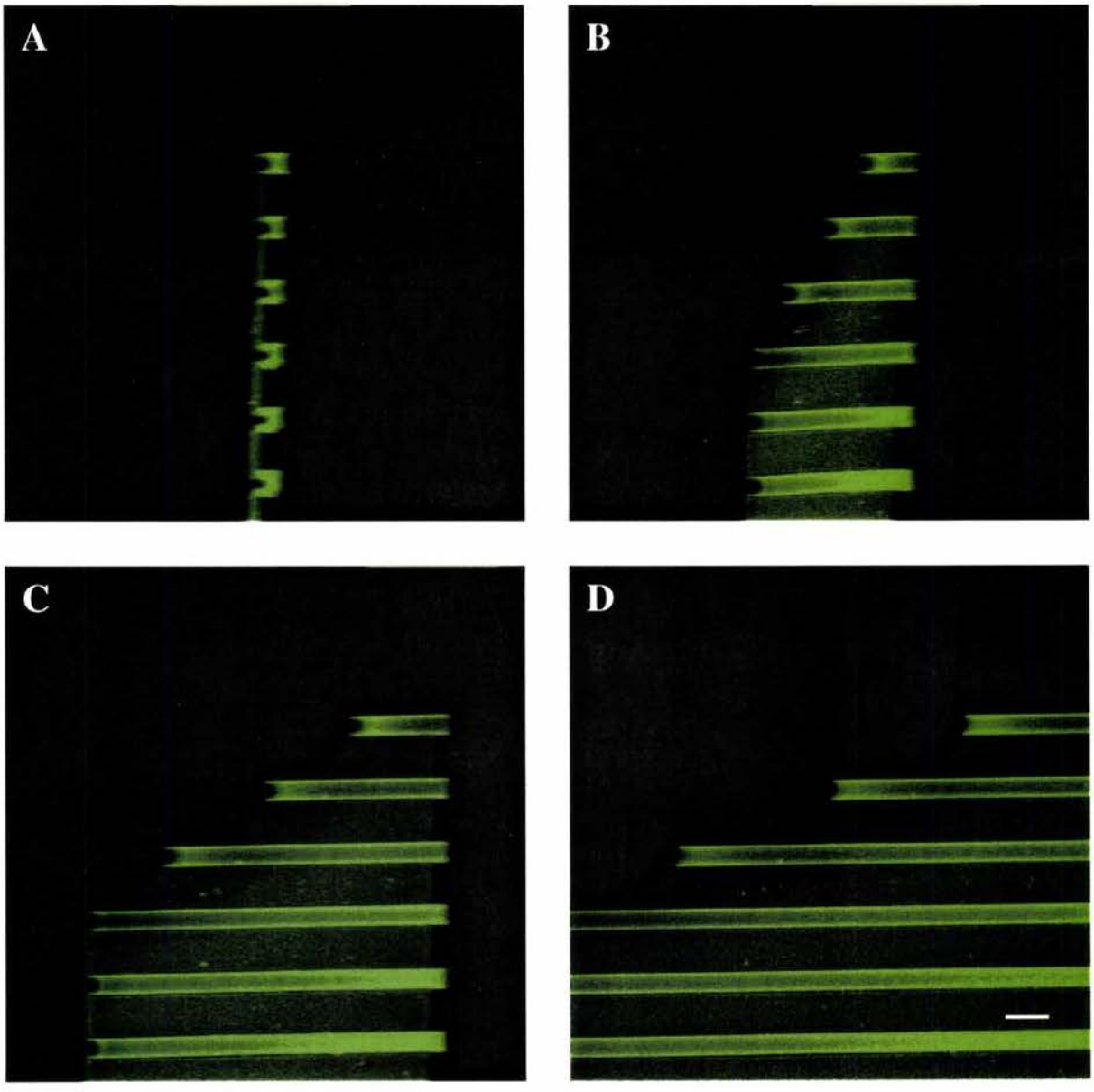

Figure 4-3. Confocal images of the FITC-conjugated laminin on micropatterned (10 x 20 x 3 μm) PS substrates. (A-D) A three-dimensional (3-D) representation of the PS substrate was reconstructed showing how more laminin was concentrated at the walls and base of the groove regions. Each image is the result of shifting the angle of the view of the 3-D image starting at (A) the cross-section and rotating 90° toward the (D) the last plane of the reconstruction. This substrate was imaged at the interface where the laminin adsorbed and did not adsorb on the PS substrate. Scale bar, 20 μm.

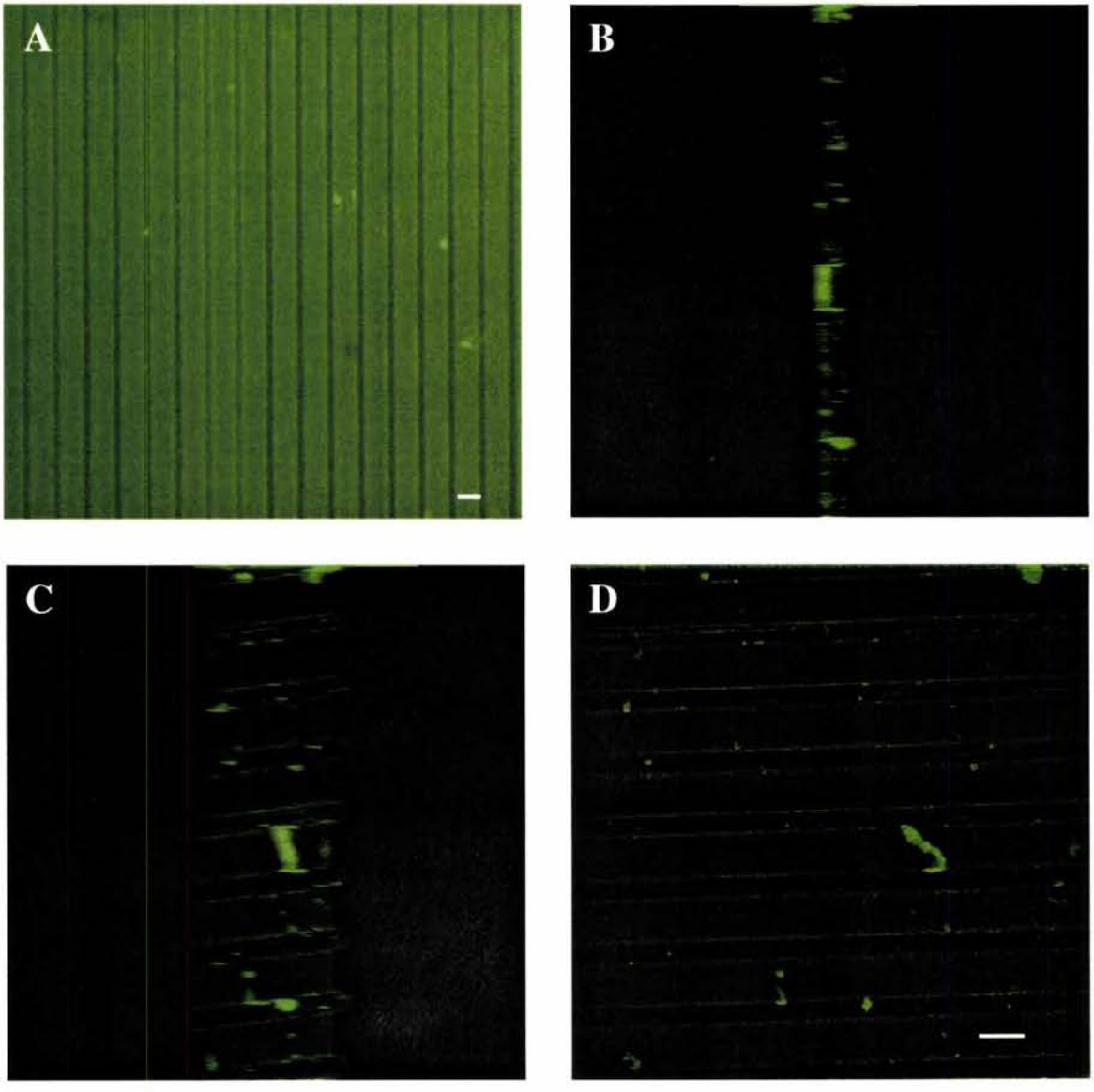

Figure 4-4. Fluorescent and confocal images of the FITC-conjugated laminin on micropatterned (10 x 20 x 3 μm) PS substrates. (A) Fluorescent image showing the FITC- conjugated laminin evenly distributed over the surfaces of the PS substrate after rinsing with PBS. Scale bar, 20 μm. (B-D) Confocal image of a reconstructed three-dimensional representation of the PS substrate showing how laminin fluoresced with a lower intensity due to the washing effect of the PBS rinse. Each image is the result of shifting the angle of the view of the 3-D image starting at (B) the cross-section and rotating 90° toward the (D) the last plane of the reconstruction. Scale bar, 20 μm.

the grooves initially. The control substrates without FITC-conjugated laminin adsorbed to the surface did not exhibit any fluorescence.

After performing the laminin assays, it was discovered that the most effective procedure for laminin adsorption was applying the laminin for 15-20 minutes, removing the excess solution by perpendicular suction with a micropipette, and letting the substrate dry at room temperature for at least four hours and then immediately seeding the substrates with the astrocytes. Due to surface tension effects, this method of adsorbing the laminin resulted in more laminin localizing in the grooves than on the mesa surface of the substrate. All further experiments were conducted with laminin adsorbed to the PS substrates.

4.3 Astrocyte Seeding and Histological Cell Staining / Immunocytochemistry

Astrocytes were seeded onto micropatterned/non-patterned film surfaces (mentioned above) with adsorbed PLL (100-1000 μg/ml borate buffer) or laminin (10-100 μg/ml EBSS) adsorbed on the surface and those without PLL or laminin at initial densities varying from 7,500 to 100,000 cells/cm^2. Histological and immunocytochemical staining procedures were used to enhance the visibility of the astrocytes on the polystyrene substrates. Live cell staining procedures were used to observe astrocyte behavior and morphology as they grew on the PS substrates. One of two methods of staining was used to enhance the visibility of the cells during experimentation. The cells were labeled in cell suspension prior to cell seeding and relabeled after they were seeded on the substrates if necessary using one of two stains, the lipophilic tracer, $DiIC_{18}$ (DiI), or membrane permeant tracer, carboxyfluorescein diacetate succinimdyl ester (CFDA SE). When staining with DiI, the cells appeared red using the tetramethyl-rhodamine isothiocyanate (TRITC) filter. After staining with CFDA SE, the astrocytes appeared green using the FITC filter. Initially, DiI was used in experiments with the astrocytes on the PS substrates. For most experiments with the astrocytes on the PS films, the CFDA SE tracer was used for live cell staining. The CFDA SE stain was found to be a more effective stain because it stained the astrocytes uniformly while the DiI tended to stain only the membrane of the Golgi body of the cell rather than the entire cell (Figure 4-5). The CFDA SE allowed better visualization of the processes of the astrocytes (Figure 4-5). This tracer gave a strong fluorescence signal from the cultured cells for four to five days depending on the proliferation rate of the astrocytes.

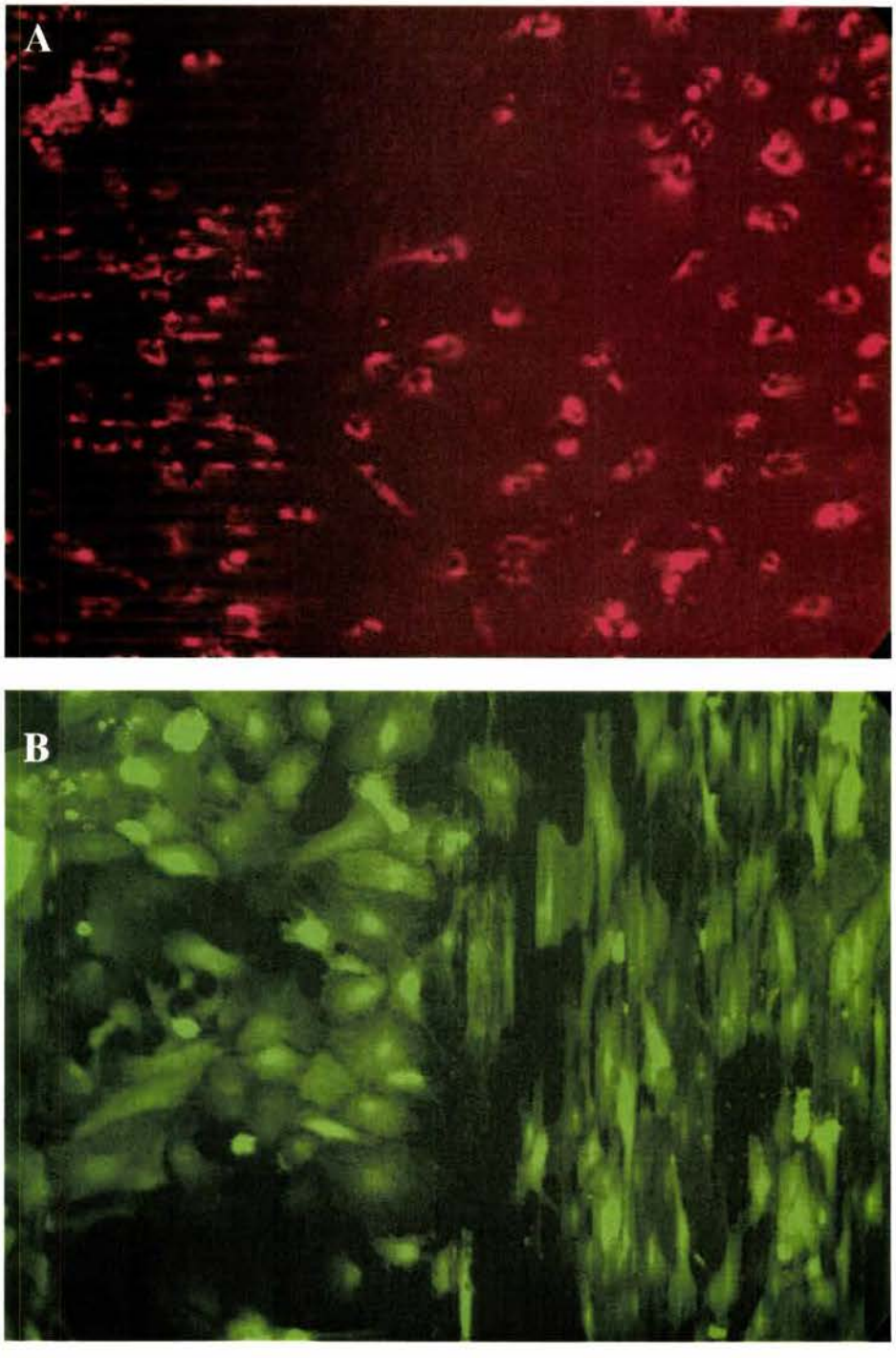

Figure 4-5. (A) Astrocytes labeled with DiI in cell suspension. (B) Astrocytes were labeled with CFDA SE in cell suspension. In (A) and (B), astrocytes were seeded on 10 x 20 x 3 μm/ non-patterned and 10 x 10 x 4 μm/ non-patterned PS substrates, respectively.

Immunocytochemistry was used to determine what percentage of the cells in the cultures were, in fact, type-1 astrocytes. Astrocytes were identified on the basis of the presence of glial fibrillary acidic protein (GFAP) immunoreactivity. Cultures were also screened with MAP-2ab and RIP antibodies for neurons and oligodendrocytes, respectively. It was determined that in astrocyte cultures seeded onto coverslips, over 85% of the cells were immunopositive for GFAP and, therefore, were astrocytic in nature (Figure 4-6). No immunoreactivity was observed with the MAP2-ab and RIP antibodies verifying that the cultures were free of neurons and oligodendrocytes, respectively. Furthermore, for cells seeded on laminin coated PS substrates (square films consisting of 0.5 cm^2 of patterned substrate adjacent to 0.5 cm^2 of non-patterned substrate), over 90% of the cells on these substrates were immunopositive for GFAP (Figure 4-7). These percentages verify that the vast majority of cells observed on the PS substrates were astrocytes.

Two histological stains, phalloidin and DAPI, were used on the preparations following fixation alone or fixation and immunocytochemistry. F-actin microfilaments were labeled with Alexa Fluor 568 phalloidin (PHALL). In addition to the GFAP antibodies, it enabled examination of the orientation of the filamentous cytoskeleton of the astrocytes on the PS substrates (Figure 4-8). Nuclei of the astrocytes were stained with DAPI. This stain allowed the visualization of the nuclei on the PS substrates and counting of the total number of cells adhering to the substrate after 24 or 72 hours (Figure 4-8).

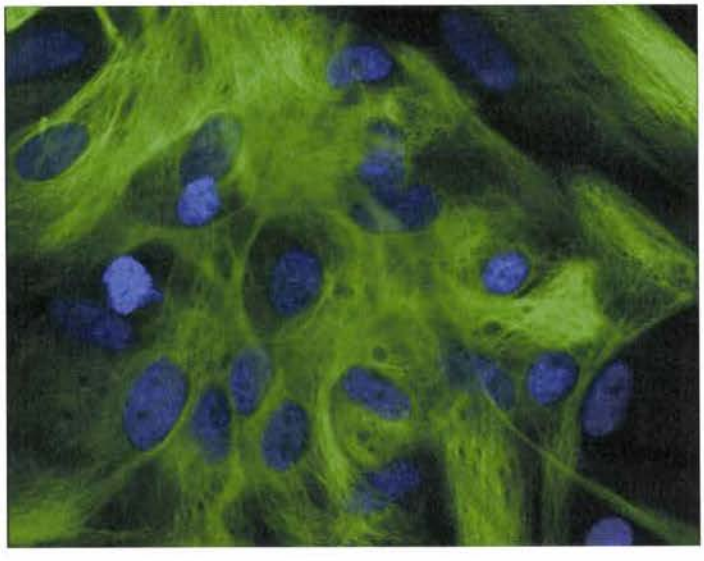

Figure 4-6. Astrocyte cultures used for seeding onto PS substrates were immunopositive for mGFAP. This is a merged image created by superimposition of mGFAP and DAPI fluorescence images.

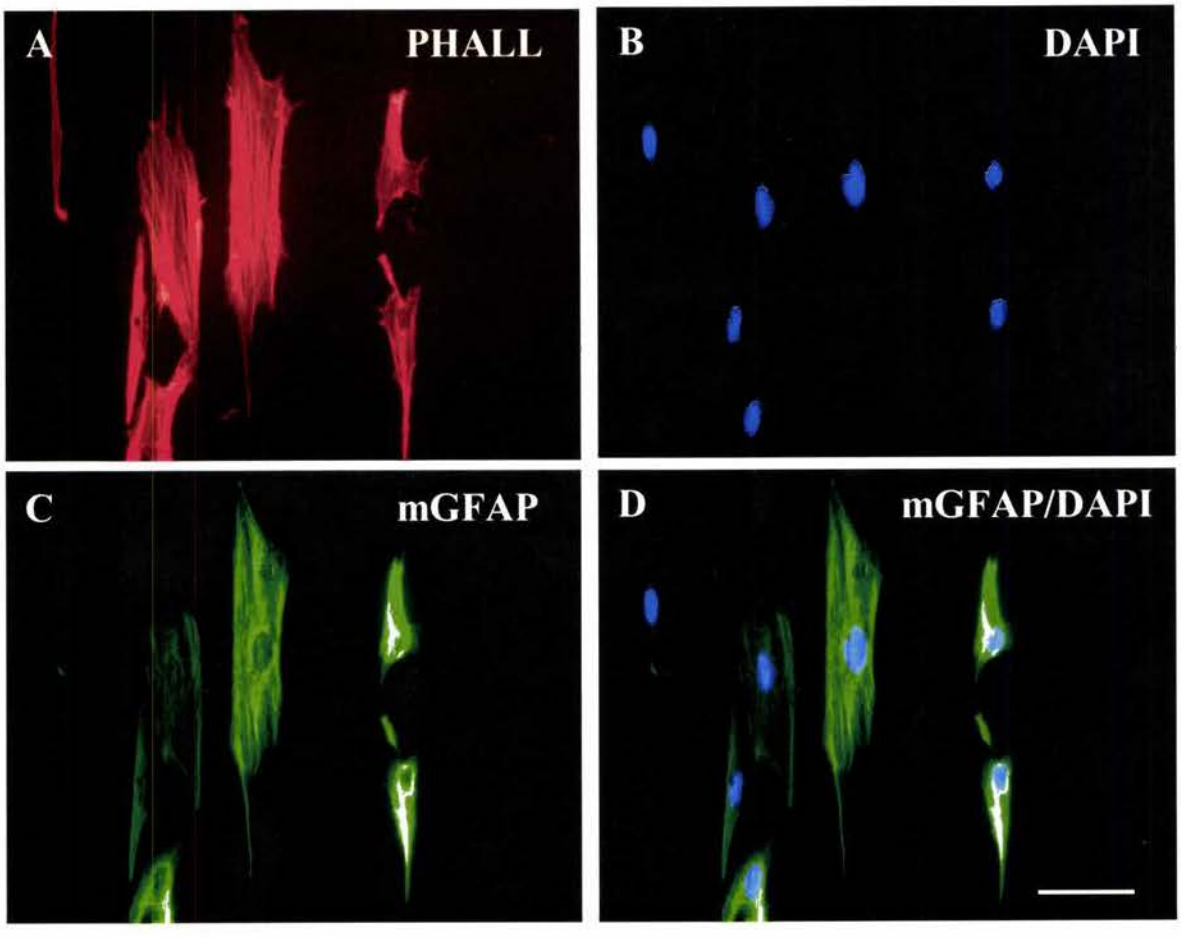

Figure 4-7. Expression of astrocytic marker by enriched astrocytes cultures on laminin coated micropatterned (10 x 20 x 3 μm) PS substrates (grooves at 90°). (A, B) Fluorescent images of phalloidin stained F-actin and nuclei of astrocytes stained with DAPI and immmunoreactivity for (C, D) mGFAP. (D) Merged image created by superimposition of mGFAP and DAPI fluorescence images. Images were taken from substrate fixed at 24 hours after seeding. Scale bar, 60 μm.

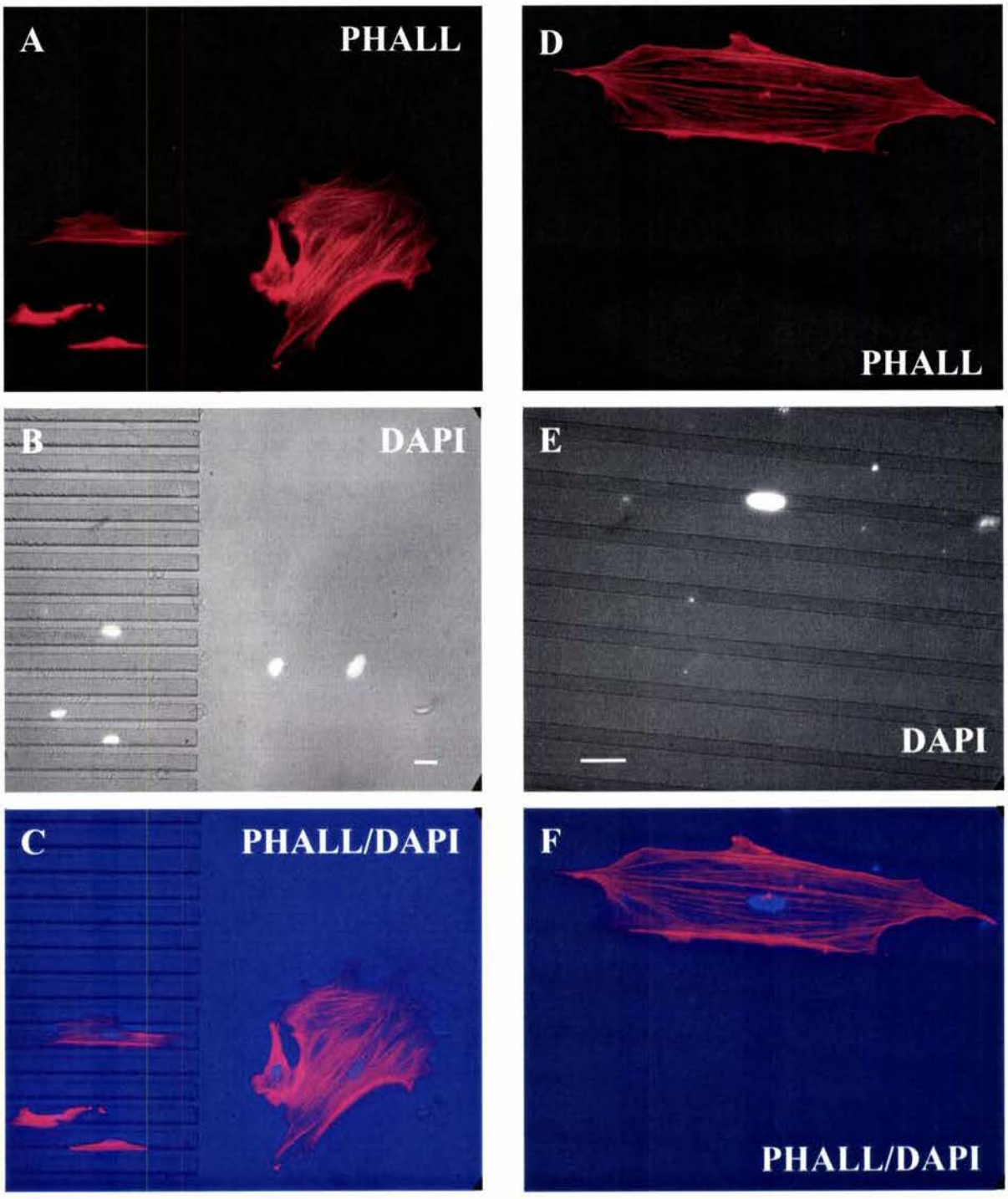

Figure 4-8. Fluorescent images showing histological staining of astrocytes on PS substrates. (A, D) The F-actin filaments of the astrocytes were labeled with Alexa Fluor 568 phalloidin. (B, E) The nuclei of the astrocytes were labeled with DAPI. (C, F) Merged image created by superimposition of phalloidin (F-actin) and DAPI (nuclei) fluorescence images. (A- C) and (D-F) are same location images taken with 20X and 40X objectives, respectively. Scale bars, 20 μm.

4.4 Physical Guidance on the Micropatterned Substrates

A valuable technique for fabricating microgrooves with various pattern sizes and spacings on polystyrene films was developed. The effects of the three-dimensional topographical pattern on cell behavior *in vitro* were studied by observing astrocytes seeded onto the micropatterned PS substrates. Pattern optimization was performed by our group in the recent past using dorsal root ganglia and Schwann cells [1-3]. By seeding Schwann cells and neurons separately on polymeric substrate surfaces and observing cell behavior, the dimensions of the micropatterns etched into the substrate surface were optimized. Various groove widths, groove spacings, and groove depths were studied to select the pattern that resulted in the best cell alignment. Substrates with patterns of 10 x 10 μm and 10 x 20 μm were found to provide the best Schwann cell and neurite alignment [1-3]. Depths of 2, 3 and 4 μm were further evaluated for cell alignment. Neurite alignment was most affected by groove depth with groove depths greater than 2 μm acting as physical barriers enabling better alignment of the cells [1, 2]. These results corresponded to other observations that deeper grooves produce larger cellular guidance response and extent of orientation increases with groove depth [4].

To study the physical guidance of astrocytes on micropatterned PS films, the above pattern dimensions were used with the assumption that astrocytes will exhibit behavior similar to Schwann cells and dorsal root ganglia. The behavior and morphology of astrocytes on the patterned substrates was compared to that on non-patterned substrates. On the non-patterned substrates, the astrocytes possessed a flattened, spread morphology (Figure 4-9). Process extension in any particular direction was not observed. In contrast, on the patterned substrates, the astrocytes were observed as having highly elongated extensions of their filamentous cytoskeleton, both F-actin microfilaments and glial intermediate filaments, in the direction of the grooves (Figure 4-9). Thus, it was apparent that the behavior of the astrocytes was influenced by the three-dimensional topography of the substrate. These cells were uniformly aligned in the direction of the grooves on substrate patterns of 10 x 10 x 4 μm and 10 x 20 x 3 μm. The 10 μm groove width directed the astrocytes to extend their filaments along the inside of the groove or at the boundary between the groove and the mesa. The groove spacings of 10 μm and 20 μm influenced the cells to spread in the direction of the grooves.

The astrocytes were observed as having one or a combination of reactions to the topography of the substrate. The cells exhibited (1) extension of their filaments along the inside of the groove, (2) extension of their filaments along a mesa in the direction of the groove, (3) extension of their

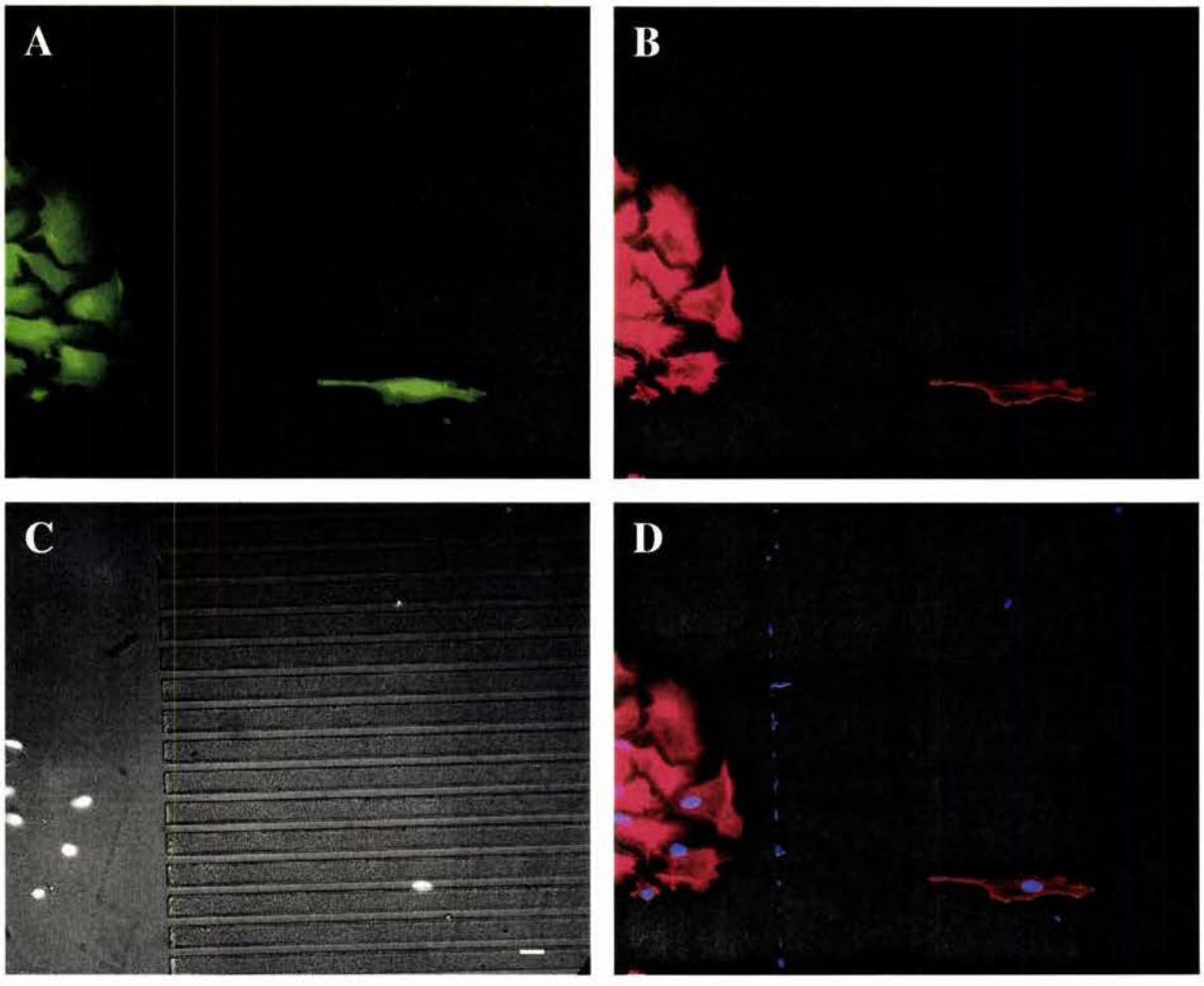

Figure 4-9. Fluorescent images of astrocytes cultured on 10 x 20 x 3 μm/ non-patterned PS substrates. An astrocyte aligned along the groove on the patterned side (right side) while astrocytes were oriented randomly on non-patterned side (left side) of substrate. (A) Astrocytes were stained with CFDA SE. (B) The F-actin microfilaments were stained with Alexa Fluor 568 phalloidin. (C) The nuclei of the astrocytes were stained with DAPI. (D) Merged image created by superimposition of phalloidin (F-actin: red) and DAPI (nuclei: blue) fluorescence images. (A-D) Same location images taken with a 20X objective. Scale bar, 20 μm.

filaments along the step edge or boundary between the groove and the mesa eventually extending filaments down inside a groove, (4) extension of their filaments from the cell body inside a groove to the mesa and growth along the mesa in the direction of the groove, and (5) bridging across grooves with filaments aligning on the mesas on either side of the groove. It has been hypothesized that the astrocytes preferred the mesa of the cell, as it was inherently rougher than the groove surface. This was a result of the silicon wafer surface etched by RIE and was observed in SEM images (Figure 4-10). Steps have not been taken to characterize the roughness of the mesas or the grooves. It was thought that cell-to-cell communications may have also played a role in astrocyte behavior. In some instances, the topographical control of the patterned substrates may be limited by chemical factors released by the astrocytes in response to their environment. Astrocytes were observed extending filaments to other astrocytes and/or migrating toward nearby astrocytes on patterned (Figure 4-11) and non-patterned substrates. Furthermore, astrocytes adhering to the substrate as an aggregate of cells were observed spanning grooves and trying to conform to the patterned substrates (Figure 4-12).

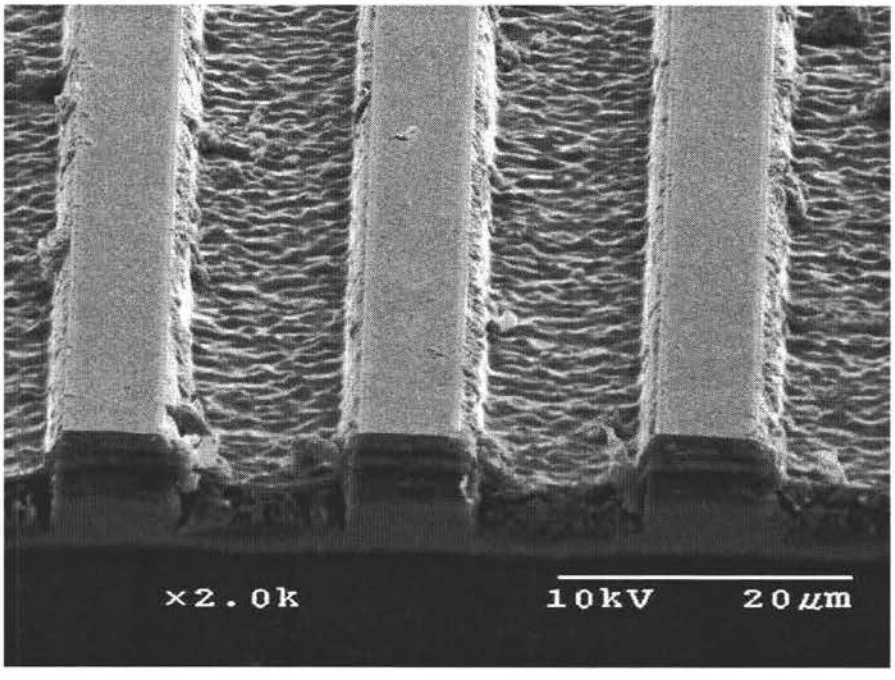

Figure 4-10. An SEM image of a patterned silicon wafer having groove dimensions of 10 x 10 x 4 μm etched using RIE. Scale bar, 20 μm.

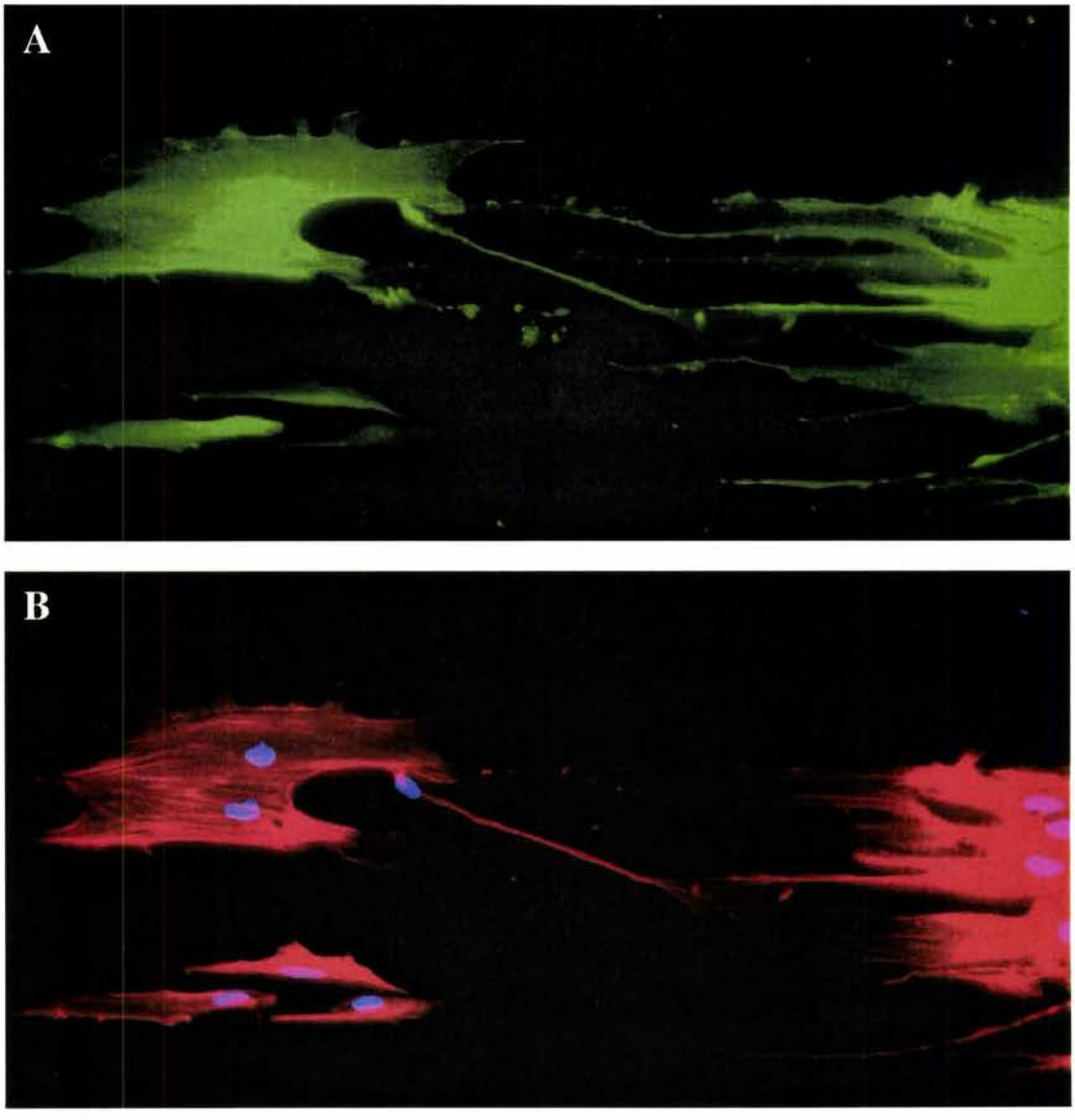

Figure 4-11. Astrocytes on micropatterned PS substrates (grooves at 0°) extending processes from one group of astrocytes to another. (A) Astrocytes were labeled with CFDA SE in cell suspension. (B) Merged image created by superimposition of Alexa Fluor 568 phalloidin (F-actin: red) and DAPI (nuclei: blue) fluorescence images. (A and B) Same location images taken with a 20X objective.

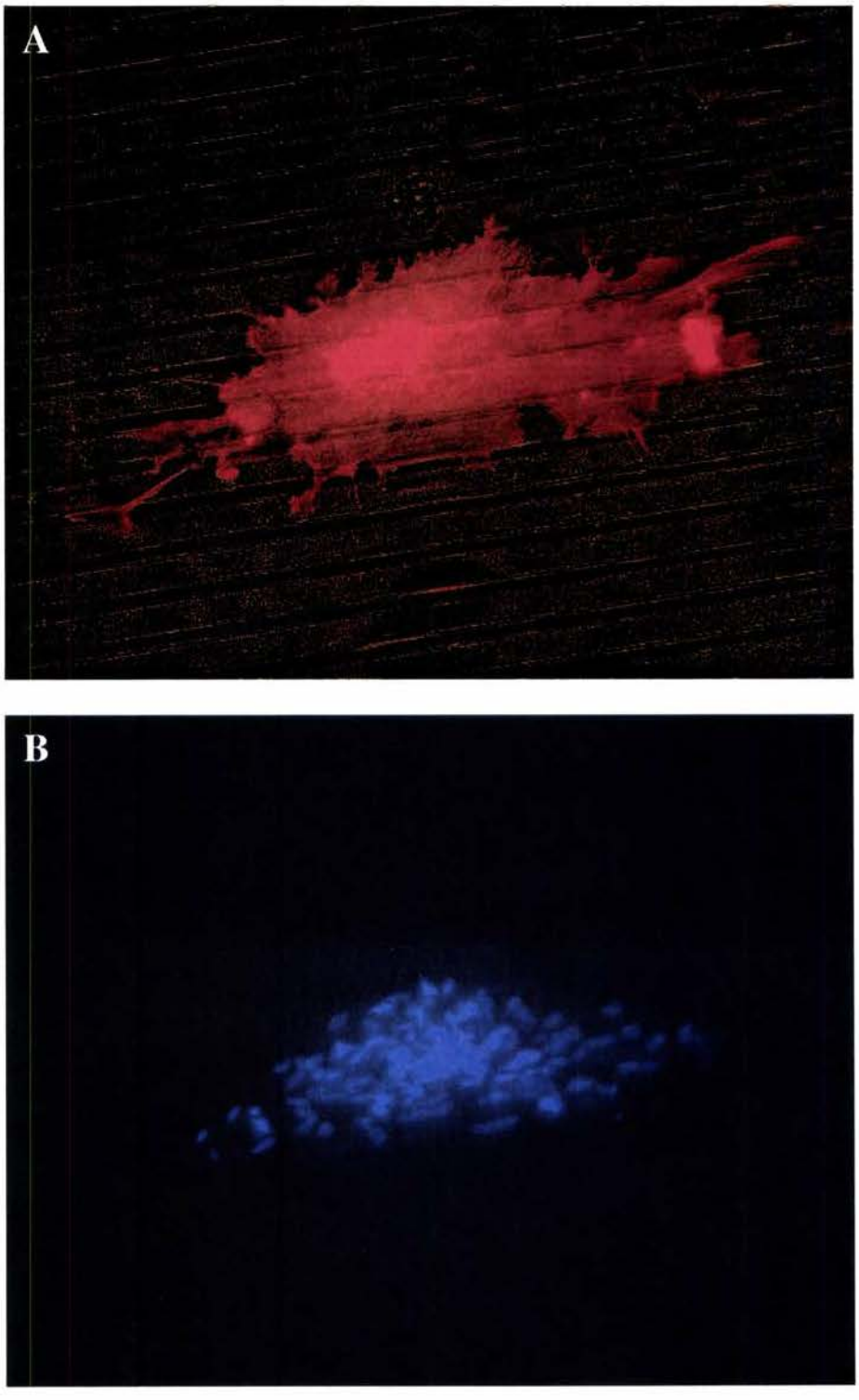

Figure 4-12. An aggregate of astrocytes was observed spreading across and spanning grooves on 10 x 20 x 3 μm PS substrates. (A) The F-actin filaments of the astrocytes were stained with phalloidin. (B) The nuclei of the astrocytes were stained with DAPI. (A and B) Same location images taken with 20X objective.

Astrocyte orientation on the 10 x 20 x 3 μm patterned (no laminin) and non-patterned (no laminin) PS substrates was analyzed and compared. Cell orientation was measured by MetaMorph software as the angle of the longest chord through each astrocyte relative to the horizontal axis of the imported image. Statistical analysis was performed on the values of the differences between the orientation of the cell and the orientation of the groove on the substrate. Therefore, lower means of orientation reveal that the cell is closer to following the orientation of the groove/mesa pattern. Cell alignment was determined by whether the longest chord through the individual astrocyte made an angle of $\leq 20°$ with the direction of the grooves. The proportion of cells falling in this group as well as those whose longest chord made an angle of $\leq 10°$ with the direction of the grooves were calculated. For an initial cell seeding density of approximately 20,000 cells per substrate, the evidence suggested that cell orientation on the patterned substrates was significantly different than on the non-patterned substrates with the same trend observed after 24 and 72 hours. Figure 4-13 shows the distributions of cell orientation (taken as the difference between the orientation of the grooves and the astrocytes orientation) on 10 x 20 x 3 μm patterned and non-patterned substrates. It can be seen astrocytes on the control or non-patterned substrates were randomly oriented while the majority of astrocytes on the patterned substrates were aligned in the direction of the grooves. It was estimated that a significantly higher percentage of cells aligned on patterned substrates than non-patterned substrates within 20° and 10° of the direction of the grooves (Figure 4-14). The estimate of the percentage of cells growing at an angle of $\leq 20°$ with the direction of the grooves was 70% for patterned substrates and 20% for non-patterned substrates. The estimate of the percentage of cells growing at an angle of $\leq 10°$ degrees with the direction of the grooves was 49.3% for patterned substrates and 10.8% for non-patterned substrates ($\alpha = 0.05$). In an effort to influence adhesion and spreading of cells on the substrate and increase the percentage of cells aligning to the direction of the grooves, chemical modifications to the PS substrate were investigated.

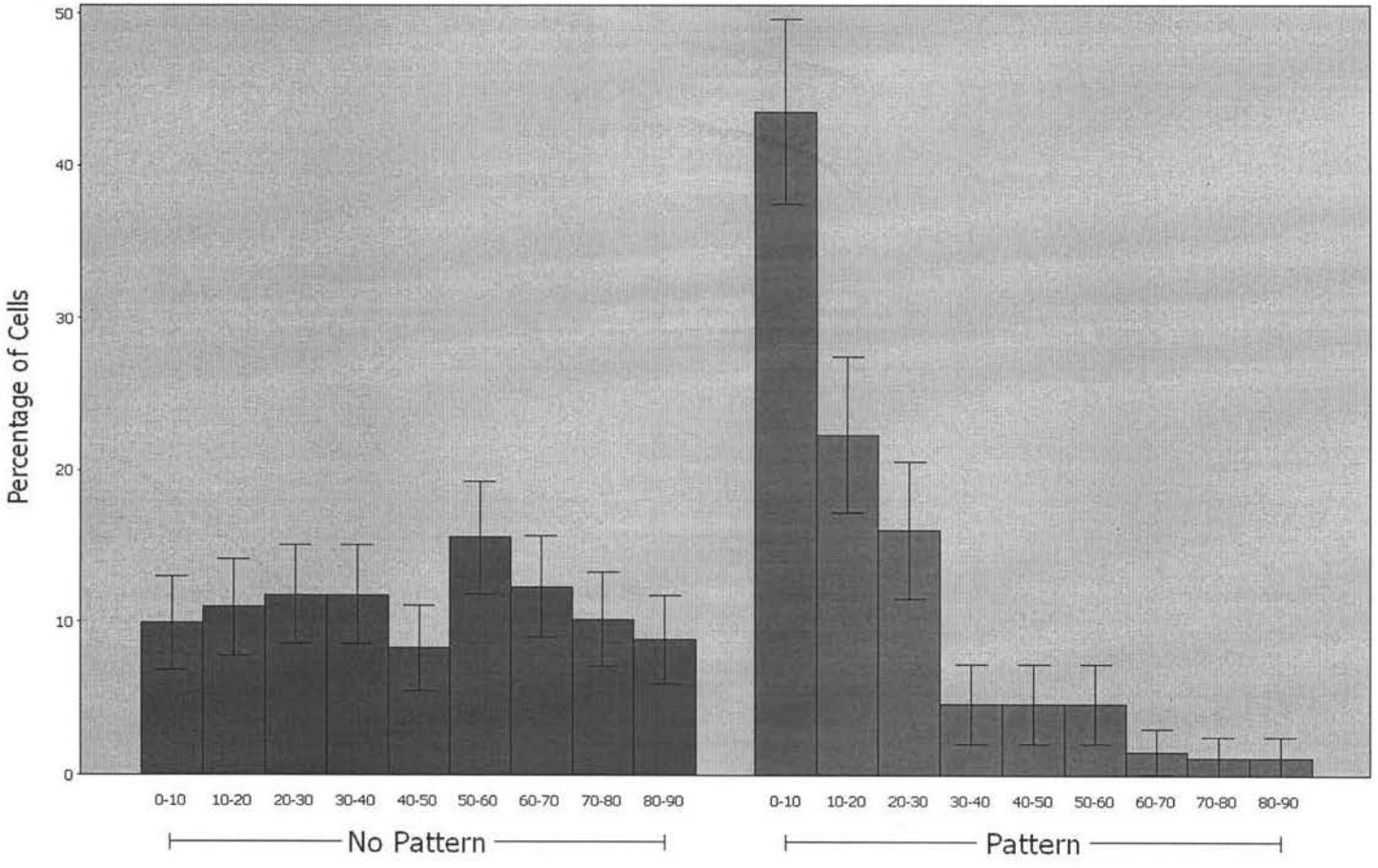

Figure 4-13. The distribution of the astrocyte orientation on 10 x 20 x 3 μm patterned and non-patterned PS substrates (without laminin) for an initial seeding density of 20,000 cells per cm^2. The data were grouped in 10° sectors from 0° to 90°. Data shown are mean values ±1 standard deviation of N= 372 (individual astrocyte measurements) for No Pattern and N= 255 for Pattern.

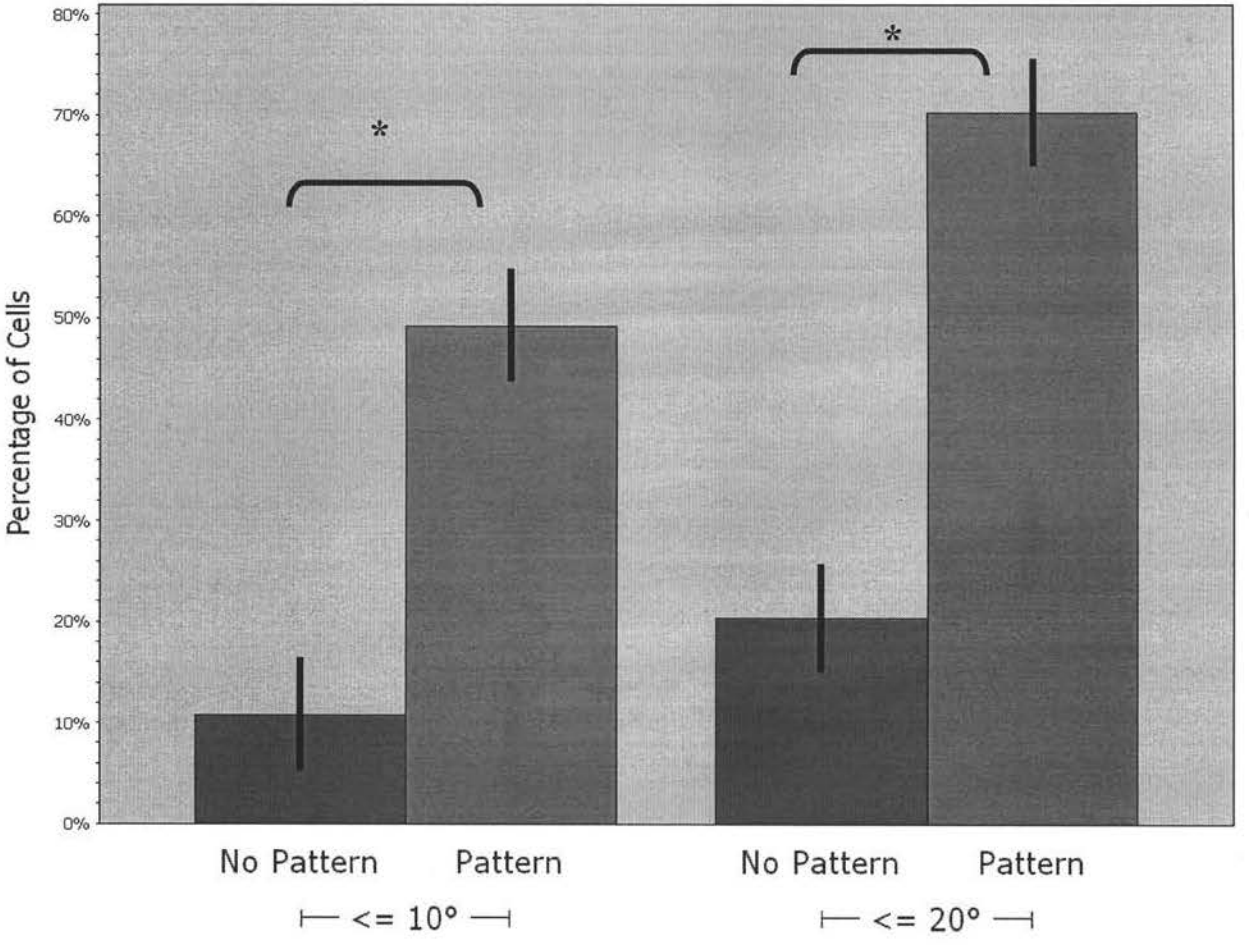

Figure 4-14. The effect of topography on astrocyte orientation on PS substrates. For an initial seeding density of 20,000 cells per cm^2, the 10 x 20 x 3 μm pattern had a significant effect on the orientation of the astrocytes with respect to the groove direction. The percentage of astrocytes aligning within ≤ 10° and ≤ 20° of the groove direction is demonstrated for 24 and 72 hours. Error bars represent ±1 standard error of the estimate of the mean (s.e.m.) percentage of cells (N= 5 for Pattern and N= 5 for No Pattern for each test : ≤ 10° and ≤ 20°). Statistically significant differences are marked with an asterisk ($P < 0.05$).

4.5 Chemical Guidance Modifications

To improve cell adhesion and spreading of the astrocytes, poly-L-lysine or laminin were adsorbed to the PS substrates. Poly-L-lysine (PLL) at 100 μg/ml in borate buffer was used to coat the PS substrates. This concentration was used after reviewing procedures used in other laboratories applying PLL to non-degradable substrates for astrocytes studies. PLL did not improve astrocyte adhesion or spreading on the PS substrates. In studies with astrocytes seeded onto PLL coated substrates at various seeding densities from approximately 15,000 cells per substrate to 100,000 cells per substrate, there were no significant differences in the morphology or numbers of cells on PLL coated substrates versus substrates not coated with PLL. Laminin, a large (~850 kDa) noncollagenous multidomain glycoprotein, was applied to the PS substrates and evaluated. This protein is a major component of the extracellular matrix and had domains specifically for cell adhesion. The concentrations of laminin used in experimentation were 10 or 100 μg/ml in EBSS. Astrocyte adhesion was estimated by evaluating the total cell count for defined regions on the non-patterned substrates. It was observed that laminin improved cell adhesion cell spreading for an initial cell seeding density of 20,000 cells/substrate with no significant differences between the low and high laminin concentrations. On LAM- NO PATT substrates, after 24 hours in the presence of laminin (10 μg/ml EBSS), cell adhesion was significantly improved and approximately 3 times more cells adhered to the PS substrates with laminin than without laminin (Figure 4-15). To account for the exponential rate of growth of the astrocytes, a natural log transformation was used for the statistical analysis of the cell counts per substrate area. Using this transformation, cell adhesion was significantly improved on LAM- NO PATT substrates after 24 hours and after 72 hours as compared to NO LAM- NO PATT substrates analyzed at the same time periods. However, there was no significant difference in the effect of laminin between the 24 and 72 hour data analyzed. At each time period, approximately 3 times more cells adhered to the PS substrates with laminin than without laminin.

At an initial cell seeding density of 20,000 cells per cm^2, astrocyte orientation was evaluated. The astrocytes exhibited wide processes spread over the laminin coated substrate surface with similar trends in orientation measurements observed and measured after 24 and 72 hours. Astrocytes adhered to LAM- NO PATT PS substrates and exhibited spreading their filaments as compared to

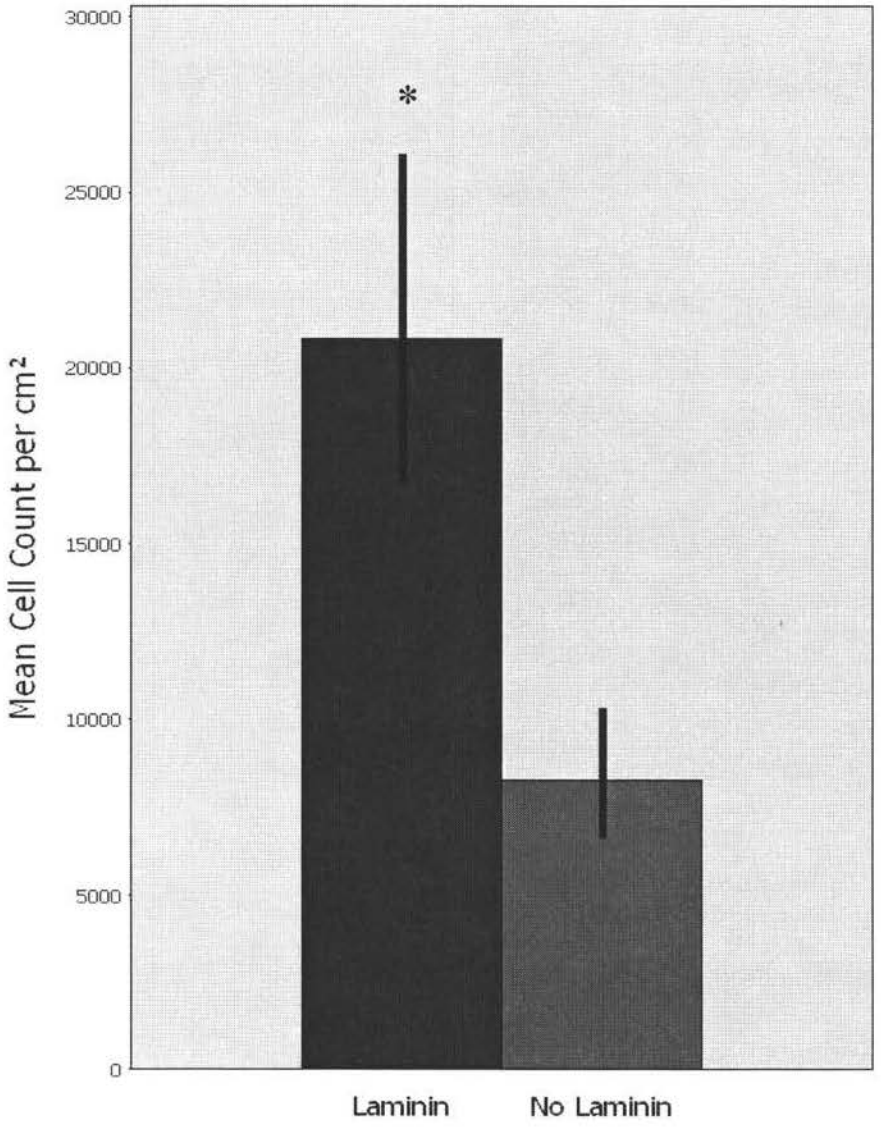

Figure 4-15. The effect of laminin on astrocyte adhesion to the non-patterned PS substrates at an initial seeding density of 20,000 cells per cm^2. The mean cell density was estimated for cell adhesion after 24 hours. A natural log transformation was used for statistical analysis of cell count per substrate area and the values were retransformed for presentation here. Data shown are mean values ± s.e.m. ($N = 3$ for Laminin and $N = 3$ for No Laminin). Statistically significant differences are marked with an asterisk ($P < 0.05$).

NO LAM- NO PATT PS substrates where the cells remained in small clusters with little spreading from the cluster over time (Figure 4-16). Overall, the astrocytes on NO LAM- NO PATT PS substrates appeared smaller with shorter processes and more circular in shape. On the non-patterned substrates, with or without laminin, the astrocytes were oriented randomly and were not aligned in any particular direction. The percentages of cells growing at an angle of $\leq 20°$ on the LAM- NO PATT and NO LAM- NO PATT PS substrates were 20.3% (Figure 4-17). The percentages of cells growing at an angle of $\leq 10°$ were 8.3% for the LAM- NO PATT PS substrates and 10.8% for NO LAM- NO PATT PS substrates (Figure 4-17) ($\alpha = 0.05$). Due to the improvement of astrocyte adhesion to laminin and the alignment resulting from growth on the micropatterned substrates, the combined effect of laminin on the behavior of astrocytes on the 10 x 20 x 3 μm pattern was examined.

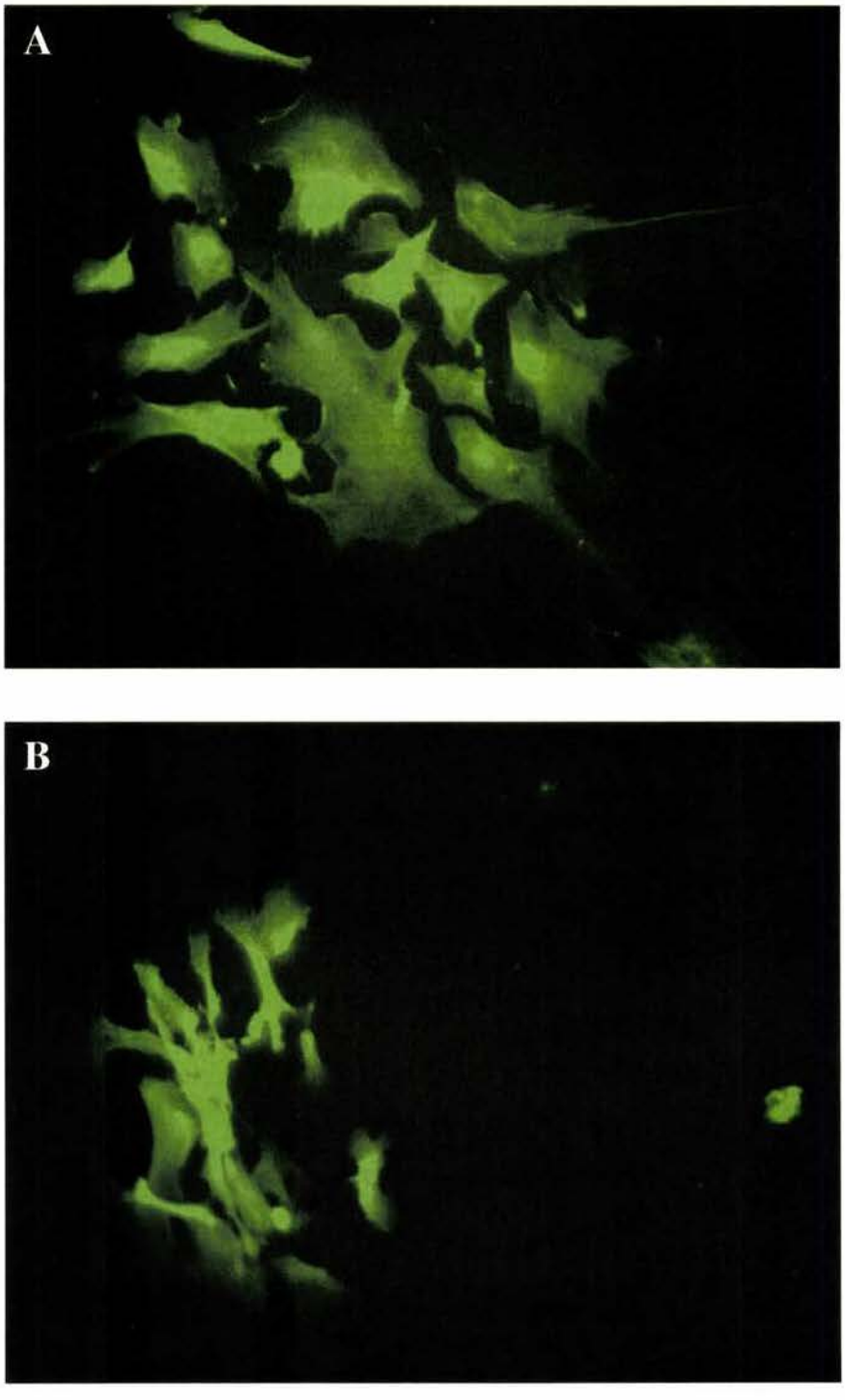

Figure 4-16. Astrocytes cultured on non-patterned substrates for 72 hours. (A) A PS substrate coated with laminin at 10 μg/ml in EBSS. (B) PS substrate not coated with laminin. Astrocytes were stained with CFDA SE in cell suspension.

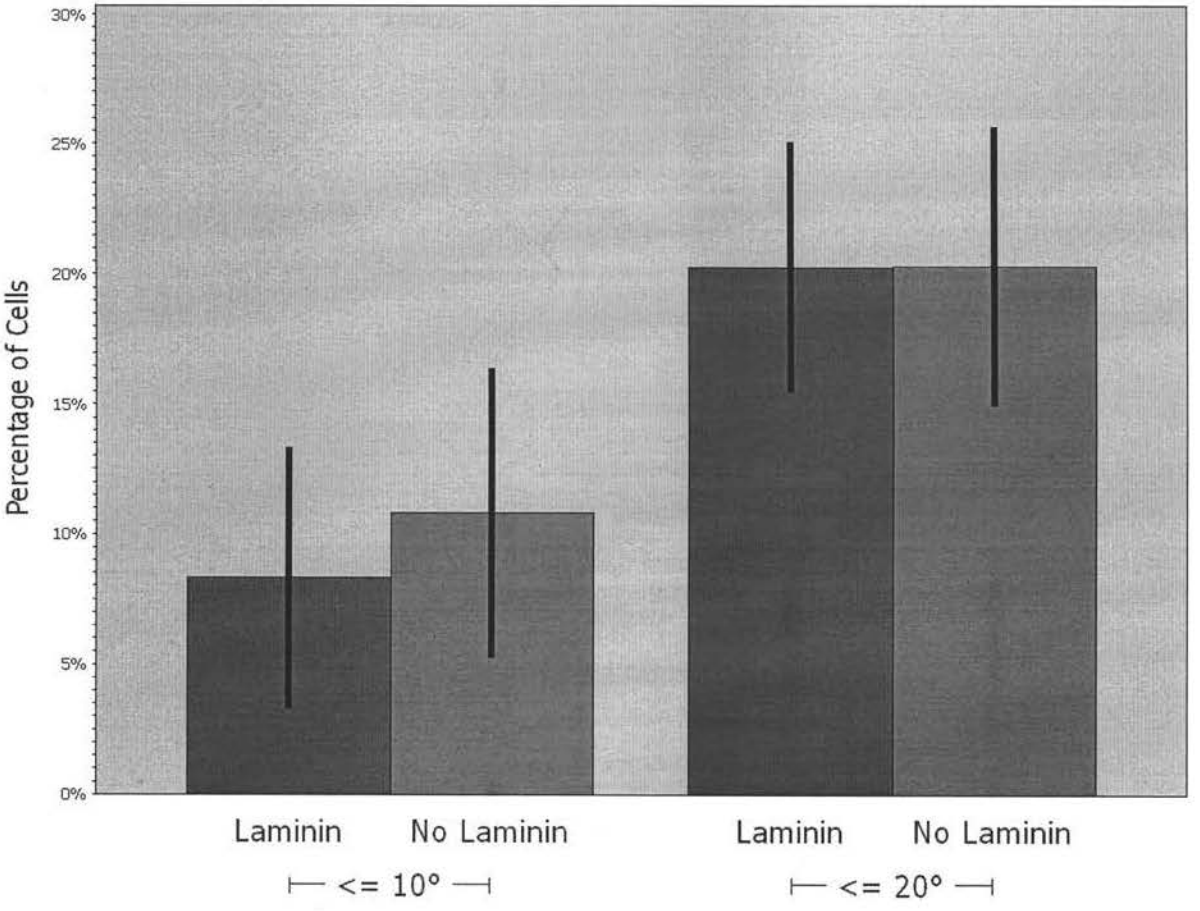

Figure 4-17. The effect of laminin on astrocyte orientation on non-patterned PS substrates. The percentage of astrocytes aligning within ≤ 10° and ≤ 20° of the groove direction is demonstrated. The data presented here is a combination of 24 and 72 hour data as similar trends were observed after each time point. Error bars represent ±1 standard error of the estimate of the mean (s.e.m.) percentage of cells (N= 5 for No Laminin and N= 6 for Laminin for each test: ≤ 10° and ≤ 20°).

4.6 Chemical and Physical Guidance

Using the combination of adsorbed laminin as a chemical cue and the topography of the patterned substrate for physical guidance, directed astrocyte growth was investigated. The behavior of the astrocytes on the micropatterned (10 x 20 x 3 μm) / non-patterned substrate surfaces coated with laminin (10 μg/ml EBSS) and those not coated with laminin was analyzed for three seeding densities of approximately 7500, 13,000 and 20,000 cells per cm^2. The synergistic effects of the chemical and physical guidance cues of the laminin coated micropatterned PS substrate were studied in terms of astrocyte adhesion and directed growth.

4.6.1 Laminin and astrocyte behavior on the patterned polystyrene substrates

Laminin was selectively deposited on the PS substrates by applying a surface tension based technique. Using this technique, more laminin was localized in the groove region than the mesas promoting alignment of the astrocytes. The astrocytes were exposed to more laminin per area in the grooves than on the surface of the mesas. The combination of laminin and the three-dimensionality of the grooves provided directional guidance for the astrocytes.

The effect of laminin on astrocyte adhesion was measured quantitatively on all substrate types. For an initial seeding density of 20,000 cells per cm^2, it was determined that adsorbing laminin (10 μg/ml in EBSS) onto the surface of the micropatterned (10 x 20 x 3 μm) PS substrate resulted in the adhesion of significantly more cells to the substrate after 24 hours than non-coated substrates (Figure 4-18) (α= 0.05). There was no significant evidence of a difference between the number of cells adhering to patterned and non-patterned PS substrates (α= 0.05). Cell adhesion and spreading of the astrocytes were improved on the LAM- PATT PS substrates without lessening the effect of the physical guidance of the pattern. Improved cell adhesion on laminin coated substrates was expected, as the laminin is an ECM protein that has two or more domains that bind to laminin receptor proteins on the surface of cells. It is responsible for many cell-basement membrane interactions including adhesion, migration and proliferation. As seen in Figure 4-19, astrocytes observed on LAM-PATT substrates were flattened and aligned in the direction of the grooves. On NO LAM-PATT substrates, alignment was still observed, however, due to the astrocytes remaining in tight clusters, a lower proportion of the cells was oriented in the direction of the grooves as compared to astrocyte alignment on LAM-PATT substrates.

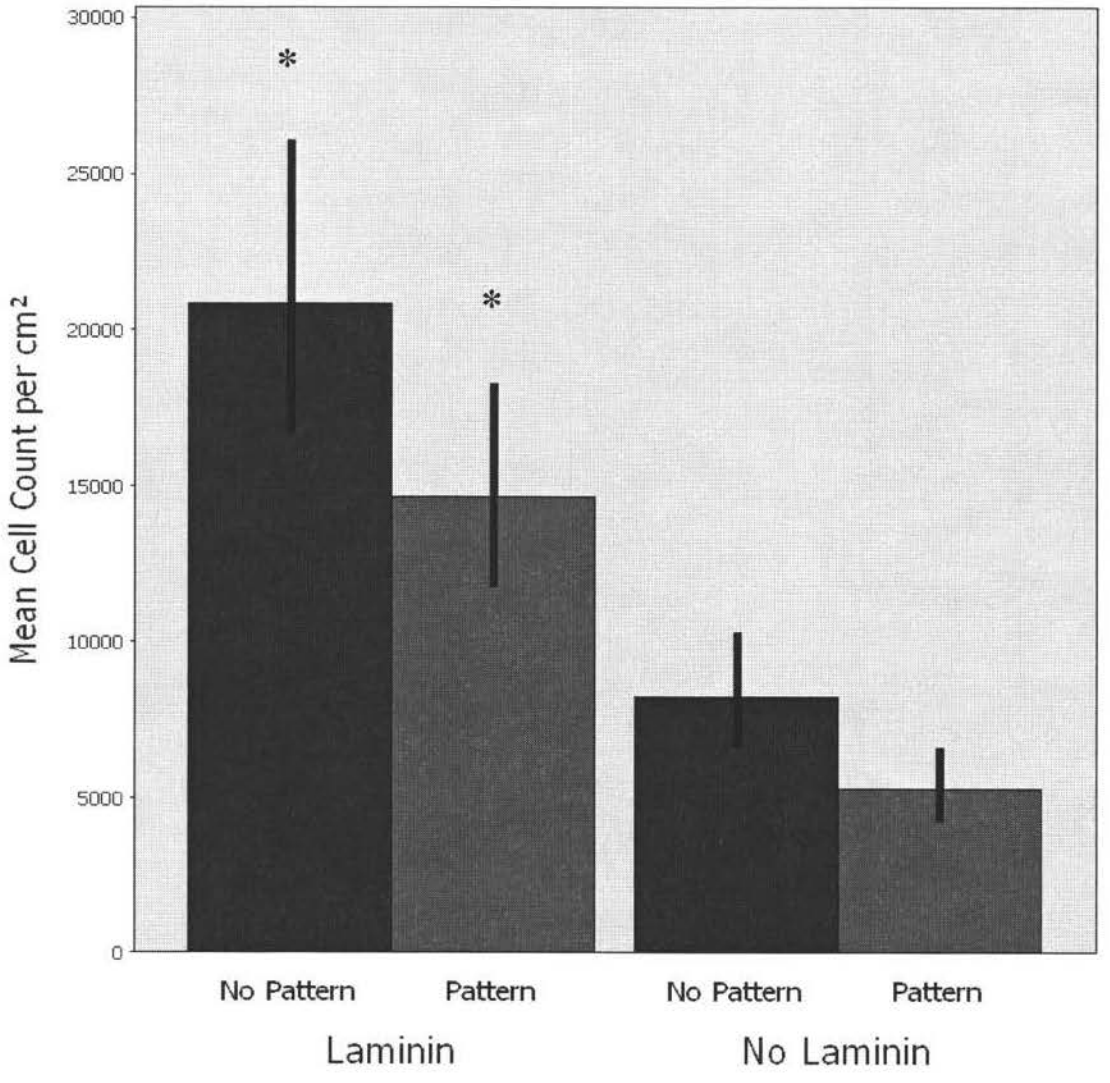

Figure 4-18. The effect of laminin (10 µg/ml) on the number of astrocytes adhering to the 10 x 20 x 3 µm patterned and non-patterned substrates PS substrates for an initial seeding density of approximately 20,000 cells per cm^2. The mean cell density was estimated for cell adhesion after 24 hours. A natural log transformation was used for statistical analysis of cell count per substrate area and the values were retransformed for presentation here. Data shown are mean values ± s.e.m. ($N = 6$ For Laminin and $N = 6$ for No Laminin). Statistically significant differences are marked with an asterisk ($P < 0.05$). All laminin coated substrates had significantly higher cell densities than those without laminin.

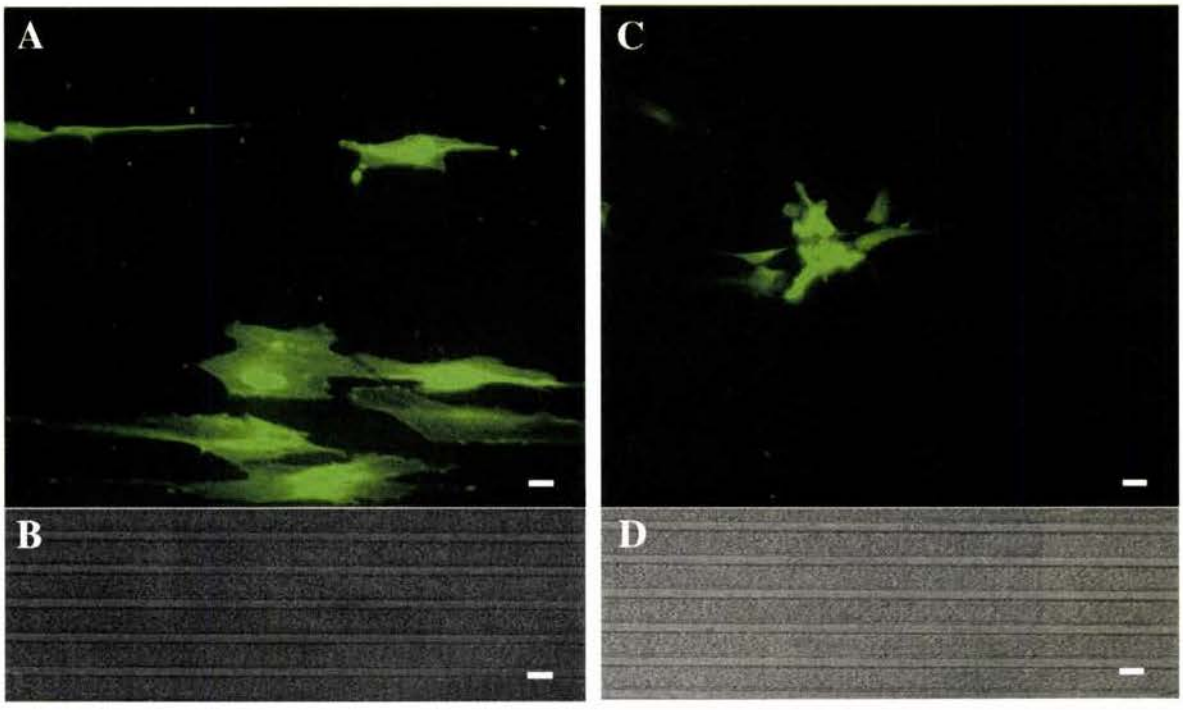

Figure 4-19. Astrocytes on 10 x 20 x 3 μm patterned PS substrates (grooves at 0°). (A) Fluorescent image of astrocytes seeded on a laminin coated (10 μg/ml in EBSS) patterned PS substrate. Astrocytes were spread out on these substrates and aligned in the direction of the grooves. (B) Light microscopy image of the laminin coated patterned PS substrate onto which the cells were seeded. (C) Fluorescent image of astrocytes seeded onto a patterned PS substrate without laminin. A lower proportion of astrocytes aligned on these substrates due to clustering of the cells. (D) Light microscopy image of the patterned PS substrate without laminin onto which the cells were seeded. (A and C) Cells were labeled with CFDA SE in cell suspension prior to seeding. Images were taken from PS substrate fixed 72 hours after seeding. (A-D) Scale bars = 20 μm.

4.6.2 Astrocyte adhesion and alignment on patterned polystyrene substrates

The chemical and topographical effects of the laminin coated micropatterned PS substrate were studied in terms of astrocyte adhesion and alignment. Adhesion was estimated by evaluating the total cell count for defined regions on the four types of PS substrates. The proportion of astrocytes whose longest chord makes an angle of $\leq 20°$ with the direction of the grooves was used as a measure of cell alignment in these studies. The proportion of cells falling in this group as well as those whose longest chord made an angle of $\leq 10°$ with the direction of the grooves were also evaluated.

4.6.2.1 *Effect of the pattern and the level of laminin on astrocyte alignment*

The combination of laminin and the three-dimensionality of the grooves provided directional guidance for the astrocytes on the PS substrate (Figure 4-20). For an initial seeding density of 20,000 cells per cm^2, the micropatterned (10 x 20 x 3 μm) PS substrates with laminin (10 μg/ml in EBSS) in the grooves were found to have a significant effect on astrocyte alignment with similar trends observed and measured after 24 and 72 hours. The laminin concentrated in the grooves improved initial cell adhesion and elaboration of astrocyte processes in the direction of the grooves significantly. The distributions of cell orientation (taken as the difference between astrocyte orientation and the orientation of the grooves) for the patterned and non-patterned substrates with adsorbed laminin on the surface are presented in Figure 4-21. Again, it can be seen that astrocytes on the control or LAM-NO PATT substrates were randomly oriented while the majority of astrocytes on the LAM-PATT substrates were aligned in the direction of the grooves. It was estimated with $\alpha = 0.05$ that a significantly higher percentage of cells aligned on LAM-PATT substrates than on LAM-NO PATT substrates within 10° and 20° of the direction of the grooves (Figure 4-22). The percentage of cells growing at an angle of $\leq 20°$ with the direction of the grooves was 85.5 % for LAM-PATT substrates and 20.3% for LAM-NO PATT substrates. The percentage of cells growing at an angle of $\leq 10°$ with the direction of the grooves was 60% for LAM-PATT substrates and 8.3% for LAM-NO PATT substrates ($\alpha = 0.05$).

The effect that the pattern had on directing astrocyte alignment was significantly different for micropatterned PS substrates with adsorbed laminin as compared to those without laminin. From statistical analysis performed on the astrocyte orientation data, it was determined with $\alpha = 0.05$ that the presence of laminin had a significant effect on the alignment of the astrocytes on the patterned substrates. For an initial seeding density of 20,000 cells per cm^2, the influence of the laminin coated

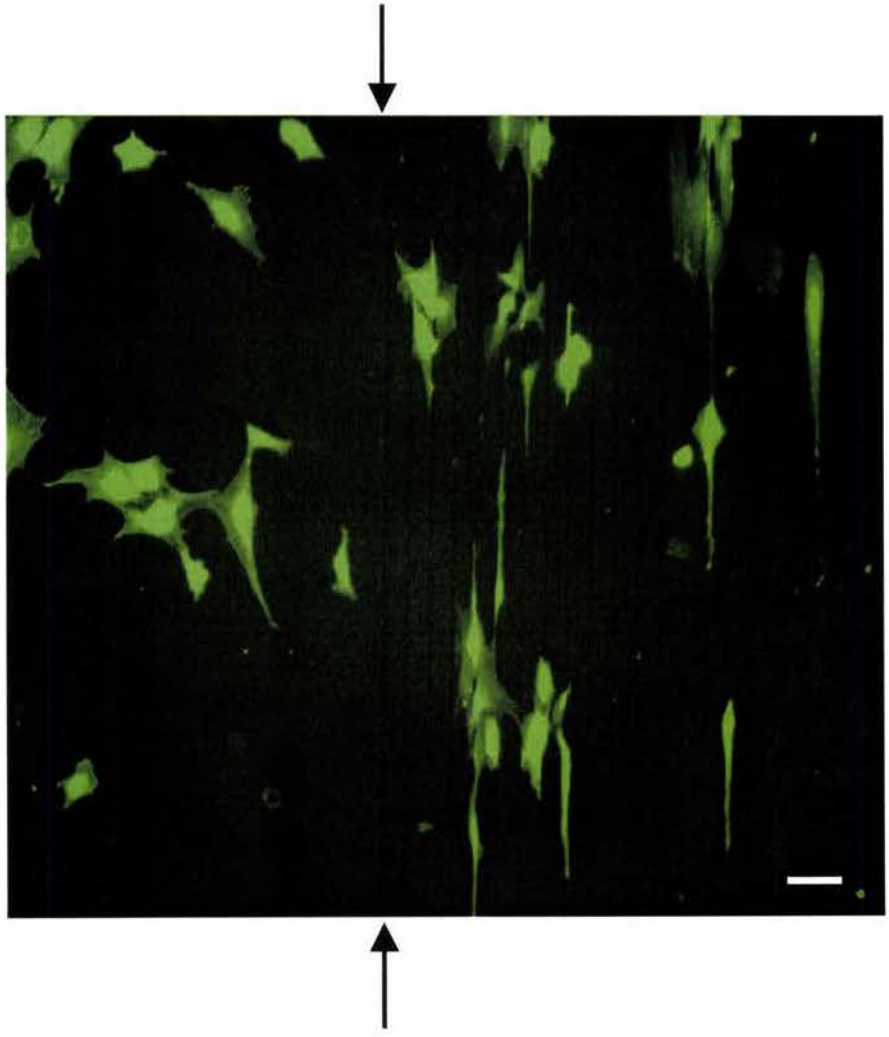

Figure 4-20. Astrocytes cultured on a laminin coated (10 μg/ml in EBSS) PS substrate. On the 10 x 20 x 3 μm LAM-PATT/ LAM-NO PATT substrate, astrocytes are aligned in the direction of the grooves on the patterned side (grooves at 90°; right of the arrows) while astrocytes were oriented randomly on the non-patterned side (left of the arrows) of the substrate. Astrocytes were stained with CFDA SE in cell suspension prior to seeding. Images were taken from PS substrate fixed 24 hours after seeding. Scale bar = 30 μm.

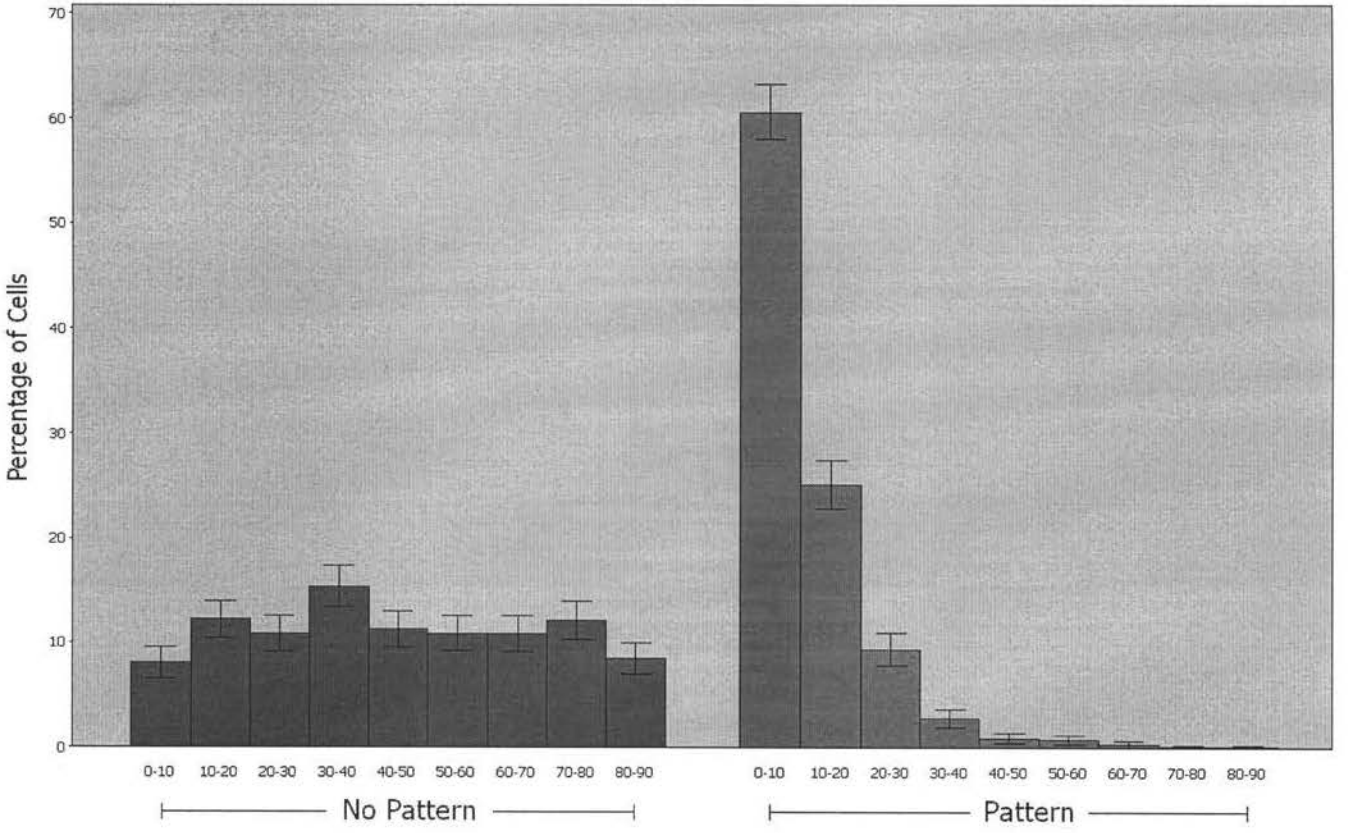

Figure 4-21. The distribution of the astrocyte orientation on 10 x 20 x 3 μm patterned and non-patterned PS substrates in the presence of laminin (10 μg/ml) for an initial seeding density of 20,000 cells per cm^2. The data were grouped in 10° sectors from 0° to 90°. Data shown are mean values ±1 standard deviation of $N = 1287$ (individual astrocyte measurements) for LAM- NO PATT and $N = 1325$ for LAM-PATT.

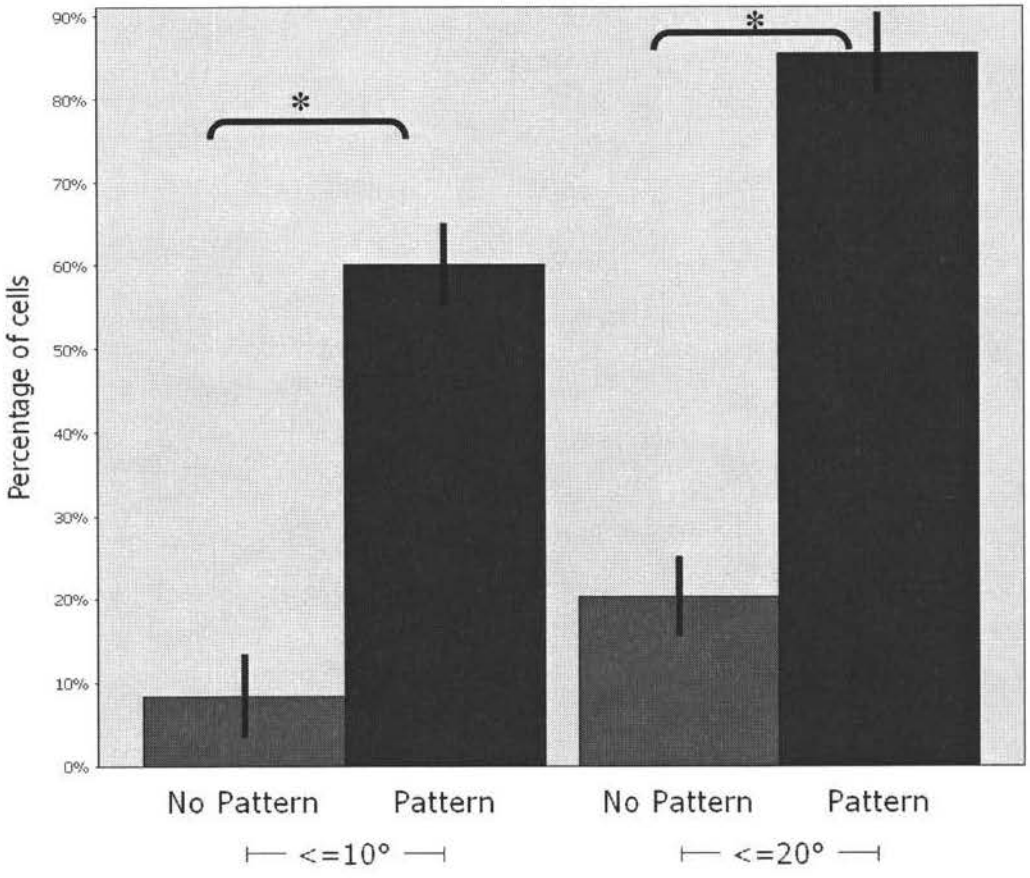

Figure 4-22. The effect of physical and chemical guidance cues on astrocyte orientation on PS substrates. For an initial seeding density of 20,000 cells per cm^2, the laminin coated (10 µg/ml in EBSS) patterned (10 x 20 x 3 µm) substrate had a significant effect on the orientation of the astrocytes with respect to the groove direction. The percentage of astrocytes aligning within ≤ 10° and ≤ 20° of the groove direction is demonstrated for 24 and 72 hours. Error bars represent ± s.e.m. percentage of cells ($N = 6$ for LAM-PATT and $N = 6$ for LAM-NO PATT for each test: ≤ 10° and ≤ 20°). Statistically significant differences are marked with an asterisk ($P < 0.05$).

10 x 20 x 3 μm patterned substrate to direct alignment within 20° and within 10° of the groove direction was compared to that on micropatterned substrates without laminin. A significantly higher percentage of cells aligned in direction of the grooves on LAM-PATT substrates than NO LAM-PATT substrates. The percentage of cells growing at an angle of ≤ 20° with the direction of the grooves was 85.5% ± 4.8% for LAM-PATT substrates and 70.3% ± 5.4% for NO LAM-PATT substrates ($\alpha = 0.05$; standard errors for 6 substrates are reported here). The percentage of cells growing at an angle of ≤ 10° with the direction of the grooves was 60% ± 5% for LAM-PATT substrates and 49.3% ± 5.6% for NO LAM-PATT substrates ($\alpha = 0.05$; standard errors for 6 substrates are reported here).

4.6.2.2 *Effect of cell seeding density on astrocyte adhesion and alignment*

In an effort to determine the most effective seeding density for alignment, astrocytes were cultured at initial seeding densities of approximately 7500, 13,000 and 20,000 cells per cm^2. PS substrates with laminin adsorbed at 10 μg/ml EBSS onto the surface resulted in a significantly higher proportion of attached cells at all seeding densities tested (Figure 4-23) with no significant evidence of a difference between the number of cells adhering to patterned and non-patterned substrates ($\alpha = 0.05$). Furthermore, the influence of the 10 x 20 x 3 μm pattern to direct alignment within 20° (Figure 4-24) and within 10° (Figure 4-25) of the groove direction was evaluated over all three seeding densities. The percentages of astrocyte alignment on the PS substrates were not significantly different for the initial seeding densities examined ($\alpha = 0.05$).

With seeding densities higher than 20,000 cells/cm^2, clustering of cells was more likely and the astrocytes became contact inhibited. Individual astrocytes did not have enough space in the area surrounding them to sense the topography of the substrate and therefore were not able to become oriented in the direction of the grooves. Furthermore, when too many astrocytes were cultured on the substrate, the effect of the topography of the substrate was decreased due to a monolayer of cells spanning the grooves (Figure 4-26). It was also observed that if the cells were not extensively triturated, cell clumping would occur. Proper evaluation of alignment could not be performed in these cases due to tight clusters of astrocytes that could not be individually measured in terms of orientation.

The combination of physical and chemical guidance cues had a significant effect on the alignment of the astrocytes on polymer films *in vitro*. Seeding the astrocytes at the initial densities ranging from 7500 to 20,000 cells/cm^2, over 85% alignment (≤ 20° with the direction of the grooves)

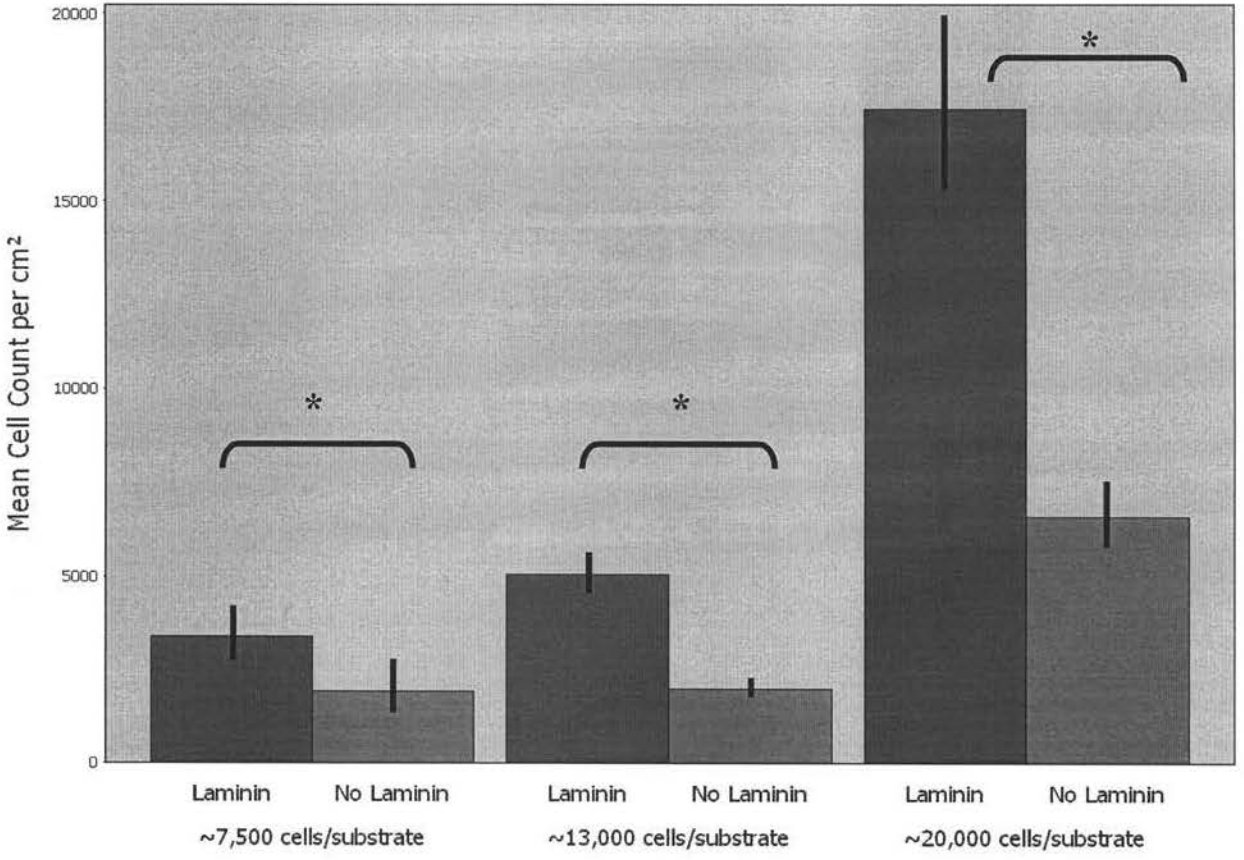

Figure 4-23. Effect of laminin on astrocyte adhesion to 10 x 20 x 3 μm micropatterned/non-patterned PS substrates. The mean cell densities on laminin coated substrates versus substrates without laminin were estimated for initial seeding densities of approximately 7500, 13,000, 20,000 cells per cm^2. The data presented here is for cell adhesion after 24 hours and was pooled across LAM-PATT and LAM-NO PATT substrates. Data shown are mean values ± s.e.m. ($N = 8$ for 7500 cells per cm^2; $N = 10$ for 13,000 cells per cm^2; $N = 12$ for 20,000 cells per cm^2). Statistically significant differences are marked with an asterisk ($P < 0.05$).

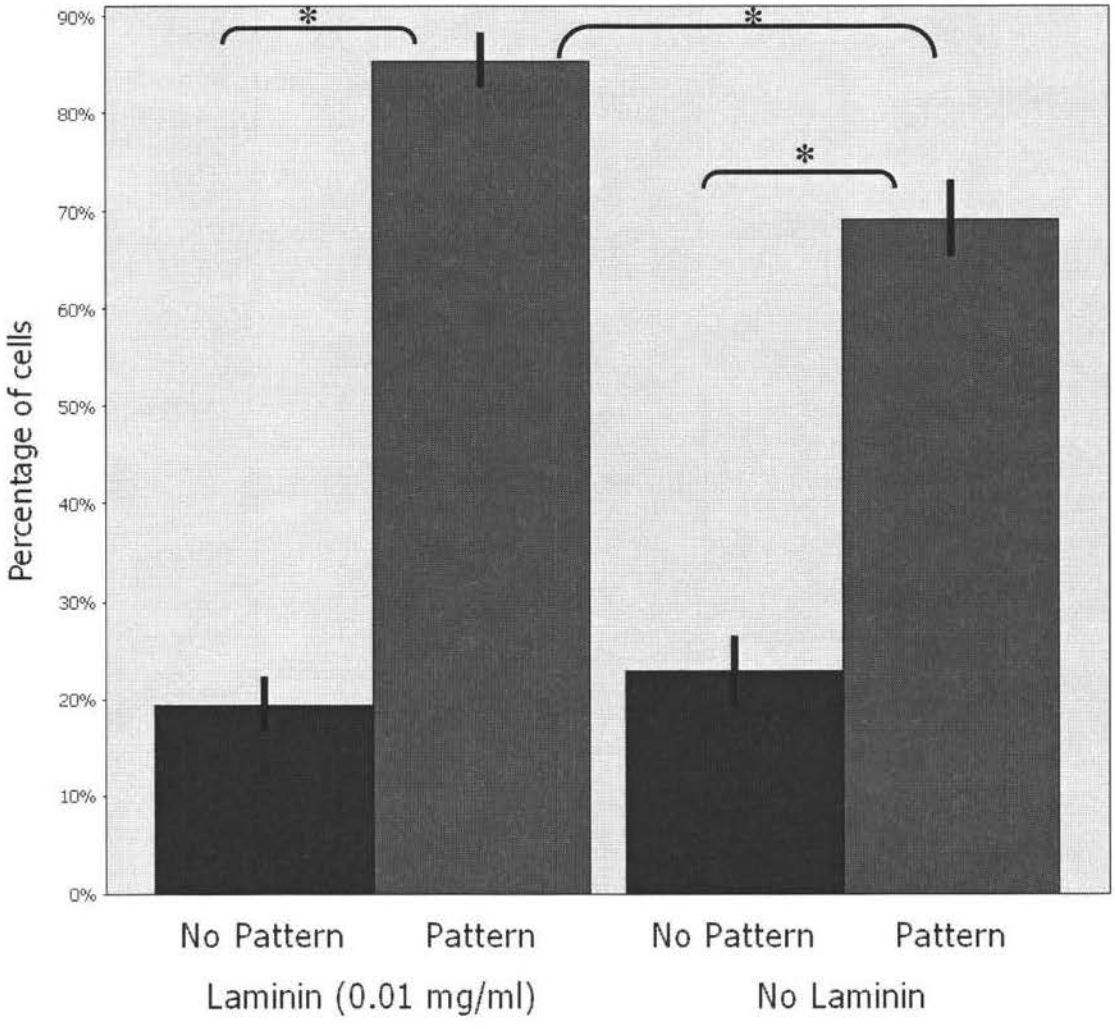

Figure 4-24. The effects of chemical and physical guidance across initial seeding densities of 7500, 13,000, and 20,000 cells per cm^2. The percentage of astrocytes growing at an angle of $\leq 20°$ with the direction of the grooves (on 10 x 20 x 3 μm patterned substrates) is demonstrated. The data presented here was pooled across all seeding densities and time periods analyzed. Data shown are mean values ± s.e.m. ($N = 24$ for No Laminin and $N = 36$ for Laminin). Statistically significant differences are marked with an asterisk ($P < 0.05$).

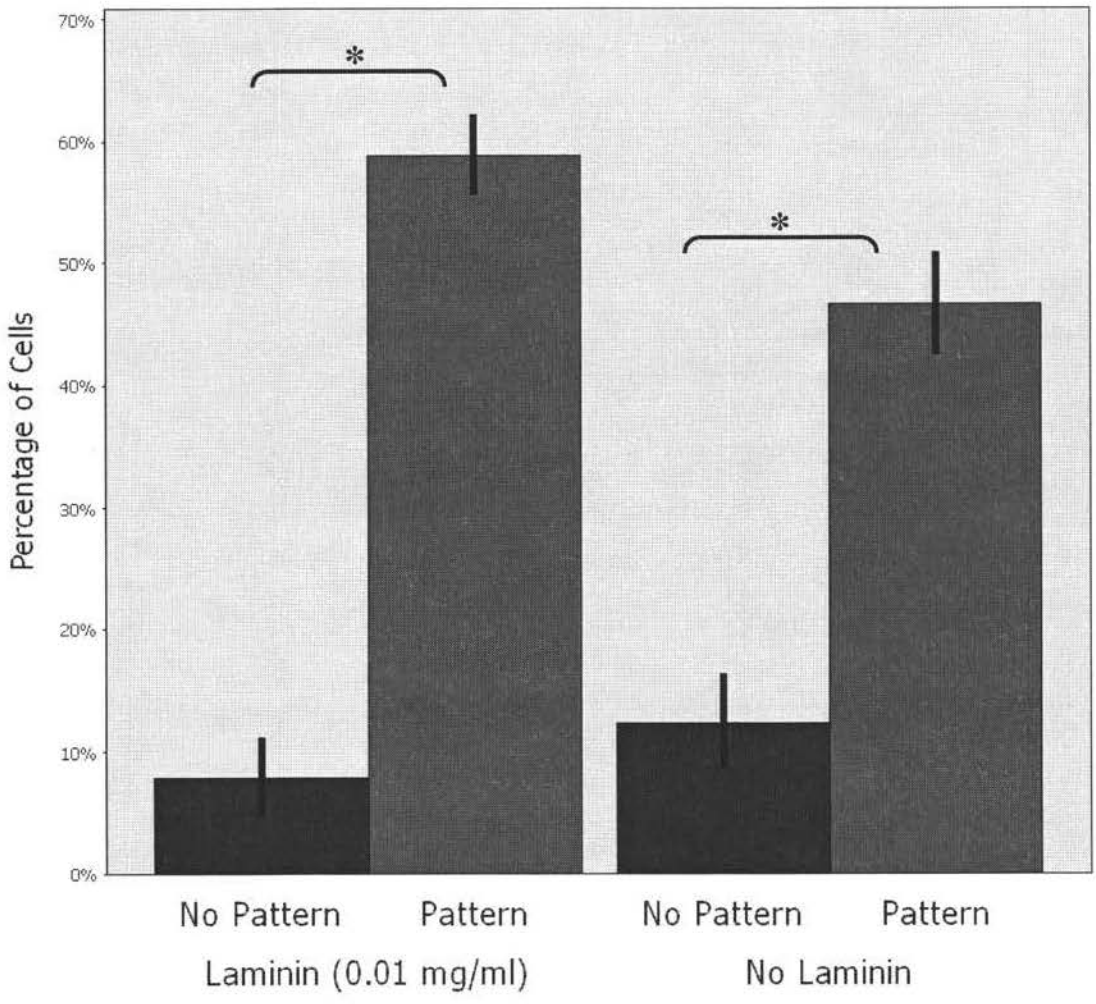

Figure 4-25. The effects of chemical and physical guidance across initial seeding densities of 7500, 13,000, and 20,000 cells per cm^2. The percentage of astrocytes growing at an angle of $\leq 10°$ with the direction of the grooves (on 10 x 20 x 3 μm patterned substrates) is demonstrated. The data presented here was pooled across all seeding densities and time periods analyzed. Data shown are mean values ± s.e.m. ($N = 24$ for No Laminin and $N = 36$ for Laminin). Statistically significant differences are marked with an asterisk ($P < 0.05$).

was achieved on the micropatterned PS substrates with laminin adsorbed on the surface. In this range of initial seeding densities, the astrocytes appeared highly elongated and extended cytoskeletal filaments in the direction of the grooves and along groove boundaries. Therefore, it is not only the individual cues but a combination of chemical (adsorbed laminin) and physical (the micropatterned substrate) cues that are required for directional guidance of astrocytes. Aligning astrocytes in a chemically modified three-dimensional environment results in a substrate that can provide a permissive environment *in vitro* for guided regeneration within the central nervous system.

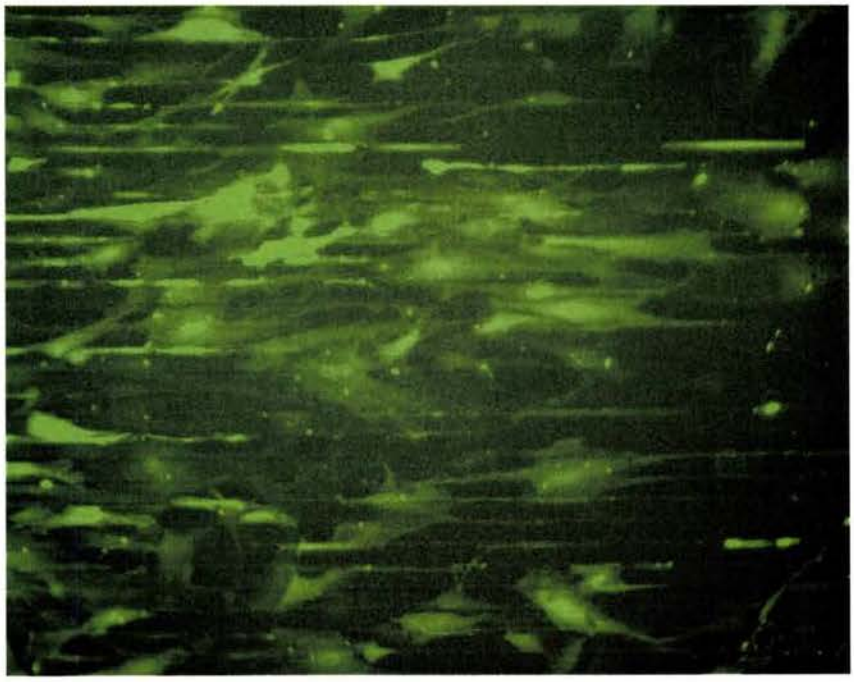

Figure 4-26. Astrocytes were cultured on a 10 x 20 x 3 μm PS substrate at a density of approximately 30,000 cells per cm^2. Many cells are spanning grooves. Although alignment was still observed, the percentage of astrocytes aligned was lessened by clustering of cells and contact inhibition. Astrocytes were stained with CFDA SE in cell suspension.

References Cited

1. Miller, C., S. Jeftinija, and S. Mallapragada, *Synergistic effects of physical and chemical guidance cues on neurite alignment and outgrowth on biodegradable polymer substrates.* Tissue Engineering, 2002. **8**(3): p. 367-378.
2. Miller, C.A., S. Jeftinija, and S.K. Mallapragada, *Micropatterned Schwann Cell-Seeded Polymer Substrates Significantly Enhance Neurite Alignment and Outgrowth.* Tissue Engineering, 2001. **7**: p. 705-715.
3. Miller, C.A., et al., *Oriented Schwann cell growth on micropatterned biodegradable polymer substrates.* Biomaterials, 2001. **22**: p. 1263-1269.
4. Curtis, A. and C. Wilkinson, *Topographical control of cells.* Biomaterials, 1998. **18**(24): p. 1573-1583.

5. CONCLUSIONS

In an effort to promote optic nerve regeneration *in vivo*, directional growth of astrocytes has been achieved on polymer substrates *in vitro*. Using a combination of physical and chemical guidance cues, the behavior and morphology of astrocytes has been investigated on micropatterned polystyrene substrates. These substrates provided topographical guidance while adsorbed laminin presented chemical cues for cell adhesion and spreading. By mimicking the processes that occur in the developing central nervous system where astrocytes are thought to guide migrating neuronal precursors, the integration of physical, chemical and biological cues can be applied to an *in vivo* experiment to facilitate optic nerve regeneration.

Polystyrene (PS) was used for fabricating micropatterned solvent cast substrates. Conventional photolithographic techniques and reactive ion etching or deep reactive ion etching were used to prepare silicon wafers having desired micropatterns that were imprinted onto the PS substrates using solvent casting. Direct etching was also experimented with to create micropatterns on the PS substrates. Based on previous pattern optimization with Schwann cells and dorsal root ganglia on biodegradable polymer substrates, the PS substrates were imprinted with patterns of 10 x 10 x 3 μm, 10 x 10 x 4 μm and 10 x 20 x 3 μm. These substrate dimensions had a significant effect on astrocyte orientation.

The micropatterned PS substrates had a significant influence on astrocyte orientation. This was evaluated on 10 x 20 x 3 μm micropatterned substrates. The astrocytes exhibited extension of their filaments along the inside of the groove region of the PS substrates as well as on the mesas in the direction of the groove. The astrocytes sensed the boundaries of the groove and aligned to within 20° and 10° of the groove direction. Over 70% of the astrocytes aligned within 20° and nearly 50% aligned within 10° of the groove direction on these PS substrates without any chemical cues presented.

Using a surface tension based technique for laminin application on the micropatterned substrates, more laminin was selectively adsorbed to the groove region. As a result, the astrocytes were exposed to more laminin per area in the grooves than on the surface of the mesas. Applying laminin resulted in significant improvement in astrocyte adhesion and spreading of F-actin microfilaments and intermediate filaments on the PS substrates. After 24 and 72 hours, approximately 3 times as many cells adhered to substrates with adsorbed laminin on the surface than those without

laminin. As a component of the ECM, the laminin also exhibits a chemotrophic effect by binding trophic factors in the culture media and those released by cells. Such trophic factors are then available to the other cells in the culture to enhance migration, proliferation and cell spreading. The adsorbed laminin allowed significantly greater astrocyte adhesion and promoted alignment of the astrocytes on the 10 x 20 x 3 μm micropatterned PS substrates.

The physical and chemical guidance provided by the laminin coated micropatterned PS substrates had a significant effect on the alignment of the astrocytes on the 10 x 20 x 3 μm. The presence of laminin had a significant effect on the alignment of the astrocytes on the micropatterned PS substrates as compared to those substrates not coated with laminin. Over 85% of the astrocytes aligned within 20° and 60% aligned within 10° of the groove direction on the PS substrates with adsorbed laminin on the surface.

Over the three initial astrocytes seeding densities examined (7500, 13,000 and 20,000 cells per cm^2), similar trends were seen in terms of astrocyte adhesion and alignment. Adsorbing laminin at 10 μg/ml EBSS onto the PS substrate resulted in the adhesion of significantly more cells to the substrate than to PS substrates without laminin. The percentages of astrocytes aligning on the micropatterned PS substrates were not significantly different among the three seeding densities.

These results demonstrate the effect that micropatterned substrates coated with laminin have on promoting the directional guidance of growing astrocytes *in vitro*. It is the combination of the topographical and chemical cues that provided the maximum effect on astrocyte behavior. The integration of the biological influence of the aligned astrocytes and the physical and chemical cues presented here can generate a permissive environment for specific cellular behavior such as the selective differentiation of neural stem cells. The understanding gained from this integration of guidance cues to control neural stem cell differentiation at the cellular level has possible applications in guided nerve regeneration using conduits. Conduits that combine the physical guidance effects of the micropatterned polymer substrates, chemical guidance mechanisms as well as the biological cues provided by astrocytes to direct neural stem cell differentiation and outgrowth provide an environment that has the potential to support regeneration of the diseased or injured optic nerve *in vivo*.

6. FUTURE WORK

There are many applications for chemically modified micropatterned polymeric guidance substrates. Microfabrication techniques offer the potential to create microdies and growth substrates having various shapes and patterns. Using such techniques, topography as well as the biochemical composition of a substrate can be changed on a cellular level. Cell-cell as well as cell-substrate interactions can be controlled using micropatterning methods. Specific patterns can be easily transferred onto polymer substrates and modified for investigation into the behavior of numerous cell types. Integrating these techniques with microelectronics and/or micromechanical components is extremely valuable to the study of cell function.

Gaining insight into the biology of neural stem cells and directing NSC outgrowth will provide useful information for *in vitro* and *in vivo* experimentation into the regeneration and repair of the central nervous system (CNS), specifically the optic nerve. Manipulating a combination of physical, chemical and biological cues at the cellular level, directed and accelerated neural stem cell (NSC) differentiation, outgrowth, and alignment *in vitro* is currently under investigation. Preliminary experiments have involved culturing adult hippocampal progenitor cells (AHPCs) on laminin-coated and non-coated micropatterned polystyrene (PS) substrates (Figure 6-1). Cell bodies were found on the mesas as well as in the grooves on the micropatterned substrate. Processes of the AHPCs were extensive on the mesas and often formed elaborate arborizations. Establishing that growth and

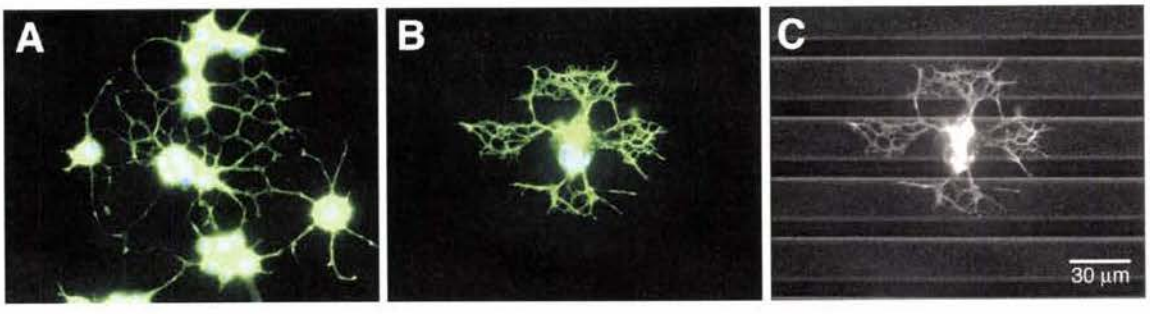

Figure 6-1. AHPCs growing on laminin coated PS substrates. A) AHPCs on a non-patterned PS substrate. B) AHPCs on 10 x 20 x 3 µm PS substrate. A and B) Merged image created by the superimposition of green fluorescent protein (GFP) and DAPI fluorescence images.
C) Merged image created by the superimposition of GFP and DIC images. Images captured after 72 hours *in vitro*.

alignment on these substrates is comparable to results obtained with the astrocytes is the first objective. Providing a permissive substrate for selective AHPC differentiation is also a primary goal of these studies. Astrocyte and AHPC co-cultures on micropatterned PS substrates will be used to investigate AHPC differentiation and the trophic and tropic factors involved.

Another goal of this project is to investigate the cellular mechanisms of optic nerve repair by creating an interface between biological and non-biological systems such as microelectronics. Microfabrication techniques are being used to develop a micropatterned PS conduit with embedded arrays of microelectrodes that can serve as an electrical cue in the directed growth of regenerating axons. Cells can be cultured directly onto this substrate for *in vitro* experimentation. The microelectrodes can be used to stimulate nerve regeneration as well as for selectively recording electrical signals from axons located in particular grooves of the micropatterned substrates. The cells in the grooves can be selectively stimulated electrically through gold electrodes located at both ends of the grooves (Figure 6-2). With such a device, an interface between optic nerve axons and retinal prosthesis can be created. This approach provides a system that can be potentially used for the transmission of electrical signals from microelectronic components through a bioartificial optic nerve to the brain where these signals are decoded and interpreted as visual images. With such a system, greater understanding and control of CNS function and repair can be accomplished.

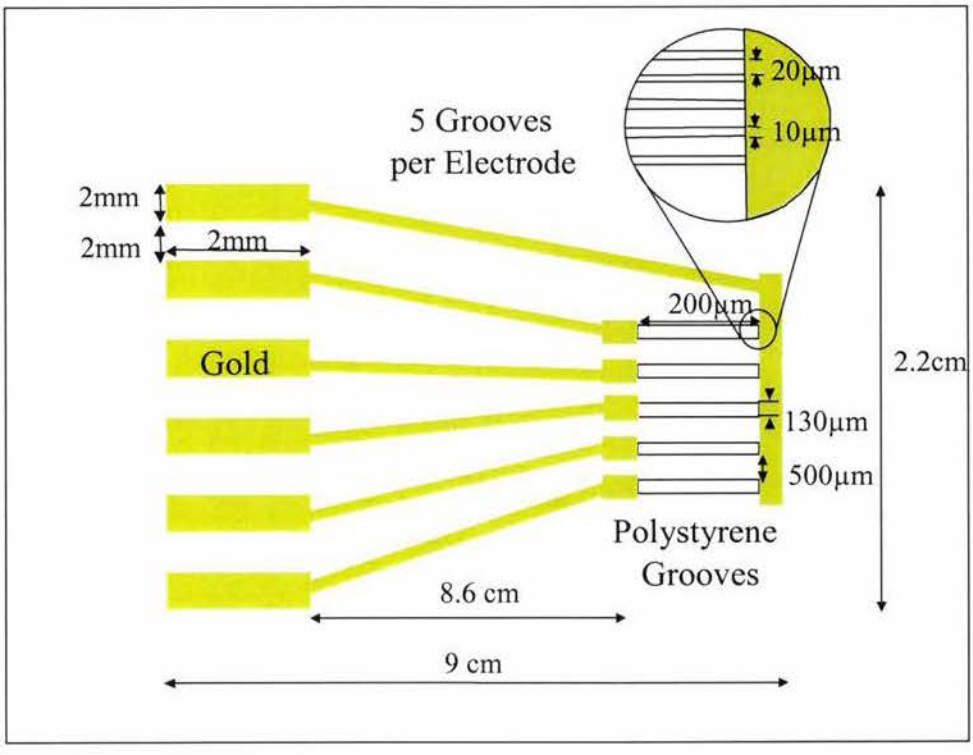

Figure 6-2. The proposed design for creating an embedded array of microelectrodes connected to the micropatterned PS substrate. Microfabrication techniques are being used to develop this device.

Substance	Source Company	Source City and State	Item Number
Alexa Fluor 568 Phalloidin	Molecular Probes	Eugene, OR	A-12380
Bovine Serum Albumin	Sigma Chemical Co.	St. Louis, MO	A-9647
Carboxyfluorescein Diacetate Succinimidyl Ester	Molecular Probes	Eugene, OR	C-1157
D-(+)-Glucose	Sigma Chemical Co.	St. Louis, MO	G-7021
DAPI	Molecular Probes	Eugene, OR	D3571
DiIC18	Molecular Probes	Eugene, OR	D282
Dimethyl Sulfoxide	Sigma Chemical Co.	St. Louis, MO	D-2650
Earle's Balanced Salt Solution	Gibco	Grand Island, NY	14155-063; 12459-012
Fetal Bovine Serum	HyClone	Logan, UT	SH00371.03
Fluorescein Isothiocyanate	Fisher Scientific	Pittsburgh, PA	AC119252500
Goat Serum	Sigma Chemical Co.	St. Louis, MO	S-6898
Halothane	Sigma Chemical Co.	St. Louis, MO	H169
L -glutamine	Sigma Chemical Co.	St. Louis, MO	G-8540
Laminin	Sigma Chemical Co.	St. Louis, MO	L-2020
Minimal Essential Medium	Gibco	Grand Island, NY	11090-081
Papain	Sigma Chemical Co.	St. Louis, MO	P-4762
Penicillin-Streptomycin	Gibco	Grand Island, NY	15140-122
Poly-*L* -Lysine	Sigma Chemical Co.	St. Louis, MO	P-1274
Sodium Bicarbonate	Sigma Chemical Co.	St. Louis, MO	S-5761
Sodium Pyruvate	Sigma Chemical Co.	St. Louis, MO	S-8636
Triton-X-100	Fisher Scientific	Pittsburgh, PA	Fisher Scientific #BP151-100
Trypan Blue 0.4%	Gibco	Grand Island, NY	15250-061
Trypsin	Sigma Chemical Co.	St. Louis, MO	T-4665
Trypsin Inhibitor	Sigma Chemical Co.	St. Louis, MO	T-9253

Antibodies	Source Company	Source City and State	Item Number
Primary Ab			
Anti-GFAP (mouse IgG)	ICN Immunobiologicals	Costa Mesa, CA	69-110
Anti-GFAP (rabbit IgG)	Sigma Chemical Co.	St. Louis, MO	G-9269
Anti-Laminin	Sigma Chemical Co.	St. Louis, MO	L-9393
Anti-MAP-2ab (mouse IgG)	Sigma Chemical Co.	St. Louis, MO	M-1406
Anti-RIP (mouse IgG)	Developmental Studies Hybridoma Bank	University of Iowa Iowa City,IA	
Secondary Ab			
Goat anti-mouse IgG (H+L) Alexa Fluor 488	Molecular Probes	Eugene,OR	A-11001
Goat anti-mouse IgG (H+L) Alexa Fluor 546	Molecular Probes	Eugene,OR	A-11003
Goat anti-rabbit IgG RITC	Southern Biotechnology	Birmingham,AL	Fisher Scientific #OB 403003
Goat anti-rabbit IgG TRITC	Sigma Chemical Co.	St. Louis, MO	T-5268

ACKNOWLEDGMENTS

I would like to thank those providing funding for this project. This project was supported by grants from the National Science Foundation (BES 9983735) and the Department of Energy (W-7405-Eng-82).

I would like to give special thanks to my major advisor Surya Mallapragada for the initial project idea as well as for her patience and optimism. I would also like to thank my committee members: Donald Sakaguchi and Richard Seagrave. I would especially like to acknowledge Don Sakaguchi for imparting his knowledge of histological staining and immunocytochemical techniques and advice on the project as a whole.

I would like to acknowledge Dr. Fred Gage of The Salk Institute for Biological Studies, La Jolla, CA, for his gift of the adult hippocampal progenitor cells to the Sakaguchi lab that were made available to us through a collaboration with Don Sakaguchi.

There are several people that offered much assistance in the development of this project that I would like to acknowledge. Bob Doyle offered his expertise in astrocyte cell culture as well as microscopy techniques that was invaluable to my project. I would like to also thank Gary Tuttle for his instruction with equipment used at the Microelectronics Research Center (MRC). Dave Schimdt also provided necessary information on the RIE and DRIE procedures used at the MRC. The undergraduate students that I have worked with have provided much help with this project especially Tony Dupre - for creating and imaging the polystyrene substrates and help with animal dissections, Mike Todd - for his expertise in microfabrication techniques and creation of the polystyrene substrates and Renee Esser - for her help with image analysis using MetaMorph.

I would like to acknowledge several others for their advice, encouragement and technical support: Cheryl Miller, Anthony Witt, Al Landin, Brian Anderson, Anil Gannepalli, Brandon Vogel, Mike Determan, Amy Determan, Dan Kuster, Matt Harper, Karen Stranghoener, Jason Gruenhagen, Deann Pitman, Kathye Law, Wendy Ortmann and Jody Danielson. I would also like to thank the Iowa State University Laboratory Animal Resources personnel for the care of the animals and Eric Rowe for overseeing the rat colony.

I would also like to thank my family and friends, especially my mother, Sheila Behr, for being there for me. Very special thanks to Justin for his ingenious statistical skills and, most of all, for his undying patience, support and encouragement.